Dynamic Factors of Bacteriorhodopsin:

Regulation Key Points in Helices B, C and F.

Alejandro Perálvarez Marín

Departament de
Bioquímica i de
Biologia Molecular.
Unitat de Biofísica

Universitat Autònoma de Barcelona

IBB

Dynamic Factors of Bacteriorhodopsin: Regulation Key Points in Helices B, C and F.

Alejandro Perálvarez Marín

Memòria de la Tesi presentada per optar al Grau de Doctor en Bioquímica i Biología Molecular per la Universitat Autònoma de Barcelona.

Aquest treball ha estat realitzat a la Unitat de Biofísica del Departament de Bioquímica i de Biología Molecular, i a l'Institut de Biotecnología i Biomedicina de la Universitat Autònoma de Barcelona, sota la direcció dels Doctors Esteve Padrós i Morell i Enrique Querol i Murillo.

Dr. Esteve Padrós i Morell Dr. Enrique Querol i Murillo

Març de 2005

A los que siempre han confiado y confían en mí,
a mi familia, a mis amigos, a mi amor;
a los sueños que embargan mi vida,
a todo lo que queda por descubrir,
a mí.

Alx.

Las manos ociosas son el instrumento del diablo.

???

But if you've got enough naivety
and you've got conviction,
then the answer is perfect for you.

Greg Graffin.

CONTENTS

CHAPTER I. 3

I. INTRODUCTION 5

I.1. Purple Membrane and Bacteriorhodopsin 8

I.2. Retinal 10

I.3. Photocycle 12

I.4. Blue form of Bacteriorhodopsin 16

I.5. Role of Helix C in Bacteriorhodopsin 16

I.6. Function of Threonines / Prolines in transmembrane proteins 19

-Threonine (Thr): 19

-Proline (Pro): 19

-Relationship between Thr and Pro: 21

I.7. Focusing on Thr90 and Pro91 in BR 21

I.8. Role of helix-embedded prolines in BR: an example for transmembrane proteins. 25

I.9. References 30

CHAPTER II. 35

II. OBJECTIVES 37

CHAPTER III. 39

Abstract 40

III.1. Introduction 41

III.2. Material and methods 42

III.3. Results 44

III.4. Discussion 49

III.5. References 51

CHAPTER IV. 53

Abstract 54

IV.1. Introduction 55

IV.2. Material and Methods 57

IV.3. Results 59

IV.4. Discussion 69
IV.5. References 74
CHAPTER V 77
Abstract 78
V.1. Introduction 79
V.2. Materials and Methods 82
V.3. Results 84
V.4. Discussion 92
V.5. References 98
CHAPTER VI 103
Abstract 104
VI.1. Introduction 105
VI.2. Materials & Methods 106
VI.3. Results & Discussion 109
VI.4. References 118
CHAPTER VII 121
VII. GENERAL DISCUSSION 123
VII.1 Thr90 124
VII.2. Pro91 127
VII.3 Thr90-Pro91 motif 129
VII.5. Helix-embedded prolines Pro50 and Pro186 132
-Pro50 132
-Pro186 133
-Embedded-Prolines in Bacteriorhodopsin 134
VII.6. Role of Prolines in Transmembrane Helices 135
VII.7. Analysis of the Role of Prolines in the stability of Bacteriorhodopsin 137
VII.7.References 139
CHAPTER VIII 141
VIII. CONCLUSIONS 143
Index of Figures and Tables 147

the seeds of inspiration never germinated in my mind,
the beacon of awakening is somewhere that I can't find.

Bad Religion.

CHAPTER I.

INTRODUCTION

I. INTRODUCTION

In a cell, either prokaryotic or eukaryotic, there are plenty of functions to perform. Most of these functions are carried out by proteins. In a first approach depending on their location, proteins can be soluble or transmembrane or amphitropic. Transmembrane proteins function, goes from signal transduction, ion channels, energy transduction, structural role to cell recognition among others. If one protein should be considered the perfect model for studying transmembrane proteins, this is Bacteriorhodopsin (BR). For the last 30 years BR has been widely studied, laying down the basis for a lot of further knowledge on transmembrane proteins.

BR is a seven helix transmembrane protein, and it is produced by an Archaeobacteria named *Halobacterium salinarum*, which is found in salt mines and salt lakes, in fact, high salt concentration and warm habitats **(Fig. I.1)**. This halophile aerobic organism is capable of producing energy, in low oxygen concentration and under illumination, through a different pathway, instead of using the electronic respiratory chain. By this alternative pathway, cells are able to survive but not to grow. BR transforms light into electrochemical energy and when coupled with an ATP synthase, light is transformed into chemical energy. Therefore, this complex represents the simplest and archaic photosynthetic system known **[1] (Fig. I.2)**. BR contains a covalently linked molecule of retinal which responses to photon stimuli **[2]**. After the light stimulus, retinal isomerizes giving rise to some conformational changes in the protein, besides of some charge movements, which create a proton gradient from the cytoplasm inner cell to the external medium **[1]**. This proton gradient is used by the ATP synthase to produce ATP **[1]**.

However, despite of being so exhaustively studied some questions remain unanswered in BR. In addition to the fact that the expression and high-amount production of this protein is achieved easily, has made of BR a good protein example for becoming extensively used as a model for characterizing some features of transmembrane proteins. Not only it is used as a model for G-protein coupled receptors, but it is also used for developing new techniques, as the improving on the crystallization and further X-ray diffraction of membrane

proteins **[3]**. Currently in the protein data bank (PDB) there are more than 50 structures of wild-type (WT) and mutant BR, as well the structure of different conformational steps of the protein called intermediates or photointermediates.

This current increasing on the number of 3D structures, some of them at high resolution, has opened new ways on the study of this protein. Nevertheless, the promising field of crystallography has not become any sort of panacea that answers everything, especially when subtle conformational changes are involved in proton function. Crystal structures turn out to be a very important tool for generating new hypothesis on the function and transport of the proton and to overcome some structural question marks.

Fig. I.1. Salt lake inhabited by *Halobacterium salinarum* with the characteristic purple coloration due to Bacteriorhodopsin.

However, crystallization methods are quite aggressive for the natural structure of the protein, because most of the native lipids are substituted by the ones used for crystallizing the protein, and the diffraction is performed at very low temperatures. Furthermore, X-ray radiation by itself may damage the protein, thus the structure obtained may only be an approach to the real one. In this way, powerful and more confident techniques are biophysical ones working with native suspensions of the protein at close-to-physiological conditions.

Examples of these techniques are FTIR, Flash Photolysis, DSC, NMR, UV-Vis Spectroscopy …

The aim of this work is focused on the determination by site directed mutagenesis of the role of certain residues that in principle are not related directly to the proton pumping function in BR. The mutant proteins are expressed in *Halobacterium salinarum*. As a candidates for performing a dynamic role on the chain of events occurring during the transport of the proton by BR, we have selected Thr90 and Pro91 due to its location in BR (in helix C), their high degree of conservation among archaeal rhodopsins (Thr90) and transmembrane GPCRs (Pro91), and finally due to its possible relationship with the kinking of the α-helix C in BR. In fact, thanks to these features, the conclusions derived from this work can be extended to other transmembrane proteins with similar characteristics.

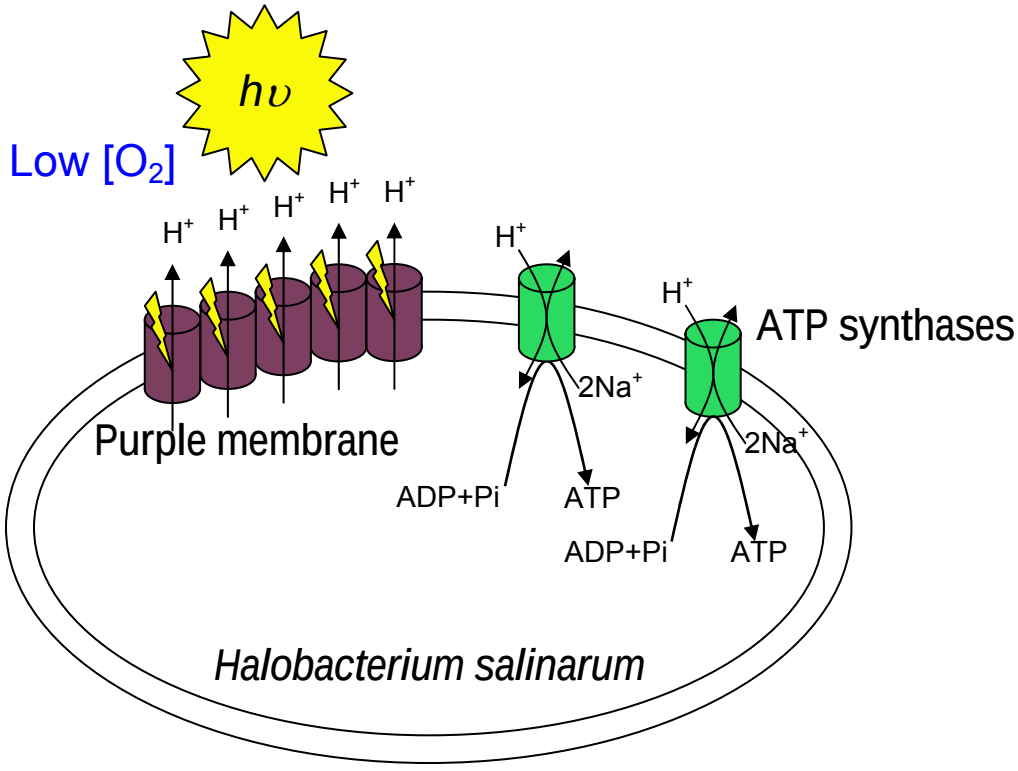

Fig. I.2. Basic scheme of light-to-chemical energy transformation carried out by *Halobacterium salinarum*. PM, which is induced by low oxygen concentration generates an electrochemical gradient of protons when stimulated by light. ATP synthases enter a proton into the cell and release two sodium molecules to the external medium through an antiport mechanism. As a result ATP molecules are produced and used as a source of energy to live until the environmental stress disappears. This is an endurance form of living, in these conditions *H. salinarum* is not capable of growing.

The goal of expressing BR in its natural environment comes from the fact that former procedures express the protein in a heterologous system as *Escherichia coli* **[4]**. Some disadvantages of this method are quite evident. *E.coli* is not able to synthesize retinal, indispensable molecule for proton pumping function. Therefore, retinal was subsequently added in the presence of some detergent concentration, and the folding of the protein was not the optimal one. In addition, *H. salinarum* has a special kind of lipids, with ether linkage, in front of the lipids of *E.coli* with ester linkage. Thus, obtaining a protein expressed in *E. coli*, yields a protein that will be post-translational modificated, solubilized to resuspend it on natural lipids and supplemented with retinal to obtain as close-to-natural protein, or a BR-like protein **[5]**.

I.1. Purple Membrane and Bacteriorhodopsin

Under conditions of anaerobe stress, *H. salinarum* stops its growing and promotes the synthesis of the so-called purple membrane (PM). This kind of membrane is distributed by patches in the cell membrane, occupying about the 50% of the membrane surface, so named because of its characteristic purple color, which evidences its presence in high salt concentration habitats **[1]**. BR represents the 75% (w/w) of the PM, while the other 25% corresponds to a mixture of ether-linked lipids as squalene, sulphate glycolipids and phosphatydilglycerolphosphates **[6]**.

Focusing on BR, the apoprotein Bacterioopsin (BO) is a protein encoded by the *bop* gene in the *H. salinarum* genome, consisting of 248 amino acids **(Fig. I.3.A)** with a molecular weight of 26 KDa **[7, 8]**. Tertiary structure consists of seven transmembrane α-helices (named from A to G) **(Fig. I.3.B)**, connected by loops at each side of the membrane. Retinal remains surrounded by the helices, in the middle of the protein, determining its two halves, the cytoplasmatic and the extracellular one. Retinal is covalently linked to the apoprotein through a protonated Schiff base with Lys216, giving rise to a chromoprotein which is called BR. Three molecules of BR are grouped forming a trimer, and then,

forming a hexagonal network of hexamers, that assumes the lattice of a natural 2D crystal **(Fig. I.3.C) [9]**.

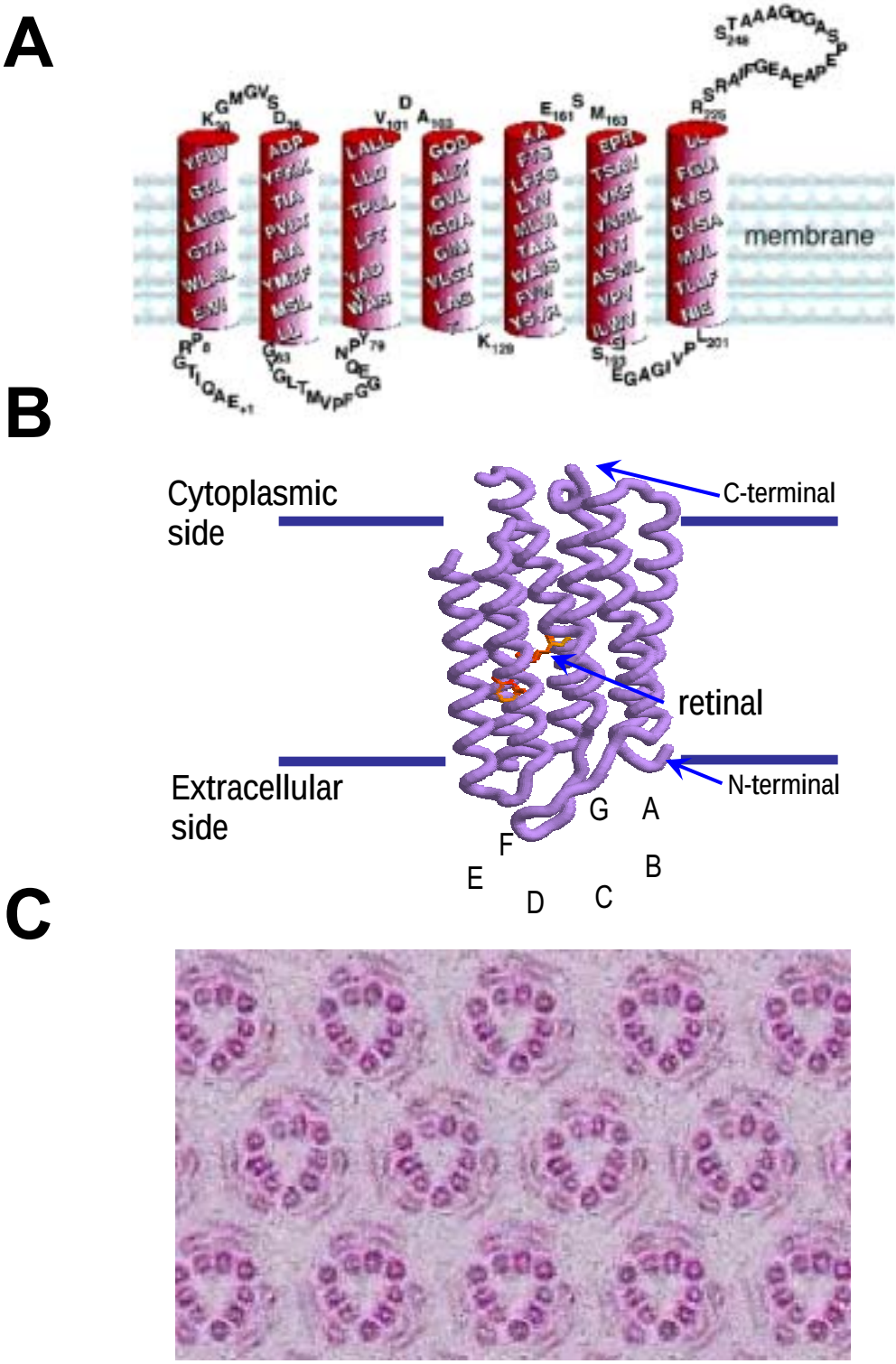

Fig. I.3. A. Primary and secondary structure of BR.B. Tertiary structure of BR. It comes from the X-ray diffraction of a crystal (PDB code 1c3w). The N- and C-terminal are not complete because they don't appear in the diffraction pattern due to their high mobility. C. The lattice of a 2D crystal is formed by three molecules of BR forming a trimer, and these trimers are later distributed forming hexamers.

I.2. Retinal

Retinal is the chromophore of the protein. It is a carotene derivative of vitamin A, so, containing a β-ionone ring. As formerly said, it is covalently linked to the protein at the Lys216 through a protonated Schiff Base **(Fig. I.4) [2]**. In its free form, retinal presents an absorbance maximum of 380 nm dissolved in ethanol. In the resting state of the protein (unphotolyzed), there is equilibrium between two forms **(Fig. I.5)**, *all-trans* and *13-cis* with a ratio of 1:2 respectively **[10]**. The absorbance maximum of this chromoprotein is 558nm, and represents the so-called Dark Adapted (DA) form. When this DA BR is illuminated, the equilibrium moves completely to a ratio of a 100% of *all-trans* retinal, yielding the Light Adapted (LA) form, with an absorbance maximum of 568 nm in WT BR.

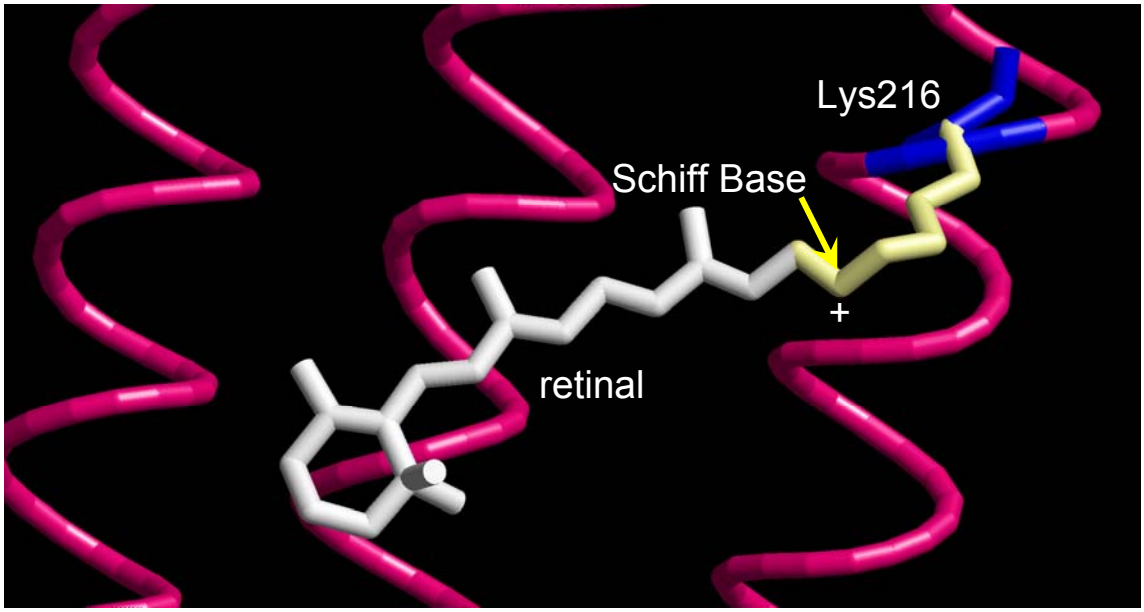

Fig. I.4. Plot of the Schiff Base between the side-chain Nitrogen of the Lysine 216 and the Carbon of the retinal molecule. The plus sign indicates the protonated state.

Retinal is mainly surrounded by hydrophobic and aromatic side chains, enclosing retinal in the proper place, which is called the Retinal Binding Pocket (RBP). Most of the retinal surrounding residues are aromatic amino acids **(Fig. I.6.A)** such as Trp (86,138,182,189) and Tyr (57, 83,185). This kind of bulky side-chain seems to be necessary to place correctly the retinal and avoid steric wrong conformations **[11-16]**. Besides these aromatic residues, there are some polar and hydrophilic (Thr90, Asp212, Asp85) and hydrophobic residues

(Leu93) in the RBP **(FIG I.6.B)**. Hydrophobic residues as Trp and Leu and the barely reactive Met seem to carry out a structural role whereas more reactive hydrophilic residues as Asp, Thr and Tyr seem to perform a more functional one.

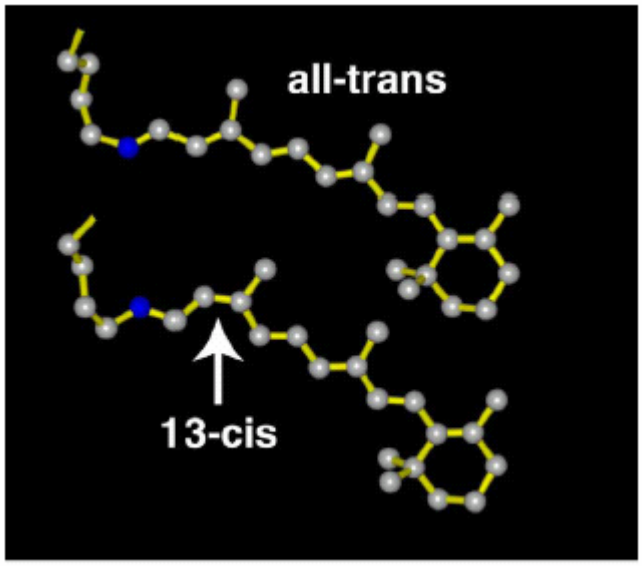

Fig. I.5. Two conformations of retinal are displayed: *all-trans* and *13-cis* retinal. [17]

Perhaps, now it is the time to insist again on the dynamic role of some residues. Residues as Thr90 or Pro186, which have no relation with the proton pathway, could be considered as relevant candidates for the transmission of conformational changes from the retinal to the protein, assuming a dynamic role. Asp85, Asp212 and Arg82 (not included in the RBP) form part of the counter-ion cloud, which stabilizes the positive charge of the Schiff Base. Some buried water molecules are also included in the counterion **[18-22]**.

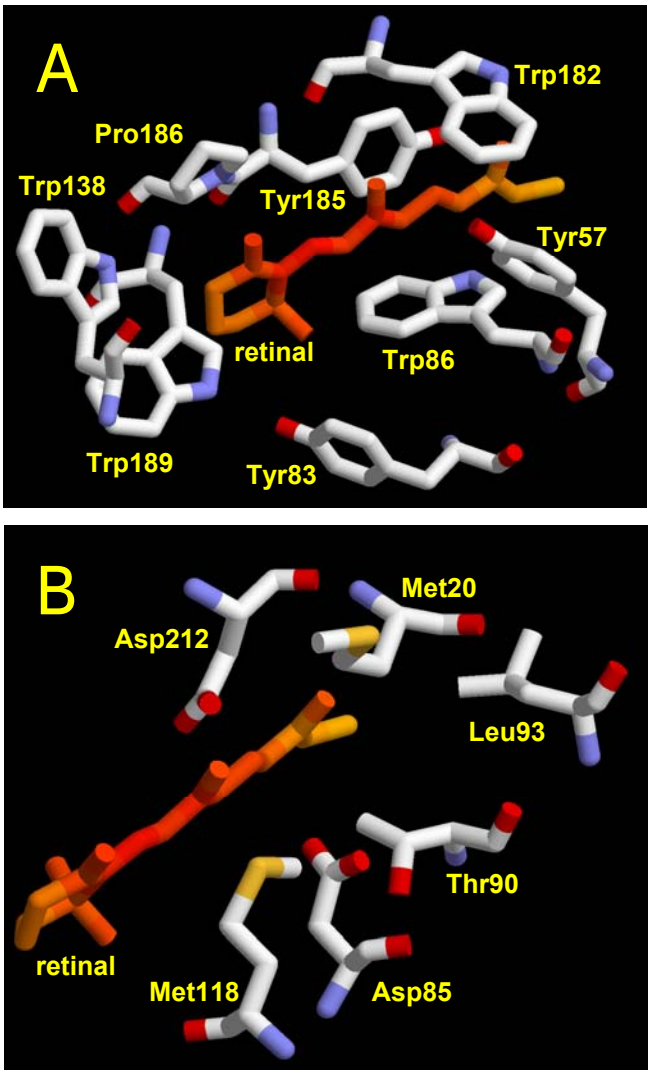

Fig. I.6. A. Set of aromatic residues surrounding retinal. Despite not being aromatic, Pro186 is included in this figure due to its proximity to Tyr185. B. Non-aromatic residues enclosing retinal. Thr90 is emphasized, although not considered as a part of the Retinal Binding Pocket, it contacts directly with retinal through steric interactions.

I.3. Photocycle

After the absorption of a photon by retinal, this molecule transmits the stimulation to the whole protein. The isomerization of the retinal after the stimulus, besides the contacts with the residues of the RBP, transduces the signal, through the different helices, from the middle of the protein to the cytoplasmic and extracellular side of the protein. The final result of this process yields the transport of a proton from the cytoplasmic to the extracellular side of the protein.

At room temperature and in the LA form, the photocycle lasts for about 10 ms. For an easy identification of the ongoing events occurring in the photocycle, they were grouped chronologically in photointermediates **(Fig. I.7)**,

from the basal state or BR going to J, K, L, M, N and the late O. Some conformational steps pass by in each of these photointermediates. As an example, there are available several crystallographic structures about photointermediates **[22-30]**. Some of them are derived from WT BR crystals analyzed at low temperature, trapping almost a pure intermediate. As well, some single or multiple mutations yield what should be considered a intermediate-like structure **[30]**. Besides, the existence of some different methods for crystallizing BR **[31-34]** has added more controversy to the structure field, because there are discrepancies among structures of the same intermediate **[35]**.

The important characteristics **[36]** of the intermediate states are **(Fig. I.7)**:

BR: Resting state just before beginning the photocycle. Retinal is in all-trans configuration, because the protein has to be light-adapted to start the photocycle. In this step, Schiff Base is protonated **[37, 38]**.

J: In the first 500 fs, after the photon is being absorbed by the retinal, J occurs. It is hardly detectable because it is very fast. Retinal remains in all-trans conformation and SB remains protonated. A reorganization of the electronic density of the retinal between the bonds between C=C and C-C occurs in this step. During this stage there is certain torsion of the polyenic chain of the retinal **[39]**.

K: The retinal isomerization from all-trans to 13-cis, 15-anti occurs in the transition from J to K. This 13-cis, 15-anti form, is different from the 13-cis, 15-syn form occurring in DA BR. This photointermediate is easily detectable compared to J. SB is still protonated **[39, 40]**.

L: The Asp96 becomes the most relevant residue in this photointermediate. Some waters enclosed between Asp96 and SB, moves after retinal isomerization, producing alteration in the Asp96 environment **[41]**. These movements yield a relaxation of the helices directed to surround the new conformation of the retinal. Recently, some structural studies point to certain movements in helix C during this intermediate **[26]** .

M: This is the most well-known photointermediate. The most remarkable feature in this intermediate is the SB deprotonation **[42, 43]**. The proton released

from the SB, moves to the Asp85, which becomes protonated. M intermediate consists of two photointermediates, known as M_1 and M_2.

M_1: The first movement of the proton occurs in this intermediate. SB deprotonates and the proton is taken by Asp85 **[44]**. This transfer gives rise to the release of a proton to the extracellular side by a residue or a complex known as X or Proton Release Group (PRG).

M_2: In this late M, the accessibility of the retinal changes from the extracellular to the cytoplasmic part, in fact to promote the reprotonation of the SB in the N intermediate **[45]**. Besides, some conformational changes occur in this step. The helices F and G open such in the way that the cytoplasmic half of the protein becomes an open channel to facilitate the entrance of water molecules **[46]**.

N: From M_2 to N, SB befalls protonated from Asp96, which deprotonates **[44]**. The opening of the helices in the late M, favors the entrance of water molecules, decreasing the pKa of Asp96, thus facilitating the deprotonation of this residue in favor of the SB. Between SB and the Asp96 exists a hydrogen bonded network, that allows the transit of the proton to reprotonate the SB **[46]**.

O: From M to O, Asp96 reprotonates, and the retinal reisomerizes to all-trans conformation. From which residue gets Asp96 the proton still remains unclear. Nevertheless, some hypothesis points to an antenna complex configured by Asp36, 38, 102 and 104, which would capture the proton from the bulk, to yield it to Asp96 **[47]**. During this intermediate, Asp85 is still protonated, but in the O→BR transition, this residue deprotonates and PRG protonates **[48]**.

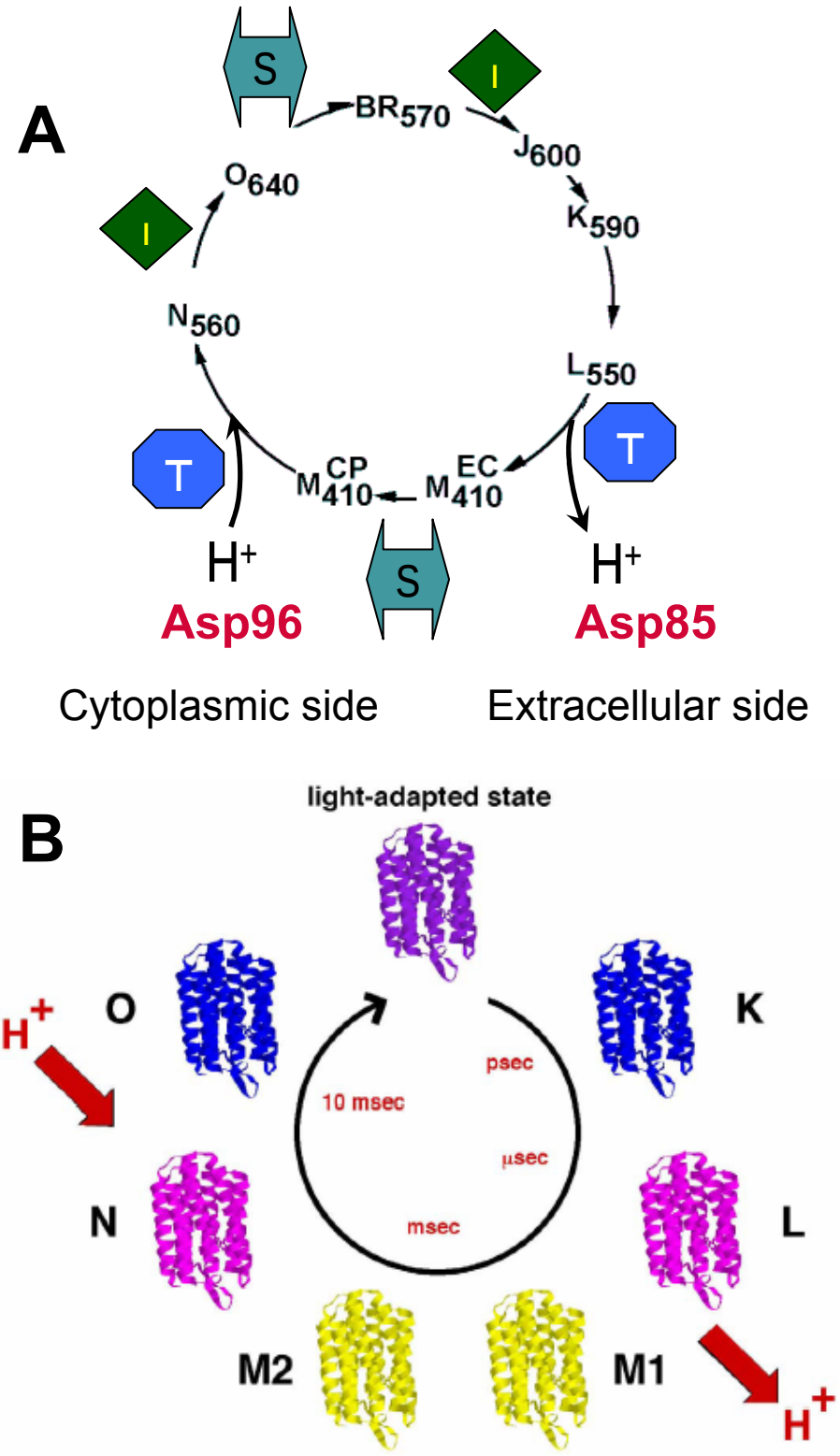

Fig. I.7.A. The BR photocycle can be defined as a sum of three different processes: Isomerization (I), Proton Transport or Translocation (T) and Switch of accessibilities (S). The first process is the retinal isomerization from all trans to 13-cis, followed by a proton transfer from the Schiff base to the proton acceptor Asp-85. Then, the accessibility of the Schiff base changes from the extracellular to the cytoplasmic side to be reprotonated from the Asp96. After reprotonation of Asp-96 from the cytoplasmic surface (O intermediate), retinal reisomerizes thermally and the accessibility of the Schiff base switches back to extracellular to re-establish the initial state. Chronologically, the photocycle seems to be divided into two halves, the first one with the main processes occurring in the extracellular side, and the second one happening in the cytoplasmic one. B. Intermediates can be identified by its maximum of absorbance (displayed as a sub index in Fig. I.6.A.), indicating an evolution in the absorption spectra shown by a color change of each intermediate. [17]

All these events described as the photocycle, should be taken into account in order to determine the path of the proton through the protein. Nonetheless, the crystal structures obtained in the last years, allow us to figure out more precisely not only the way of the proton, but also the structure of some intermediates. These structures of intermediates are obtained at low temperatures and in a non-natural environment for the protein. However, some general ideas can be inferred of each intermediate taking into account each structure. The consensus of some conformations contrasts with the controversy generated about substantial differences among the structure of one intermediate (L-intermediate) published by different groups **[26, 29, 49]**.

I.4. Blue form of Bacteriorhodopsin

At physiological conditions (neutral pH), the presence unprotonated state of Asp85, yields the average purple form of BR, which has a maximum absorbance of 558nm when it is dark-adapted. Under acidification of the medium **[50]**, Asp85 protonates, and the presence of the blue form, which absorbs near 600nm is evident. The pK_a of this group at 150 mM KCl is about 2.7. As a main feature, this low pH induced form lacks of M intermediate due to the presence of an always-protonated Asp85. Another consequence is the inability of this form to pump protons **[51]**. Another way to obtain this blue form is under the deionization of the sample. When cations are removed from the sample, the pK_a of the Asp85 rises from 2.7 150 mM KCl to 5.5 in deionized water. These two ways of obtaining the blue form yields the same specie **[52]**.

I.5. Role of Helix C in Bacteriorhodopsin

The right handed α-helix is a widespread protein secondary structure. This structure presents the following features **[53] (Fig. I.8)**:

- The R groups of the amino acids all extend to the outside.
- The helix makes a complete turn every 3.6 amino acids.
- The helix is right-handed; it twists in a clockwise direction, going from N-ter to C-ter.
- The carbonyl group (-C=O) of each peptide bond extends parallel to the axis of the helix and points directly at the -N-H group of the peptide bond

4 amino acids below it in the helix. A hydrogen bond forms between them.

As previously commented BR is a transmembrane protein and, as most of all the proteins of this kind, presents a high percentage of α-helix in the secondary structure (**Section I.1** and **Fig. I.3.B**). Almost all the relevant residues for the proton transport function (i.e. Asp85, Asp96, Arg82…) are included in the Helix C **(Fig. I.9)**. Besides this, Trp86, Arg82, Leu93 and Tyr83 are residues present in helix C that helps to conform the retinal binding pocket and to maintain the native structure. Recent studies reveal that Helix C

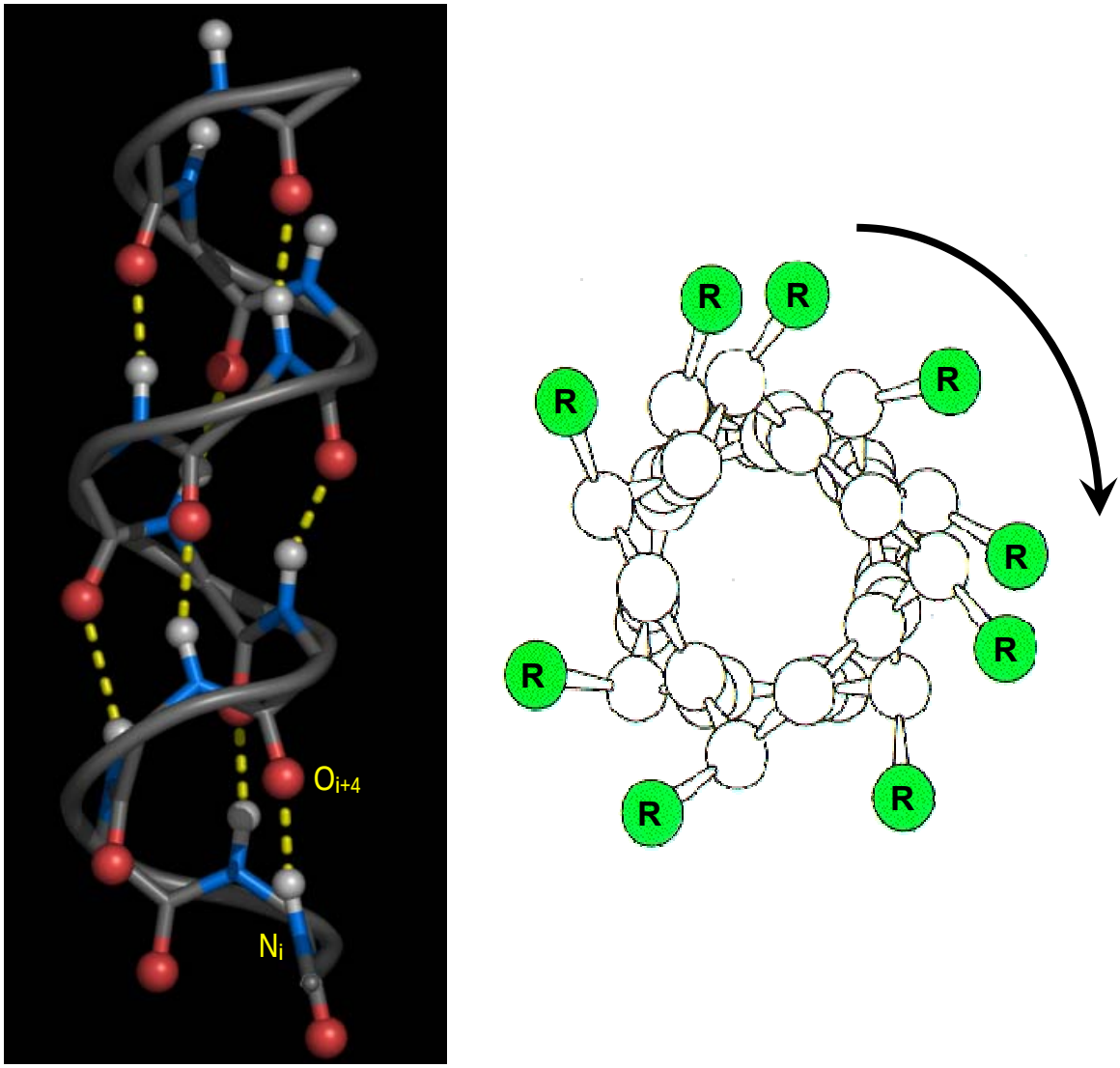

Fig.I.8 Plot of an average right-handed α-helix. The general features explained in the text are presented. The amino acid R-group is displayed in green. Oxygen and Nitrogen are represented in red and blue respectively.

moves during L intermediate. All these features convert helix C in a very relevant helix. On the other hand, it is known that BR suffers numerous conformational changes during the photocycle, so there must exist some residues especially involved in them, thus having a dynamic role. As an approach to understand this dynamic role, Thr90 and Pro91 in helix C have been tested, as candidates. We have also checked Pro50 in helix B and Pro186 in helix F.

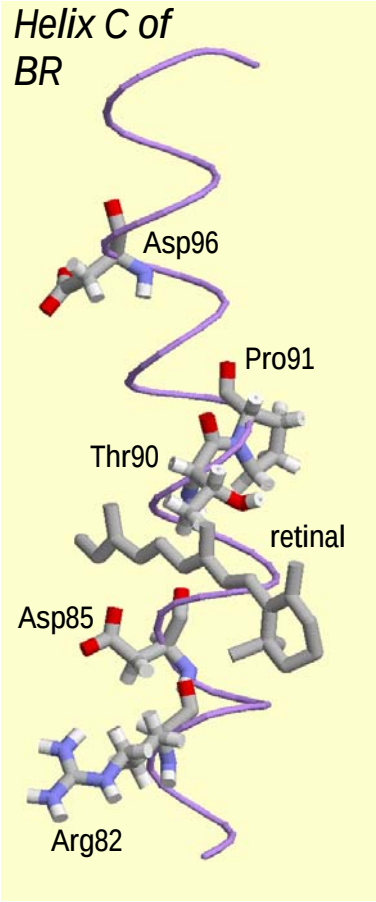

Fig. I.9. Disposition of the residues related to proton pumping in Helix C. Moreover Thr90 and Pro91 are displayed to show the kinking of this helix. These two residues are not directly involved in the translocation of the proton through the BR channel. Retinal is also shown.

It is observable that the major changes are present in helices G, F, B and C **[45]**. Besides helix G, containing Lys216 where retinal is attached, helices B, C and F have a common feature that is the presence of a Pro near the middle of the helix. Therefore, it is worth to note that these helices have some deviation from what a standard α-helix should be. This could be related to the presence of these Pro. Nevertheless, some recent structures of mutants of these Pro reveal

that the helices remain almost unaltered when these residues are substituted **[54, 55]**. It is clear that the crystallographic structures are equivalent to static pictures of the resting state; therefore, analysis of dynamic features of BR becomes a very interesting matter.

I.6. Function of Threonines / Prolines in transmembrane proteins

-Threonine (Thr): This amino acid contains an aliphatic hydroxyl group that makes this amino acids reactive and hydrophilic **(Fig. I.10)**. The R group (hydroxyl) of this residue, barely deprotonates, and its pK_a is above 14. Thr through its aliphatic hydroxyl, when placed in the inner structure of a protein, for instance in the middle of an α-helix, is able to perform hydrogen bonding with neighbor residues. This property confers more flexibility to the Thr-containing-structure. A Thr in the middle of an α-helix may act as a hinge, kinking the helix, thus becoming a good residue to favor conformational changes. The hydroxyl group of Thr interacts, in an α-helix, with the i-4 residue, increasing the degree of kinking of a helix. In the case of BR, there are several Thr along its sequence. The most interesting cases are Thr46, Thr47 and Thr89, Thr90. Both sets of neighbor Threonines, are quite near of a Pro, Pro50 in the case of Thr46-47 and Pro91 in the case of Thr89-90.

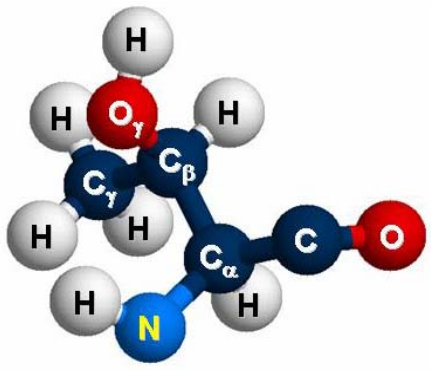

Fig. I.10. Molecular plot of Threonine.

-Proline (Pro): This is perhaps one of the most singular and interesting residues among all. The average features of an amino acid are not present in Pro **(Fig. I.11)**. The side chain consists of a saturated 5 member ring (pyrrolidine

ring). It is the only amino acid, with its side chain going back to form a covalent linkage to the peptidic nitrogen. This yields some special characteristics. First of all, proline has not the ability of acting as a hydrogen bond donor due to lose of the hydrogen of the peptidic nitrogen. Secondly, the *cis* conformation of the X-Pro peptide bond is accessible due to the steric destabilization of the *trans* conformation **[56]** . This lability introduced by Pro, due to the inability for performing conventional hydrogen bonds, besides the easiness for changing between *cis-trans* conformation, has made of Pro, when present in an α-helix, a helix-breaker residue. Nevertheless, despite being unable of perform hydrogen bond through its peptidyl N, Pro is frequently found in the middle of α-helices, where this residue can help the helix to adopt the optimal disposition to establish helix-helix interactions **[57, 58]**. Although Pro leads to the kinking of the α-helix, this residue is able to stabilize the structure through the establishment of a non-conventional hydrogen bond with its C_δ, which in addition controls the puckering of the pyrrolidine ring. C_δ is able to interact with the 3rd (i-3) and/or the 4th (i-4), or even with the 5th previous residues (bond type 3, 4, 4/3, 5/4/3 …). This alternative hydrogen bonding is derived from the fact that $C\gamma$ of Pro in an α-helix introduces a clash **(Fig. I.12)** with the peptydil O of the i-4 residue that prevents the bending of the helix in this direction **[59]**.

There are several Pro in BR, such as Pro8, Pro50, Pro77, Pro91, Pro 186, Pro200…But the most important ones, due to its supposed functional and structural relevance are beyond any doubt, Pro50, Pro91 and Pro186.

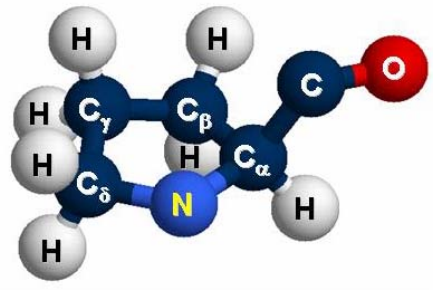

Fig. I.11. Molecular plot of Proline.

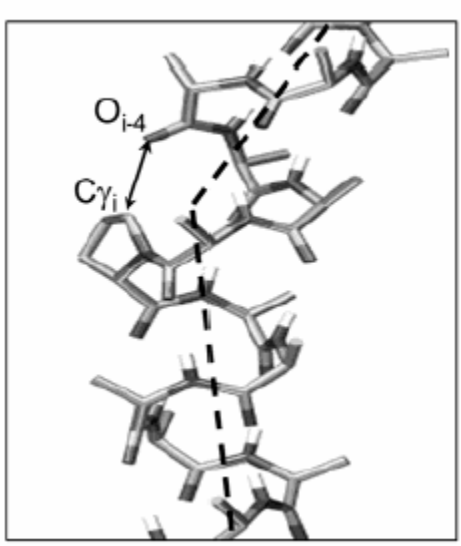

Fig I.12. Diagram of a proline residue in a helix, highlighting how the loss of an *i* ← (*i* - 4) H-bond and the distortion (steric clash) induced by the close contact of the Cγ atom of the proline ring at position *i* with the carbonyl O atom of residue *i* - 4 leads to a change in direction of the helix axes (broken lines) before and after the proline **[**59**]**.

-Relationship between Thr and Pro:

Computational studies on transmembrane proteins containing Pro, argue that the presence of Ser and Thr near Pro-kinked helices are able to modulate the degree of the kink **[60]**. Concisely, the motif Thr-Pro seems to enhance the degree of kinking of an α-helix, whereas a Thr/Ser-X-X-Pro motif could decrease the bending of the helix. In bacteriorhodopsin, some motifs of this kind are present, for instance, Thr89-Thr90-Pro91, Thr46-Thr47-X-X-Pro50 and Ser183-X-X-Pro186. The motif Thr90-Pro91 seems to enhance the distortion on the helix. Pro is supposed to kink the helix, and Thr90 seems to help increasing the kink through the interaction of its hydroxyl group with Trp86.

I.7. Focusing on Thr90 and Pro91 in BR

Several questions arise when Helix C is observed. From a functional point of view, as previously commented, the residues involved directly in proton transport are present in this helix. Is it important to maintain a correct position of these residues? Must they be located precisely around the SB all along the photocycle? Does this helix need to change the conformation to distinguish between the extracellular and the cytoplasmic events during the photocycle? As

a first approach, all these questions that should be answered with a strong "yes" seem to respond to a structural point of view. Taking into account the protein we are studying, maybe a dynamic assumption should be done, more than a structural one. Does the kink of helix C suppose any kind of distortion directed to answer all these questions?

Thr90 and Pro91 **(Fig. I.13)** directly and through their interactions, kink the helix C at the level of retinal.

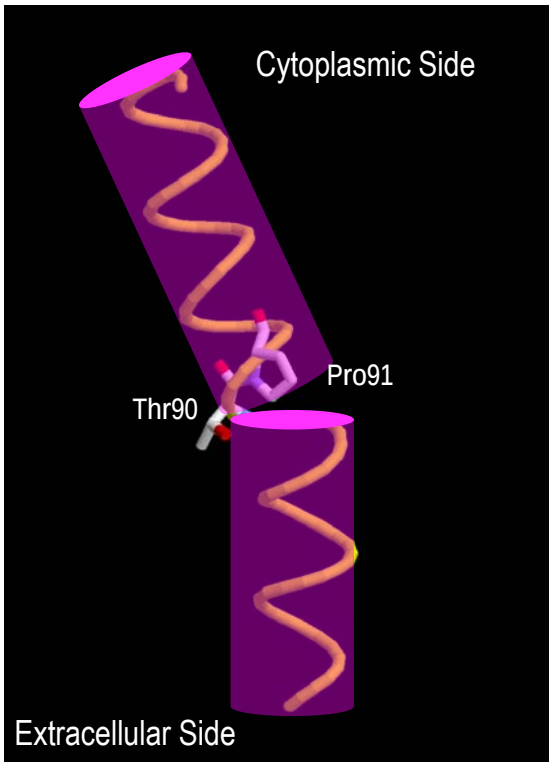

Fig. I.13. Helix C of BR kinked at the level of Thr90 and Pro91. Cylinders are overlapped to the helix to show the degree of bending.

Thr90 is a residue which potentially establishes several interactions **(Fig. I.14)**:

- Thr90 – Trp86: As a backbone hydrogen bond (typical i-4 of an α-helix), between the O of Thr90 and the N of Trp86.
- Thr90 – Trp86: Hydrogen bond involving O_γ of Thr90 and O of Trp86.
- Thr90 – Asp115: Hydrogen bond formed by the O_γ of Thr90 and the O_δ of Asp115.
- Thr90 – Retinal: Van der Wals contact between C_γ of Thr90 and the region of C_{11},C_{12},C_{13} and C_{20} of retinal.

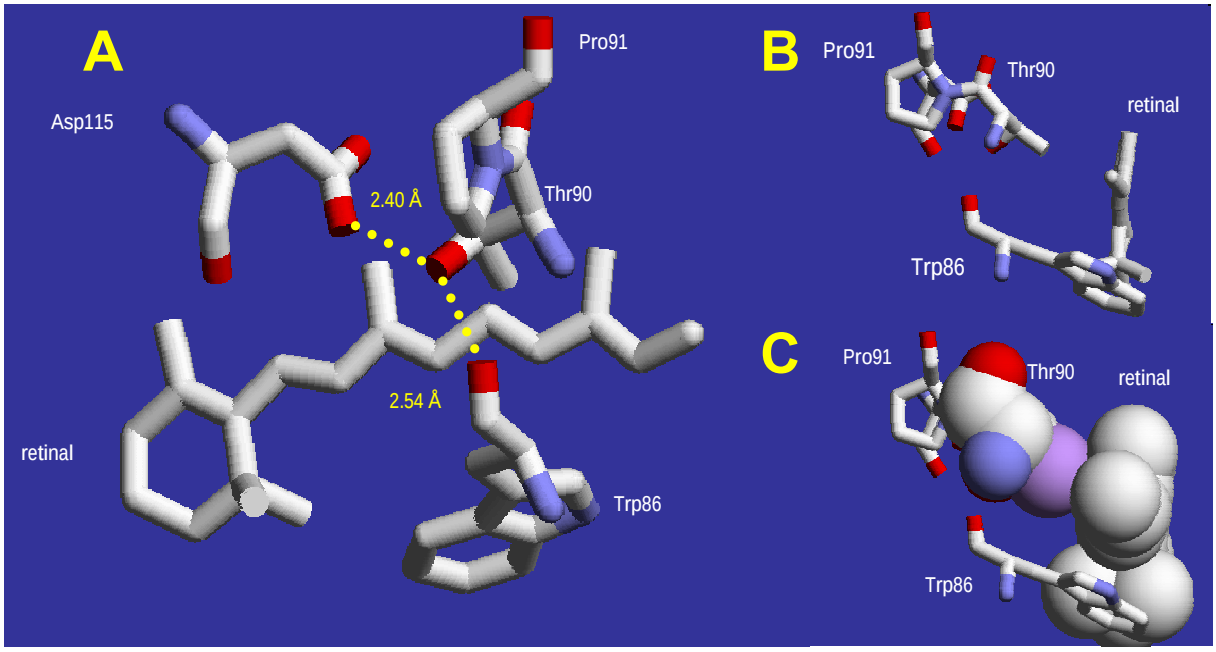

Fig.I.14. A. Hydrogen bonds formed by the –OH group of the Thr90 in BR. As indicated by the distances, these bonds are quite strong. B. Side view to display the $-CH_3$ group of Thr90 and its orientation towards retinal. C. Van der Wals spheres are plotted to notice the contact between Thr90 and the retinal. The atomic coordinates comes from the 1c3w pdb code.

Pro91 interacts through a non-conventional hydrogen bond with the Leu87 (i-4 residue) **(Fig. I.15)**. It is a type 4 interaction **[61]** (though it can also be considered a type 5/4/3). The distances of Pro91 to Phe88 (i-3) and Trp86 (i-5) are above 3.2 Å, nevertheless these interactions should not be discarded.

As a measure of the relevance of one residue among different proteins, sequence conservation studies have been performed. In order to relate BR to other transmembrane proteins such as fungal rhodopsins, GPCRs, bacterial, cyanobacteria, green alga and archaeal rhodopsins, sequence alignments **(Fig. I.16) [62-65]** and prediction studies **[66, 67]** have been carried out. In summary, alignments show a fully conserved position of Pro91 in all rhodopsins but in GPCRs. GPCRs, are hypothesized to originate from the duplication of helices occurred as the evolution of an ancestral gene. Nevertheless, according to Metzger et al. **(Fig. I.17)**, Pro91 is fully represented in GPCRs in Helix 5 (corresponding to Helix C in type 1 (archaeal) rhodopsins). In the case of Thr90, the conservation only appears among archaeal rhodopsins, indicating a limited relevance compared to Pro91.

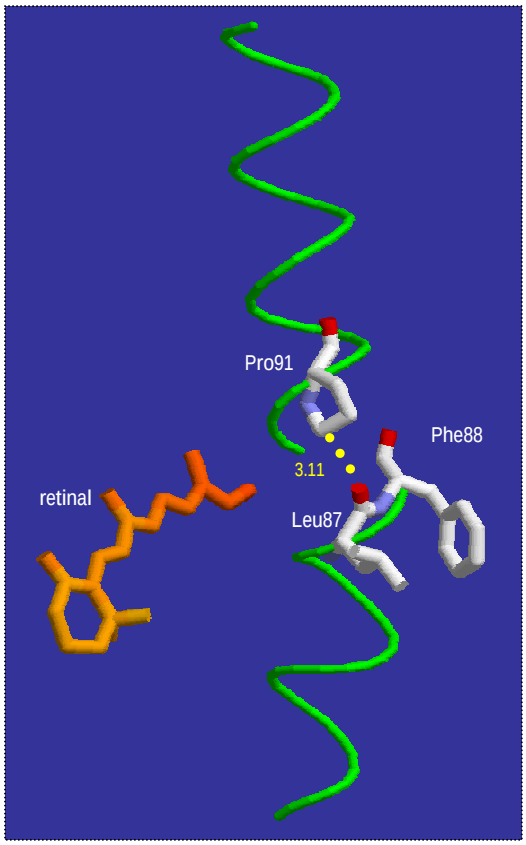

Fig.I.15. Interactions established by Pro91 in helix C. Distance from Cδ of Pro91 to Leu87 (i-4) is displayed indicating the presence of a hydrogen bond. The bond between Pro91 with Phe88 and/or Trp86 is not easily established (distance between atoms above 3.2 Å). Atomic coordinates from the 1py6 structure of the PDB.

Considering the residues interacting with Pro91, and Thr90, only Trp86 seems to be fully conserved in all rhodopsin-like (fungal, archaeal, bacterial, alga and cyanobacteria) proteins but not in GPCRs. Asp115 is almost fully conserved only within archaeal rhodopsins.The aim to focus on Thr90-Pro91 attempts to solve whether a structural static or a functional dynamic role could be assigned to this motif, even if a mixture of structure and function should be inferred, assigning to this set of residues a dynamic role.

In order to determine how Thr90 exerts a modulation over Pro91 and over Helix C single mutation of Thr90 to Alanine and Valine, and the mutation of Asp115 to Alanine have been carried out. The expected behavior of these mutations is displayed in **Fig. I.18**. Moreover, Pro91 is studied by its mutation to Ala, a substitution supposed to restore the environment for an average α-helix.

In summary, the intention is to drive an exhaustive study on the Thr90-Pro91 motif in Helix C, first of all to answer the dynamic role question in BR and

secondly to set up the basis for other transmembrane proteins with similar features.

I.8. Role of helix-embedded prolines in BR: an example for transmembrane proteins.

The study of the role of Pro91 in BR is not understandable without comparing it with the other embedded prolines present in BR. Examples of these motifs are Pro50 in Helix B and Pro186 in Helix F. The study of these prolines have been performed earlier in a heterologous system as *E.coli* is **[68, 69]**. Some differences were reported compared to wt, mostly for Pro186 mutants, despite that this system is not an optimum one **[5]**. Moreover, the conservation degree observed by prediction studies **[67]** argues for a more relevant role than the one restricted for BR. Conservation among not only archaeal rhodopsins (see **Fig. I.16**) but also in GPCRs (see **Fig. I.17**) gives the idea that BR is a perfect model to provide information about the function of these so conserved residues. If there is no assigned function for these resiudes, why are they so conserved? And, if there is any function, this can be derived to other transmembrane proteins? So, in addition of the P91A mutant, the mutants P50A and P186A were designed in order to throw some light on these questions.

In the case of the mutations of Pro50, Pro91 and Pro186, there is no need to make predictions on the structure, because the crystal structures of P50A, P91A and P186A have been recently published **[54, 55]**. These structures provide the means to determine the effect of the mutated residue on the resting BR structure. A comparison of the structures of the mutants versus WT is performed in order to assume what structural changes produce the mutations **(Fig. I.19)**. In fact, the authors of the crystals based on the 3D structures conclude that no relevant structural changes should be inferred. Nevertheless, when these publications appeared, the mutants were constructed and expressed, and almost all the studies were done, so these structures despite yielding some controversy, complement the biophysical studies performed.

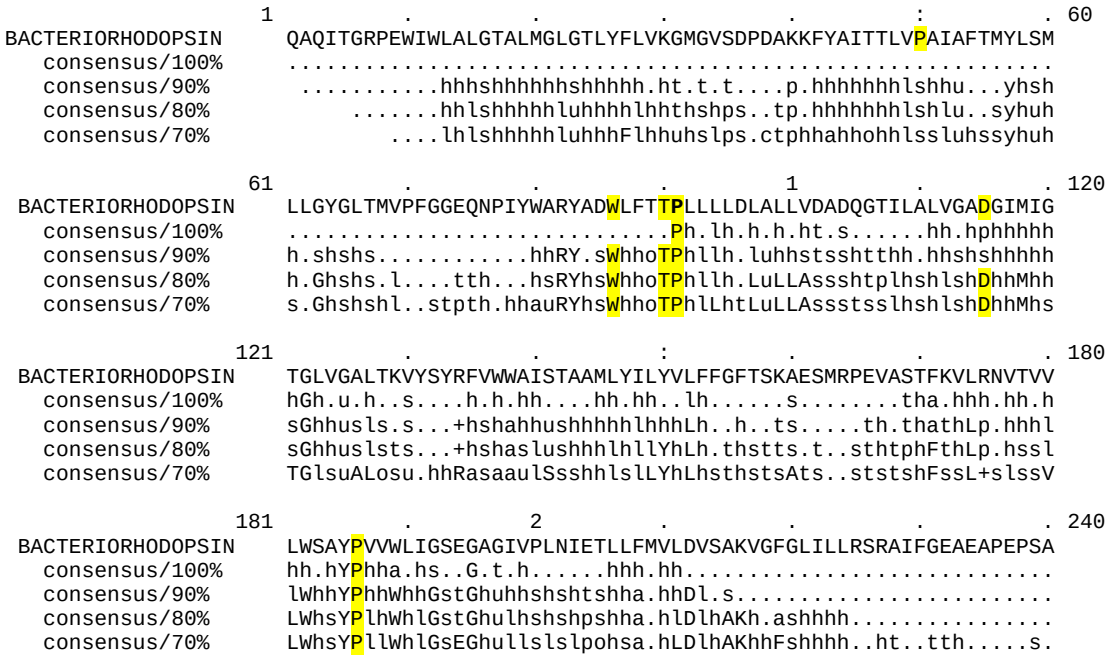

Fig. I.16. Comparison of the bacteriorhodopsin sequence to those of 28 archaerhodopsins having a coincidence of at least 25%, as shown by the multiple sequence alignment program MaxHom [70]. Amino acid sequence 1-240 is shown. The side chains with a 100% consensus are indicated in bold. Symbols: o, alcohol; l, aliphatic; a, aromatic; c, charged; h, hydrophobic; -, negative; p, polar; +, positive; s, small; u, tiny; t, turnlike [71]. Residues of interest in this work are yellow marked.

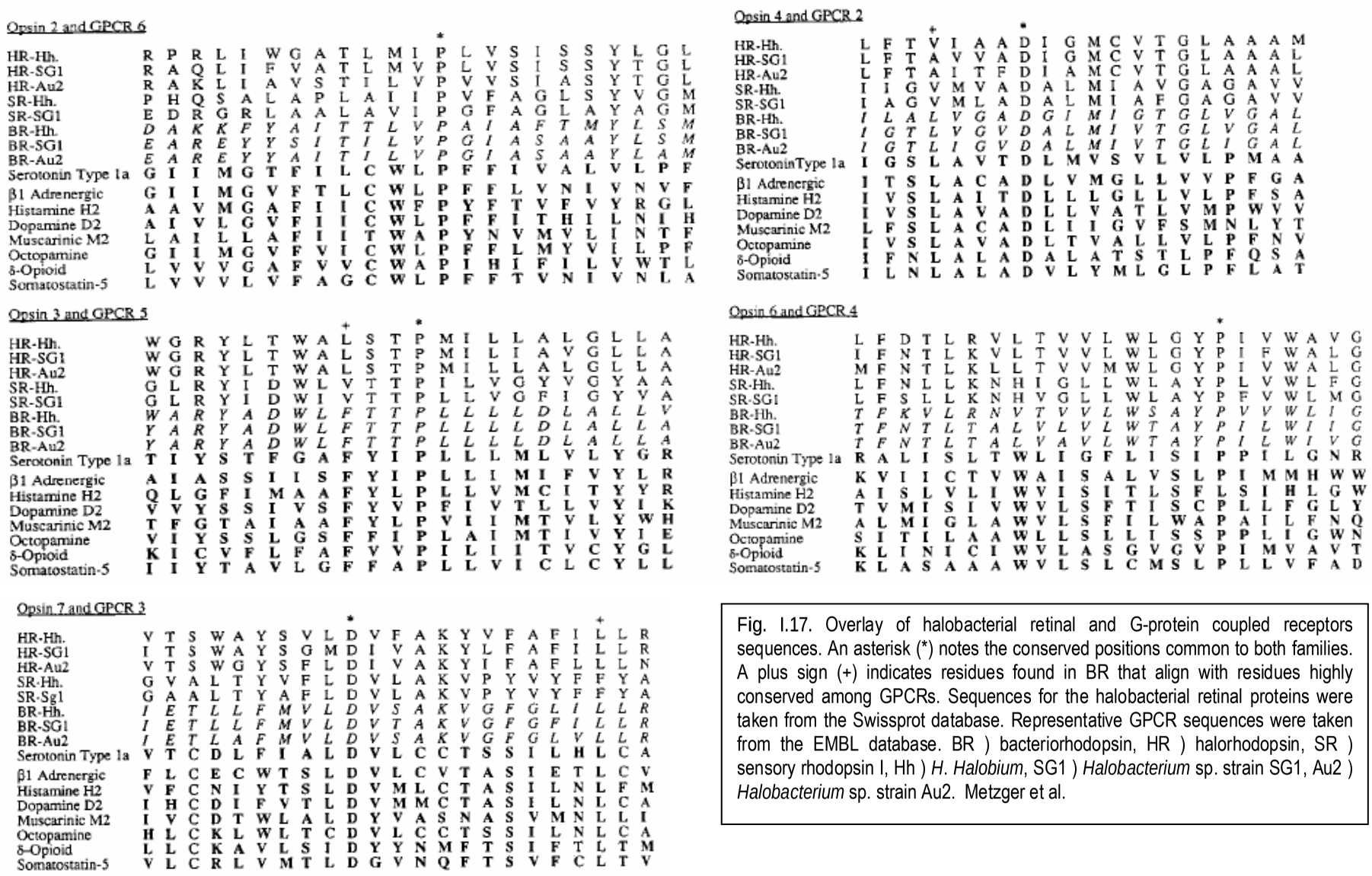

Fig. I.17. Overlay of halobacterial retinal and G-protein coupled receptors sequences. An asterisk (*) notes the conserved positions common to both families. A plus sign (+) indicates residues found in BR that align with residues highly conserved among GPCRs. Sequences for the halobacterial retinal proteins were taken from the Swissprot database. Representative GPCR sequences were taken from the EMBL database. BR) bacteriorhodopsin, HR) halorhodopsin, SR) sensory rhodopsin I, Hh) *H. Halobium*, SG1) *Halobacterium* sp. strain SG1, Au2) *Halobacterium* sp. strain Au2. Metzger et al.

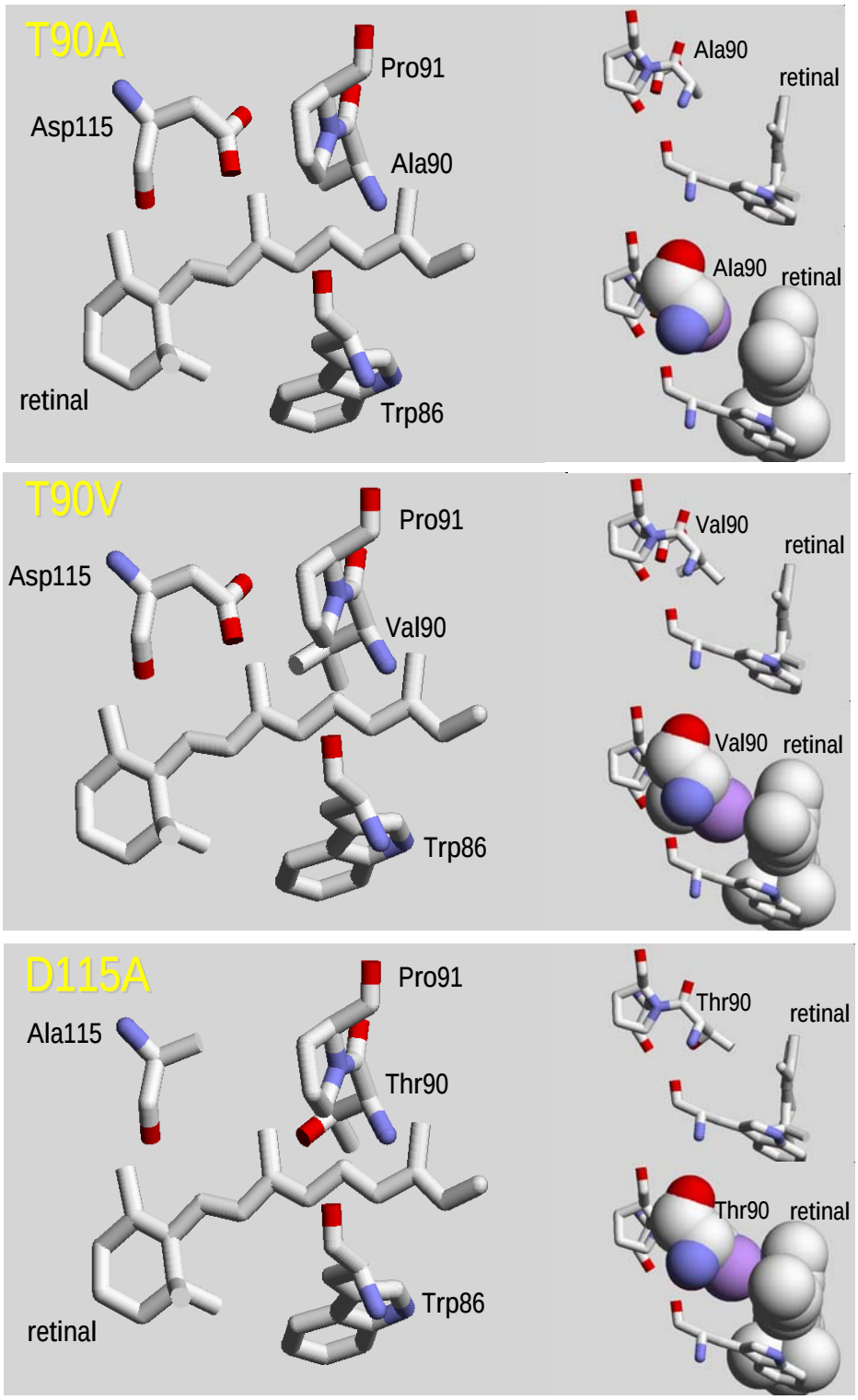

Fig.I.18. Plot of the projected mutants to study the function of Thr90. T90A mutant in comparison to WT (Fig. I.12.) loses all the interactions. Ala90 is not able to interact through hydrogen bonding nor with Asp115 nor with Trp86. The Van der Wals contact is not possible as well. T90V as T90A loses the hydrogen bond with Asp115 and Trp86, nevertheless, the side chain of Valine is supposed to emulate the steric contact with retinal. D115A mutant cannot form hydrogen bond between Thr90 and Asp115. The contact between retinal and Thr90 remains unaltered.

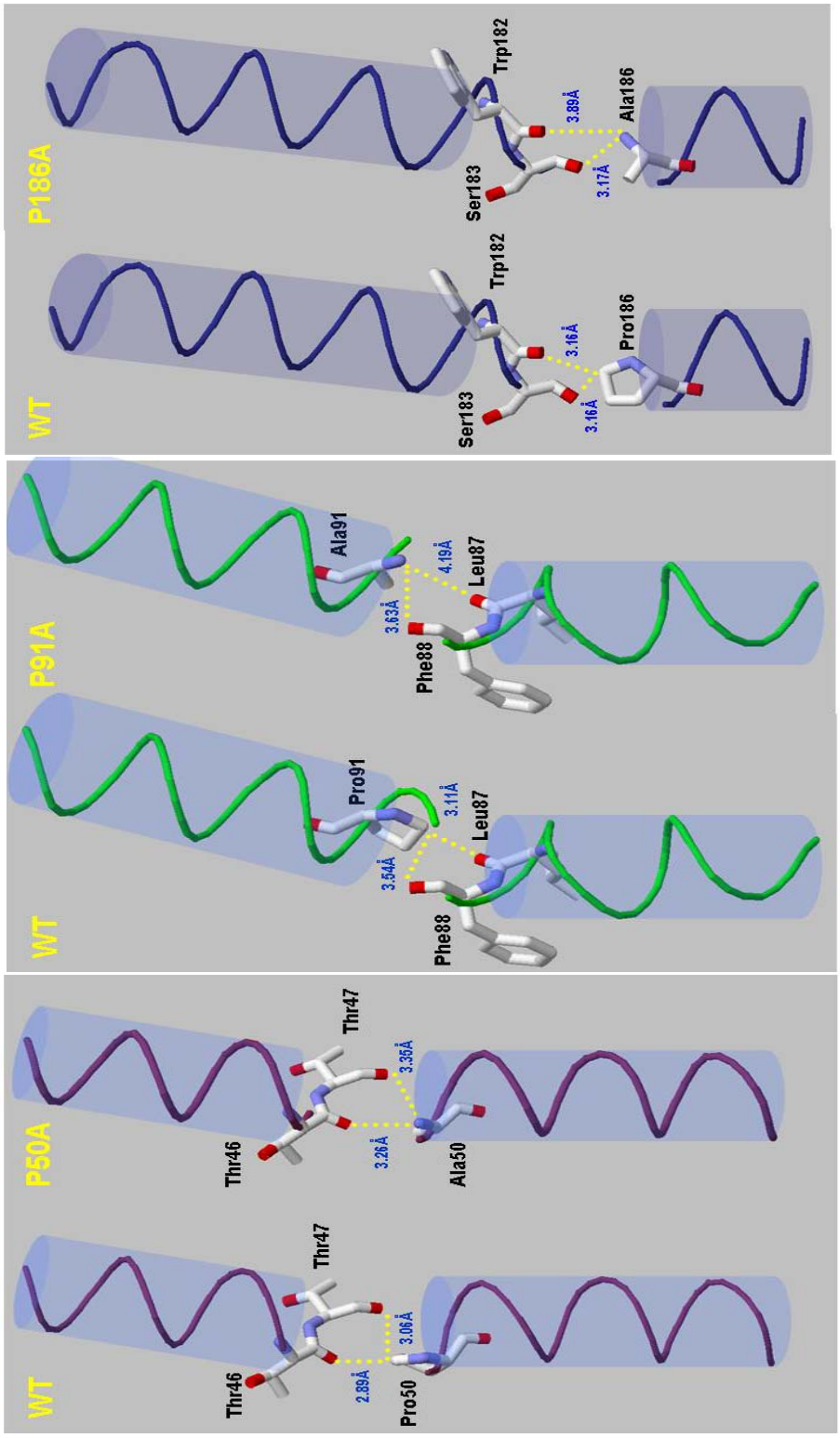

Fig. I.19. Comparison of the structures of WT (PDB code 1PY6) versus transmembranal Prolines mutants. Doted yellow lines are plotted just to display distances, not as an evidence of an hydrogen bond. The maximal distance considered for the existence of a hydrogen bond is 3.2Å, although Chakrabarti et al. showed C-H···O bonds of about 3.7 Å . The residues represented correspond to the i-3 and i-4 amino acids before Pro (i). In the case of WT, the distance considered reflects the space between the Cδ of the Pro versus the peptydil Oxygen of the i-3 and the i-4 residue. In the case of the mutant structures, the distance represented is the one between the peptydil Nitrogen of the Ala respect the peptydil Oxygen of the i-3 and the i-4 residue. The PDB code for the mutants P50A, P91A and P186A are 1PXR, 1Q5J and 1Q5I respectively.

I.9. References

1. Oesterhelt, D. and B. Hess, Reversible photolysis of the purple complex in the purple membrane of Halobacterium halobium. Eur J Biochem, 1973. **37**: p. 316-326.
2. Oesterhelt, D. and W. Stoeckenius, Rhodopsin-like protein from the purple membrane of Halobacterium halobium. Nat New Biol, 1971. **233**(39): p. 149-52.
3. Pebay-Peyroula, E., et al., X-ray structure of bacteriorhodopsin at 2.5 angstroms from microcrystals grown in lipidic cubic phases. Science, 1997. **277**(5332): p. 1676-81.
4. Nassal, M., et al., Structure-function studies on bacteriorhodopsin. III. Total synthesis of a gene for bacterio-opsin and its expression in Escherichia coli. J Biol Chem, 1987. **262**(19): p. 9264-70.
5. Needleman, R., et al., Properties of Asp212----Asn bacteriorhodopsin suggest that Asp212 and Asp85 both participate in a counterion and proton acceptor complex near the Schiff base. J Biol Chem, 1991. **266**(18): p. 11478-84.
6. Henderson, R., The structure of the purple membrane from Halobacterium hallobium: analysis of the X-ray diffraction pattern. J Mol Biol, 1975. **93**(2): p. 123-38.
7. Ovchinnikov, Y.A., et al., The structural basis of the functioning of bacteriorhodopsin: an overview. FEBS Lett, 1979. **100**(2): p. 219-24.
8. Dunn, R., et al., The bacteriorhodopsin gene. Proc Natl Acad Sci U S A, 1981. **78**(11): p. 6744-8.
9. Blaurock, A.E. and W. Stoeckenius, Structure of the purple membrane. Nat New Biol, 1971. **233**(39): p. 152-5.
10. Scherrer, P., et al., Retinal isomer ratio in dark-adapted purple membrane and bacteriorhodopsin monomers. Biochemistry, 1989. **28**(2): p. 829-34.
11. Hatanaka, M., et al., Trp86 --> Phe replacement in bacteriorhodopsin affects a water molecule near Asp85 and light adaptation. Biochemistry, 1997. **36**(18): p. 5493-8.
12. Maeda, A., et al., Water molecule rearrangements around Leu93 and Trp182 in the formation of the L intermediate in bacteriorhodopsin's photocycle. Biochemistry, 2003. **42**(9): p. 2535-41.
13. Weidlich, O., et al., Steric interaction between the 9-methyl group of the retinal and tryptophan 182 controls 13-cis to all-trans reisomerization and proton uptake in the bacteriorhodopsin photocycle. Biochemistry, 1996. **35**(33): p. 10807-14.
14. Hashimoto, S., et al., Ultraviolet resonance Raman spectra of Trp-182 and Trp-189 in bacteriorhodopsin: novel information on the structure of Trp-182 and its steric interaction with retinal. Biochemistry, 1997. **36**(39): p. 11583-90.
15. Hashimoto, S., et al., Changes in hydrogen bonding and environment of tryptophan residues on helix F of bacteriorhodopsin during the photocycle: a time-resolved ultraviolet resonance Raman study. Biochemistry, 2002. **41**(20): p. 6495-503.

16. Petkova, A.T., et al., Tryptophan interactions in bacteriorhodopsin: a heteronuclear solid-state NMR study. Biochemistry, 2002. **41**(7): p. 2429-37.
17. Hirai, T. and S. Subramaniam, Structural insights into the mechanism of proton pumping by bacteriorhodopsin. FEBS Lett, 2003. **545**(1): p. 2-8.
18. Grigorieff, N., et al., Electron-crystallographic refinement of the structure of bacteriorhodopsin. J Mol Biol, 1996. **259**(3): p. 393-421.
19. Luecke, H., H.T. Richter, and J.K. Lanyi, Proton transfer pathways in bacteriorhodopsin at 2.3 angstrom resolution. Science, 1998. **280**(5371): p. 1934-7.
20. Kimura, Y., et al., Surface of bacteriorhodopsin revealed by high-resolution electron crystallography. Nature, 1997. **389**(6647): p. 206-11.
21. Mitsuoka, K., et al., The structure of bacteriorhodopsin at 3.0 A resolution based on electron crystallography: implication of the charge distribution. J Mol Biol, 1999. **286**(3): p. 861-82.
22. Edman, K., et al., High-resolution X-ray structure of an early intermediate in the bacteriorhodopsin photocycle. Nature, 1999. **401**(6755): p. 822-6.
23. Facciotti, M.T., et al., Structure of an early intermediate in the M-state phase of the bacteriorhodopsin photocycle. Biophys J, 2001. **81**(6): p. 3442-55.
24. Facciotti, M.T., et al., Crystal structure of the bromide-bound D85S mutant of bacteriorhodopsin: principles of ion pumping. Biophys J, 2003. **85**(1): p. 451-8.
25. Facciotti, M.T., S. Rouhani, and R.M. Glaeser, Crystal structures of bR(D85S) favor a model of bacteriorhodopsin as a hydroxyl-ion pump. FEBS Lett, 2004. **564**(3): p. 301-6.
26. Edman, K., et al., Deformation of helix C in the low temperature L-intermediate of bacteriorhodopsin. J Biol Chem, 2004. **279**(3): p. 2147-58.
27. Kamikubo, H., et al., Structure of the N intermediate of bacteriorhodopsin revealed by x-ray diffraction. Proc Natl Acad Sci U S A, 1996. **93**(4): p. 1386-90.
28. Lanyi, J.K., X-ray crystallography of bacteriorhodopsin and its photointermediates: insights into the mechanism of proton transport. Biochemistry (Mosc), 2001. **66**(11): p. 1192-6.
29. Lanyi, J.K. and B. Schobert, Mechanism of proton transport in bacteriorhodopsin from crystallographic structures of the K, L, M1, M2, and M2' intermediates of the photocycle. J Mol Biol, 2003. **328**(2): p. 439-50.
30. Lanyi, J.K., X-ray diffraction of bacteriorhodopsin photocycle intermediates. Mol Membr Biol, 2004. **21**(3): p. 143-50.
31. Faham, S. and J.U. Bowie, Bicelle crystallization: a new method for crystallizing membrane proteins yields a monomeric bacteriorhodopsin structure. J Mol Biol, 2002. **316**(1): p. 1-6.
32. Takeda, K., et al., A novel three-dimensional crystal of bacteriorhodopsin obtained by successive fusion of the vesicular assemblies. J Mol Biol, 1998. **283**(2): p. 463-74.
33. Gouaux, E., It's not just a phase: crystallization and X-ray structure determination of bacteriorhodopsin in lipidic cubic phases. Structure, 1998. **6**(1): p. 5-10.

34. Rummel, G., et al., Lipidic Cubic Phases: New Matrices for the Three-Dimensional Crystallization of Membrane Proteins. J Struct Biol, 1998. **121**(2): p. 82-91.
35. Lanyi, J.K., What is the real crystallographic structure of the L photointermediate of bacteriorhodopsin? Biochim Biophys Acta, 2004. **1658**(1-2): p. 14-22.
36. Haupts, U., J. Tittor, and D. Oesterhelt, Closing in on bacteriorhodopsin: progress in understanding the molecule. Annu Rev Biophys Biomol Struct, 1999. **28**: p. 367-99.
37. Siebert, F. and W. Mantele, Investigation of the primary photochemistry of bacteriorhodopsin by low-temperature Fourier-transform infrared spectroscopy. Eur J Biochem, 1983. **130**(3): p. 565-73.
38. Earnest, T.N., et al., Orientation of the bacteriorhodopsin chromophore probed by polarized Fourier transform infrared difference spectroscopy. Biochemistry, 1986. **25**(24): p. 7793-8.
39. Atkinson, G.H., L. Ujj, and Y.D. Zhou, Vibrational spectrum of the J-625 intermediate in the room temperature bacteriorhodopsin photocycle. Journal of Physical Chemistry A, 2000. **104**(18): p. 4130-4139.
40. Atkinson, G.H., et al., Picosecond time-resolved fluorescence spectroscopy of K-590 in the bacteriorhodopsin photocycle. Biophys J, 1989. **55**(2): p. 263-74.
41. Maeda, A., et al., Tryptophan perturbation in the L intermediate of bacteriorhodopsin: fourier transform infrared analysis with indole-15N shift. Biochemistry, 1992. **31**(50): p. 12543-5.
42. Rothschild, K.J. and N.A. Clark, Polarized infrared spectroscopy of oriented purple membrane. Biophys J, 1979. **25**(3): p. 473-87.
43. Braiman, M.S., P.L. Ahl, and K.J. Rothschild, Millisecond Fourier-transform infrared difference spectra of bacteriorhodopsin's M412 photoproduct. Proc Natl Acad Sci U S A, 1987. **84**(15): p. 5221-5.
44. Braiman, M.S., O. Bousche, and K.J. Rothschild, Protein dynamics in the bacteriorhodopsin photocycle: submillisecond Fourier transform infrared spectra of the L, M, and N photointermediates. Proc Natl Acad Sci U S A, 1991. **88**(6): p. 2388-92.
45. Subramaniam, S., et al., Protein conformational changes in the bacteriorhodopsin photocycle. J Mol Biol, 1999. **287**(1): p. 145-61.
46. Luecke, H., et al., Structure of bacteriorhodopsin at 1.55 A resolution. J Mol Biol, 1999. **291**(4): p. 899-911.
47. Brown, L.S., R. Needleman, and J.K. Lanyi, Functional roles of aspartic acid residues at the cytoplasmic surface of bacteriorhodopsin. Biochemistry, 1999. **38**(21): p. 6855-61.
48. Zscherp, C., et al., In situ determination of transient pKa changes of internal amino acids of bacteriorhodopsin by using time-resolved attenuated total reflection Fourier-transform infrared spectroscopy. Proc Natl Acad Sci U S A, 1999. **96**(10): p. 5498-503.
49. Kouyama, T., et al., Crystal structure of the L intermediate of bacteriorhodopsin: evidence for vertical translocation of a water molecule during the proton pumping cycle. J Mol Biol, 2004. **335**(2): p. 531-46.
50. Metz, G., F. Siebert, and M. Engelhard, Asp85 is the only internal aspartic acid that gets protonated in the M intermediate and the purple-

to-blue transition of bacteriorhodopsin. A solid-state 13C CP-MAS NMR investigation. FEBS Lett, 1992. **303**(2-3): p. 237-41.
51. Mowery, P.C., et al., Effect of acid pH on the absorption spectra and photoreactions of bacteriorhodopsin. Biochemistry, 1979. **18**(19): p. 4100-7.
52. Tuzi, S., et al., Location of a cation-binding site in the loop between helices F and G of bacteriorhodopsin as studied by 13C NMR. Biophys J, 1999. **76**(3): p. 1523-31.
53. Schulz, G.E. and R.H. Schirmer, Principles of protein structure. Springer advanced texts in chemistry. 1979, New York: Springer-Verlag. x, 314.
54. Faham, S., et al., Side-chain contributions to membrane protein structure and stability. J Mol Biol, 2004. **335**(1): p. 297-305.
55. Yohannan, S., et al., The evolution of transmembrane helix kinks and the structural diversity of G protein-coupled receptors. Proc Natl Acad Sci U S A, 2004. **101**(4): p. 959-63.
56. Lansing, J.C., et al., Solid-state NMR investigation of the buried X-proline peptide bonds of bacteriorhodopsin. Biochemistry, 2003. **42**(12): p. 3586-93.
57. Adamian, L. and J. Liang, Helix-helix packing and interfacial pairwise interactions of residues in membrane proteins. J Mol Biol, 2001. **311**(4): p. 891-907.
58. Orzáez, M., et al., Influence of proline residues in transmembrane helix packing. J Mol Biol, 2004. **335**(2): p. 631-40.
59. Bright, J.N. and M.S.P. Sansom, The flexing/twirling helix: Exploring the flexibility about molecular hinges formed by proline and glycine motifs in transmembrane helices. Journal of Physical Chemistry B, 2003. **107**(2): p. 627-636.
60. Deupi, X., et al., Ser and Thr residues modulate the conformation of pro-kinked transmembrane alpha-helices. Biophys J, 2004. **86**(1 Pt 1): p. 105-15.
61. Chakrabarti, P. and S. Chakrabarti, C--H.O hydrogen bond involving proline residues in alpha-helices. J Mol Biol, 1998. **284**(4): p. 867-73.
62. Ruiz-Gonzalez, M.X. and I. Marin, New insights into the evolutionary history of type 1 rhodopsins. J Mol Evol, 2004. **58**(3): p. 348-58.
63. Zhai, Y., et al., Homologues of archaeal rhodopsins in plants, animals and fungi: structural and functional predications for a putative fungal chaperone protein. Biochim Biophys Acta, 2001. **1511**(2): p. 206-23.
64. Bieszke, J.A., et al., A eukaryotic protein, NOP-1, binds retinal to form an archaeal rhodopsin-like photochemically reactive pigment. Biochemistry, 1999. **38**(43): p. 14138-45.
65. Ihara, K., et al., Evolution of the archaeal rhodopsins: evolution rate changes by gene duplication and functional differentiation. J Mol Biol, 1999. **285**(1): p. 163-74.
66. Taylor, E.W. and A. Agarwal, Sequence homology between bacteriorhodopsin and G-protein coupled receptors: exon shuffling or evolution by duplication? FEBS Lett, 1993. **325**(3): p. 161-6.
67. Metzger, T.G., et al., An analysis of the conserved residues between halobacterial retinal proteins and G-protein coupled receptors: implications for GPCR modeling. J Chem Inf Comput Sci, 1996. **36**(4): p. 857-61.

68. Mogi, T., et al., Structure-function studies on bacteriorhodopsin. VIII. Substitutions of the membrane-embedded prolines 50, 91, and 186: the effects are determined by the substituting amino acids. J Biol Chem, 1989. **264**(24): p. 14192-6.
69. Zhang, Y.N., et al., Effects of mutagenetic substitution of prolines on the rate of deprotonation and reprotonation of the Schiff base during the photocycle of bacteriorhodopsin. Photochem Photobiol, 1993. **57**(6): p. 1027-31.
70. Sander, C. and R. Schneider, Database of homology-derived protein structures and the structural meaning of sequence alignment. Proteins, 1991. **9**(1): p. 56-68.
71. Padros, E., A. Peralvarez, and M. Marquez, Bacteriorhodopsin, a light-driven proton pump. Recent Res. Devel. Biophys., 2003. **2**: p. 157-172.

You can't avoid her, She's in the air
In between molecules
Of Oxygen and Carbon Dioxide.

Weezer

CHAPTER II.

OBJECTIVES

II. OBJECTIVES

The main objective of this work is the analysis of the structural and functional role of some amino acids in Bacteriorhodopsin.

- Characterization of the motif Thr90-Pro91 in the centre of Helix C of Bacteriorhodopsin. Because Thr90 interacts with Asp115 through a hydrogen bond and with the retinal through hydrophobic interaction, the mutants T90V and D115A were taken into account. The following objectives were settled:

  ⇒ Design and construct the Bacteriorhodopsin mutants P91A, T90A, T90V and D115A by site directed mutagenesis.
  ⇒ Express the mutants in the purple membrane of *Halobacterium salinarum.*
  ⇒ Analyze the role of Thr90 and Pro91 in the properties of the protein and in the proton pumping function in particular through the study of the mutants.
  ⇒ Infer a role to the motif Thr90-Pro91 in Bacteriorhodopsin.

- Analyze the role of the other two Prolines located in transmembrane helices in BR, and to extend this role to other Transmembrane Proteins. The subsequent objectives were proposed:

  ⇒ Design and construct the Bacteriorhodopsin mutants P50A and P186A by site directed mutagenesis.
  ⇒ Express the mutants in the purple membrane of *Halobacterium salinarum*.
  ⇒ Characterize the role of Pro50, and Pro186 in Bacteriorhodopsin properties and proton pumping through the analysis of the mutants.
  ⇒ Infer a role to Helix-embedded prolines of Bacteriorhodopsin in particular and to transmembrane helices of proteins in general.

Oh oh people of the earth
Listen to the warning the seer he said
Beware the storm that gathers here
Listen to the wise man.

Queen

CHAPTER III.

THR90 IS A KEY RESIDUE OF THE BACTERIORHODOPSIN PROTON PUMPING MECHANISM

Abstract

Mutation of Thr90 to Ala has a profound effect on bacteriorhodopsin properties. T90A shows about 20% of the proton pumping efficiency of wild type, once reconstituted into liposomes. Mutation of Thr90 influences greatly the Schiff base-Asp85 environment, as demonstrated by altered λmax of 555 nm and pKa of Asp85 (about 1.3 pH units higher than wild type). Hydroxylamine accessibility is increased in both dark and light and differential scanning calorimetry and visible spectrophotometry show decreased thermal stability. These results suggest that Thr90 has an important structural role in both the unphotolysed bacteriorhodopsin and in the proton pumping mechanism.

III.1. Introduction

In the proton transport mechanism of bacteriorhodopsin (BR), two interrelated events have been recognized as fundamental: protonation/deprotonation reactions of some key amino acids and the Schiff base, and conformational changes **[1-3]**. The presence of conformational changes in BR during proton transport have been clearly described in the last years **[1-9]**, but the structural basis of these movements are not still clear. The conformational changes that originate from the retinal after photoisomerization may be the result of the consecutive retinal changes and/or protonation changes, or may evolve independently of the retinal after the first event. Three Pro residues located near the middle of the helices B (Pro50), C (Pro91) and F (Pro186) could function as hinges facilitating these movements **[10-14]**. Especially, movement of the cytoplasmic end of helix F representing a transient opening of the cytoplasmic side may be important for Asp96 reprotonation **[15-18]**. Movements of the cytoplasmic loops may also be important for proton transfer in the cytoplasmic side.

It has been described recently that Ser and Thr residues bend α helices by forming an additional hydrogen bond with the i-3 or i-4 peptide carbonyl oxygen **[19]**. This effect could become important for helix C that carries the sequence Thr89-Thr90-Pro91 and several key side chains of the proton transport mechanism (Arg82, Asp85, Asp96). The importance of Thr89 has been pointed out in several papers **[20-22]**, but Thr90 has so far received little attention. In addition to the possible induction of a bend in the helix, another interesting aspect of Thr90 is suggested by the recent three-dimensional structures of BR, which reveal the formation of an hydrogen bond between Thr90 (helix C) and Asp115 (helix D) **[23-25]**. Studies of model transmembrane helices **[26]** indicate that this may be a strong hydrogen bond. We describe in this work several properties of T90A that suggest an important structural role of Thr90 in the proton transport mechanism.

III.2. Material and methods

The T90A mutant was obtained as in the previously described procedure **[27]**. The membrane was grown and purified by the standard method **[28]**, and the mutation was confirmed from *Halobacterium salinarum* transformants by sequencing the *bop* gene from isolated DNA.

Deionised membranes were obtained after a 6-hour dialysis against Dowex 50W cation exchange resin. pH titrations were carried out by adding micro volumes of HCl or NaOH solutions to membrane suspensions ($1.5 \cdot 10^{-5}$ M BR). To avoid contamination, pH adjustment of deionised samples was done by using duplicates. Absorption spectra were taken using an integrative sphere device (to minimise the lose of signal caused by light scattering) placed in a Varian Cary 3 spectrophotometer. Absorbance changes at 615 nm as a function of pH were used to monitor the purple-to-blue transition. Experimental data were normalized to the largest value at 615 nm and fitted to the Henderson-Hasselbach equation.

DSC experiments were performed using a MicroCal MC2 instrument (MicroCal Inc, USA). Samples were dialysed previously against water adjusted to pH 7.0, giving a final protein concentration of 1.5-2 mg/ml. Experiments were done under a nitrogen pressure of 1.7 atm to avoid sample evaporation at high temperatures. Scanning speed was set at 1.5 ºK/min. Three consecutive thermograms were registered for each sample. The first informs about the heat released or taken by the protein upon temperature increase. After cooling down to room temperature, a second and a third thermograms were run to check the reversibility of the transitions. Two corrections were applied to the first thermogram: a) subtraction of the second thermogram, that acts as a blank and b) subtraction of the chemical baseline using the method of Takahashi and Sturtevant **[29]**. T_m was defined as the temperature where C_p value is maximal.

Analysis of thermal stability of dark-adapted T90A samples in H_2O ($0.75 \cdot 10^{-5}$ M) was carried out by recording absorption spectra in the UV-visible range during thermal ramps of 5 ºC steps, from 20 to 95 ºC in a Cary Bio3 spectrophotometer. Samples were allowed to stabilize for 8 min at each temperature.

Membrane suspensions ($1.5 \cdot 10^{-5}$ M BR) were reacted with 1M hydroxylamine in a medium containing 150 mM sodium phosphate (pH 7.0). Reactions under light were done using white light of 300 lux of luminance.

For liposome preparation, egg yolk phosphatidylcholine (EPC) was purified as described by Singleton et al. **[30]** and stored in chloroform solution at –20 ºC. Initial proteoliposome suspensions were obtained by adding the required amount of purple membrane suspension in 150 mM KCl, pH 7.0 to a dry film of EPC obtained by rotatory evaporation, and vortexing for 10 minutes. In all cases EPC concentration was 6 mg/mL and the lipid-to-BR ratio was 50:1 (w/w). Small proteoliposomes were obtained by high-pressure homogenisation **[31]** with a Microfluidizer 110S (Newton, USA).

Liposome size distribution was measured by dynamic light scattering using a Microtrac Ultrafine Particle Analyser 150 spectrometer (Montgomeryville, USA). Samples were diluted with their aqueous medium in order to obtain a satisfactory signal. Data acquisition time was 10 minutes.

All proton-pumping pH measurements were done in dim red light at 25 ºC. In order to avoid any pH gradient across the vesicle bilayers, the suspensions were kept in darkness for at least 30 min prior to pH measurements. After complete pH stabilisation, the sample was illuminated with yellow-filtered light of a luminance of about $8 \cdot 10^4$ lux on the sample. The initial rate of proton pumping was determined by a linear fit of the pH changes within the first ten seconds of illumination.

III.3. Results

The first evidence of the perturbed behaviour of T90A is the absorption maximum, 555 nm in the light-adapted state (see **Fig. III.1A**) as compared to 568 nm of wild type; this gives rise to a more reddish colour for the mutant. Upon acidification, T90A shows a purple-to-blue transition similar to wild type (see **Fig. III.1C**), although this mutant never reaches the λ_{max} of 603 nm in any condition analysed. In the case of deionised sample, a double-peaked absorption spectrum is obtained at acid pH (maximum at 500 nm and shoulder at 592 nm; see **Fig. III.1B**), indicative of two populations. At neutral pH, the spectrum presents a unique peak at 535 nm. Difference spectra of the sample at acid pH minus the sample at neutral pH show two positive bands at 620 and 445 nm, corresponding the blue and red forms **(Fig. III.1D)**. The λ_{max} of 535 nm at neutral pH contrasts with deionised wild type, which has a λ_{max} of 558 nm.

Table III.1 shows the apparent Asp85 pK_a values, obtained from the plots of absorbance differences at 615 nm. In all the conditions analysed, these values are higher than those of wild type, revealing that removal of the O-H group of Thr90 affects the Asp85 environment.

The hydroxylamine accessibility to the Schiff base in T90A mutant is increased as compared to wild type **(Fig. III.2)**. Under illumination, T90A has a $t_{1/2}$ of about 53 min as compared to 180 min for wild type. In the dark, T90A also shows enhanced accessibility ($t_{1/2}$ of about 4.5 h as compared to 160 h for wild type).

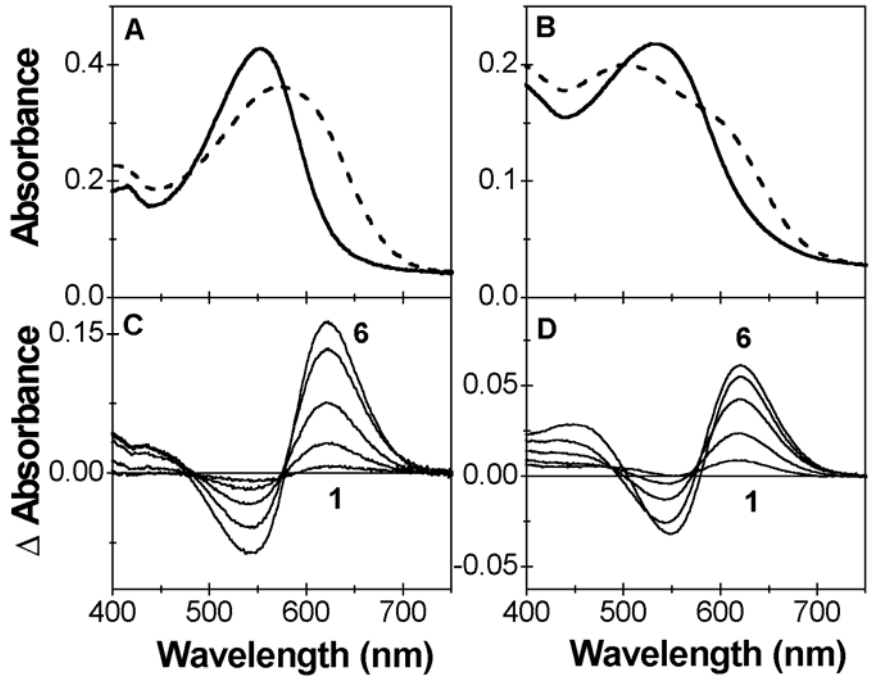

Fig.III.1. Purple-to-blue transition of dark-adapted T90A. (A) Absorption spectra of T90A in 150 mM KCl at pH 7.2 (——) and 2.0 (---). (B) Absorption spectra of deionised T90A at pH 7.0 (——) and 3.6 (---). (C) Curves 1-6 are the difference spectra (pH_i-$pH_{7.2}$) of T90A in 150 mM KCl, where pH_i values are 7.2, 6.2, 5.0, 4.1, 3.5 and 3.2. (D) Curves 1-6 are the difference spectra (pH_i-$pH_{8.0}$) of deionised T90A, where pH_i values are 7.0, 6.4, 5.9, 5.1, 4.3 and 3.6.

Table III.1.

Apparent pK_a of Asp85 (the purple-to-blue transition), as obtained from the plot of absorption changes as a function of pH.

	Asp85 pK_a	
	wild type	**T90A**
Deionised sample	5.5	6.3
H_2O	3.2	4.6
150 mM KCl	2.7	4.0

To study the role of Thr90 in the maintenance of BR structure, DSC experiments were performed. Thermograms of wild type and T90A in water at neutral pH are shown in **Fig. III.3**, after correction with instrumental and chemical baselines. Important differences in both transitions are revealed. The pre-transition, which reflects the cooperative disorganization of the hexagonal para-crystalline arrangement, shows a transition around 54 ºC, as compared to wild type at about 82 ºC. The main transition, that is a consequence of the cooperative denaturation of the tertiary structure, has a T_m of 83 ºC, as compared to 98 ºC for wild type. This indicates an easier loss of the inter-helical interactions upon temperature increase.

Changes in the visible absorption band also give information about protein denaturation, detected in this case through retinal release. Similar to wild type, when the T90A membrane suspensions are gradually heated, first appears the blue form (630 nm), followed by the appearance of the red form (approximately 460 nm) and finally, the free retinal. In accordance with DSC results, thermal stability experiments of T90A show a lower temperature of retinal release, about 85 ºC in H_2O (pH 7.0), as compared to 90ºC for wild type (data not shown).

In order to estimate proton transport efficiency, wild type BR and T90A were incorporated into liposomes using the high-pressure homogenisation method, which gives a good reproducibility **[31]**. Fig. 4 presents pH changes as a function of time of illumination, in 150 mM KCl. The initial pumping rate of T90A is about 16% of that of wild type, and the photo steady pumping amount is about 20% of wild type. Size measurements showed that both preparations had a similar liposome size distribution, with a mean diameter of about 60 nm.

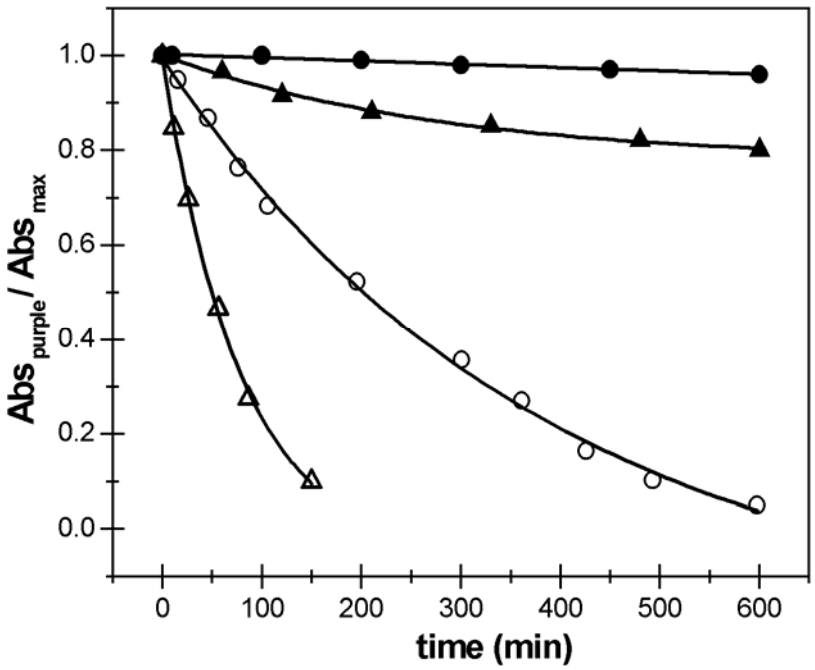

Fig.III.2. Rate of hydroxylamine reaction with wild type BR (circles) and T90A (triangles) as measured by the absorption change in the visible. The reactions were carried out in dark (filled symbols) or under illumination with light of 300 lux (empty symbols).

about 60 nm. The degree of orientation of BR into the liposomes was checked by papain digestion under conditions that cuts the C-terminal tail, followed by electrophoresis (data not shown). No significant differences were found between wild type and the T90A mutant.

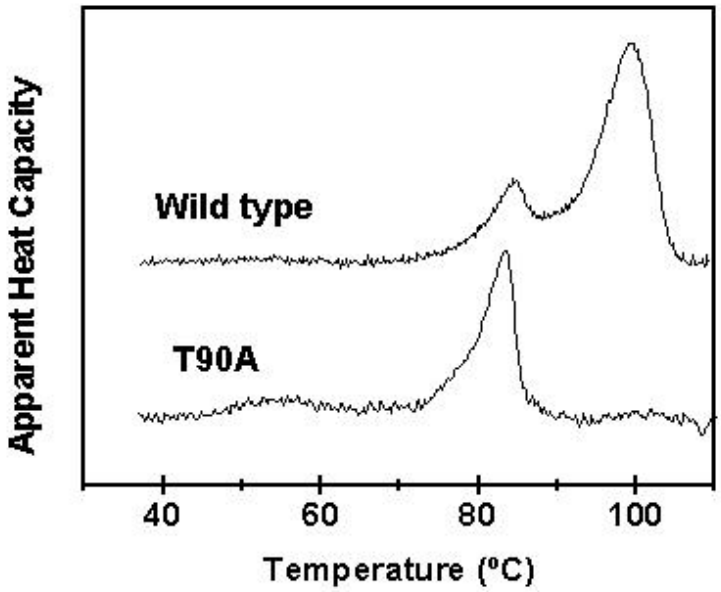

Fig. III.3. DSC thermograms of wild type and T90A. The membranes were suspended in H_2O at 1.5-2.0 mg/ml, pH 7.0. All curves were corrected with the instrumental and chemical baselines. Scans were taken at 1.5 ºK/min.

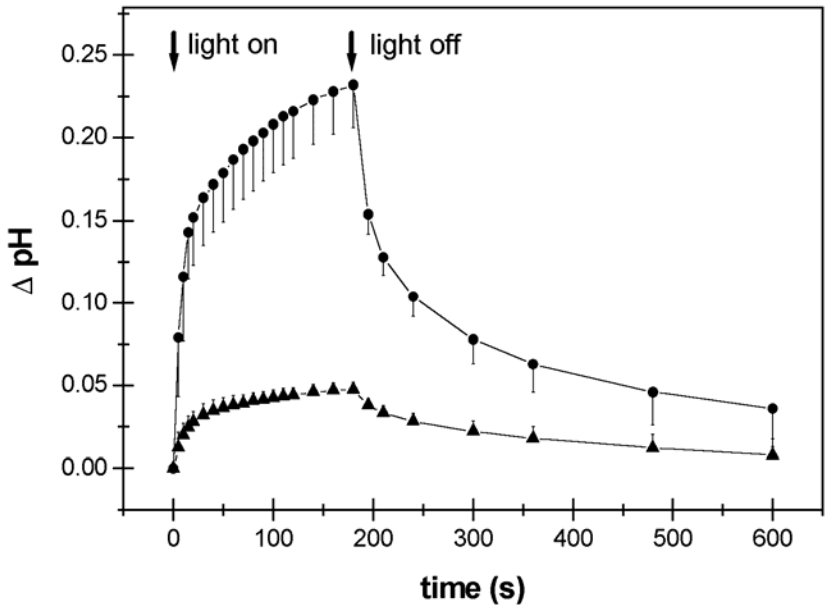

Fig. III.4. Proton pumping rates of wild type BR (circles) and T90A (triangles) incorporated into liposomes, as a function of time. Data are the mean values from 3 independent samples. The bars represent half of the corresponding standard error. The initial pumping rate of T90A was about 16% of that of wild type, and the photo steady pumping amount, about 20%.

III.4. Discussion

One important result of this work is that the T90A mutant has between 16 and 20% of the wild type proton pumping efficiency, as evidenced by the small pH changes appearing upon illumination of proteoliposome suspensions. On the other hand, the altered values of λ_{max} and of pK_a of Asp85 in the resting state argue that the Asp85/Schiff base environment is distorted by the mutation. According to the published structural models of BR, Thr90 cannot interact directly with either the Schiff base, or with Asp85, or with water molecules. Yet the $C\gamma$ of Thr90 is in Van der Waals contact with C_{11} - C_{12} of the retinal **[24, 25]**, and the disappearance of this steric interaction could explain some of the effects observed. This could be similar to the steric interaction existing between Leu93 and the 13-methyl group of the retinal **[32]**. However, due to the more lateral location of Thr90 with respect to the retinal, as compared to Leu93, we favour the view that the changes induced by the mutation are due mainly to a structural influence achieved through two different and perhaps complementary interactions of Thr90: the strong hydrogen bond formed with Asp115 (with a distance of 2.40 - 2.50 Å, according to references **23-25**) and the hydrogen bond formed with the peptide carbonyl oxygen of Trp86 (distance of about 2.55 Å). These strong hydrogen bonds may constitute key interactions for the maintenance of the correct location and bending of helix C. Even if hydrophobic interactions and water-mediated hydrogen bonds can facilitate the correct location of this helix, most likely these interactions are too weak to maintain the arrangement of helix C by themselves. In contrast, hydrogen bonding between transmembrane helices (in this case between helices C and D) is of strong nature **[26]**. Other hydrogen bonding inter-helical interactions involving helix C can also contribute to its stabilization, like Thr46 with Asp96, Tyr79 with Arg7 and Glu9, and Tyr83 with Trp189 **[25]**. However, the hydrogen bonds Thr90-Asp115 and Thr46-Asp96 are located near the middle of the helix and presumably will contribute the most to the stabilisation of helix C.

It is likely that disappearance of the hydrogen bonds formed by the O-H group of Thr90 is responsible of the effects of the mutation. For example, rupture of the inter-helical hydrogen bond formed with Asp115 is in keeping with

both the lower thermal stability of the mutant and the increased hydroxylamine accessibility. The main DSC transition, which is due to the destruction of tertiary interactions between helices including the retinal **[33]**, is about 15 ºC lower than wild type; a lower T_m for retinal release is also obtained from visible spectroscopy. Similarly, the decrease of about 28 ºC of the DSC pre-transition argues that disappearance of the interactions maintained by Thr90 decreases the compact state of the protein and confers a less stable para-crystalline arrangement. In this context, the alteration of the infrared absorbance band of Asp115 giving rise to a signal in the difference spectra of photocycle intermediates of wild type **[34, 35]** may be mainly a reflex of the strain induced over the hydrogen bond by the movement of the helices during the photocycle.

Interestingly, Trp86, Thr90 and Asp115 are highly conserved residues among homologous proteins from several halobacterial strains, giving support to the view that they are structurally important residues. Indeed, the homologous residue in halorhodopsin, Thr116, also forms hydrogen bonds with Asp141 (homologous to Asp115) in helix D and with the peptide carbonyl oxygen of Trp112 (homologous to Trp86), as revealed by the recent high-resolution structure (ref 36; PDB entry 1E12). Although at this time we can only speculate about the exact role of the Thr90-Asp115 and Thr90-Trp86 interactions, a possibility is that the Thr90-Asp115 link acts like a turning point, thus allowing the movement of helix C in the transport process, as has been readily detected by electron paramagnetic resonance spectroscopy **[5]** and X-ray diffraction **[24]**. It may be that lack of this interaction impel helix C to adopt a too separated location from the other helices, thus preventing the correct environments and interactions for the key side chains that are located in it (Arg82, Asp85, Asp96). On the other hand, Thr90 is central in the sequence Thr89-Thr90-Pro91 and this sequence has been described as capable of inducing kinks in helices **[19]**. The BR structural models effectively show a kink in helix C at the level of these amino acids. Possibly, a completely regular α helix could not form correctly the retinal cavity. This type of kink has also been involved in the conformational equilibrium between active and inactive states of G-protein coupled receptors **[19, 37]**.

III.5. References

[1] Balashov, S.P. (2000) Biochim. Biophys. Acta 1460, 75-94.
[2] Luecke, H., Schobert, B., Cartailler, J.P., Richter, H.T., Rosengarth, A., Needleman, R. and Lanyi, J.K. (2000) J. Mol. Biol. 300, 1237-1255.
[3] Subramaniam, S., Linddahl, M., Bullough, P., Faruqi, A.R., Tittor, J., Oesterhelt, D., Brown, L., Lanyi, J. and Henderson, R. (1999) J. Mol. Biol. 287, 145-161.
[4] Radzwill, N., Gerwert, K. and Steinhoff, H.J. (2001) Biophys. J. 80, 2856-2866.
[5] Rink, T., Pfeiffer, M., Oesterhelt, D., Gerwert, K. and Steinhoff, H.J. (2000) Biophys. J. 78, 1519-1530.
[6] Steinhoff, H.J., Savitsky, A., Wegener, C., Pfeiffer, M., Plato, M. and Möbius, K., (2000) Biochim. Biophys. Acta. 1457, 253-262.
[7] Oka, T., Kamikubo, H., Tokunaga, F., Lanyi, J.K., Needleman, R. and Kataoka, M. (1999) Biophys. J. 76, 1018-1023.
[8] Mollaaghababa, R., Steinhoff, H.-J., Hubbell, W.L. and Khorana, H.G. (2000) Biochemistry 39, 1120-1127.
[9] Oka, T., Yagi, N., Fujisawa, T., Kamikubo, H., Tokunaga, F. and Kataoka, M. (2000) Proc. Natl. Acad. Sci. USA 97, 14278-14282.
[10] Gerwert, K., Hess, B. and Engelhard, M. (1990) FEBS Lett. 261, 449-454.
[11] Deber, C.M., Sorrell, B.J. and Xu, G.Y. (1990) Biochem. Biophys. Res. Commun. 172, 862-869.
[12] Sankararamakrishnan, R. and Vishveshwara, S. (1993) Proteins 15, 26-41.
[13] Lu, H., Marti, T. and Booth, P. (2001) J. Mol. Biol. 308, 437-446.
[14] Ludlam, C.F., Sonar, S., Lee, C.P., Coleman, M., Herzfeld, J., RajBhandary, U.L and Rothschild, K.J. (1995) Biochemistry 34, 2-6.
[15] Kamikubo, H., Kataoka, M., Varo, G., Oka, T., Tokunaga, F., Needleman, R. and Lanyi, J.K. (1996) Proc. Natl. Acad. Sci. USA 93, 1386-1390.
[16] Koch, M.H., Dencher, N.A., Oesterhelt, D., Plohn, H.J., Rapp, G. and Buldt, G. (1991) EMBO J. 10, 521-526.
[17] Subramaniam, S., Gerstein, M., Oesterhelt, D. and Henderson, R. (1993) EMBO J. 12, 1-8.
[18] Vonck, J. (1996) Biochemistry 35, 5870-5878.
[19] Ballesteros, J.A., Deupi, X., Olivella, M., Haaksma, E.E.J. and Pardo, L. (2000) Biophys. J. 79, 2754-2760.
[20] Kandori, H., Kinoshita, N., Yamazaki, Y., Maeda, A., Shichida, Y., Needleman, R., Lanyi, J.K., Bizounok, M., Herzfeld, J., Raap, J. and Lugtenburg, J. (1999) Biochemistry 38, 9676-9683.
[21] Kandori, H., Yamazaki, Y., Shichida, Y., Raap, J., Lugtenburg, J., Belenky, M. and Herzfeld, J. (2001) Proc. Natl. Acad. Sci. USA 98, 1571-1576.
[22] Russell, T.S., Coleman, M., Rath, P., Nilsson, A. and Rothschild, K.J. (1997) Biochemistry 36, 7490-7497.
[23] Essen, L.-O., Siegert, R., Lehmann, W.D. and Oesterhelt, D. (1998) Proc. Natl. Acad. Sci. USA 95, 11673-11678.
[24] Royant, A., Edman, K., Ursby, T., Pebay-Peroula, E., Landau, E.M. and Neutze, R. (2000) Nature 406, 645-648.
[25] Luecke, H., Schobert, B., Richter, H.T., Cartailler, J.P., Lanyi, J.K. (1999) J. Mol. Biol. 291, 899-911.

[26] Zhou, F.X., Cocco, M.J., Russ, W.P., Brunger, A.T. and Engelman, D.M. (2000) Nature Str. Biol. 7,154-160.
[27] Sanz, C., Lazarova, T., Sepulcre, F., González-Moreno, R., Bourdelande, J.-L., Querol, E. and Padrós, E. (1999) FEBS Lett. 456, 191-195.
[28] Oesterhelt, D. and Stoeckenius, W. (1974) Methods Enzymol. 31, 667-678.
[29] Takahashi, K. and Sturtevant, J. M. (1981) Biochemistry 20, 6185-6190.
[30] Singleton, W.S., Gray, M.S., Brown, M.L. and White, J.L. (1965) J. Am. Oil Chem. Soc.42, 53-57
[31] Barnadas, R. and Sabés, M. (2001) Methods Enzymol. (in the press)
[32] Delaney, J.K., Schweiger, U. and Subramaniam, S. (1995) Proc. Natl. Acad. Sci. USA 92, 11120-11124.
[33] Cladera, J., Galisteo, M.L., Sabés, M., Mateo, P.L. and Padrós, E. (1992) Eur. J. Biochem. 207, 581-585.
[34] Maeda, A., Sasaki, J., Shichida, Y., Yoshizawa, T., Chang, M., Ni, B., Needleman, R. and Lanyi, J.K. (1992) Biochemistry 31, 4684-4690.
[35] Sasaki, J., Lanyi, J.K., Needleman, R., Yoshizawa, T. and Maeda, A. (1994) Biochemistry 33, 3178-3184.
[36] Kolbe, M., Besir, H., Essen, L.-O. and Oesterhelt, D. (2000) Science 288, 1390-1396.
[37] Ballesteros, J.A., Shi, L. and Javitch, J.A. (2001) Mol. Pharmacol. 60, 1-19.

And as we wind on down the road
Our shadows taller than our soul.
There walks a lady we all know
Who shines white light and wants to show
How everything still turns to gold.
And if you listen very hard
The tune will come to you at last.
When all are one and one is all
To be a rock and not to roll.

Led Zeppelin

CHAPTER IV.

THR90 PLAYS A VITAL ROLE IN THE STRUCTURE AND FUNCTION OF BACTERIORHODOPSIN

Abstract

The role of Thr90 in the bacteriorhodopsin structure and function was investigated by its replacement with Ala and Val. The mutant D115A was also studied, since Asp115 in helix D forms a hydrogen bond with Thr90 in helix C. Differential scanning calorimetry showed a decreased thermal stability of all three mutants, being T90A the least stable. Light-dark adaptation of T90A was found to be abnormal and salt-dependent. Proton transport monitored using pyranine signals was about 10% of wild type for T90A, 20% for T90V and 50% for D115A. At neutral or alkaline pH, the M rise of these mutants was faster than wild type, whereas M decay was slower in T90A. Overall, FTIR difference spectra of T90A were strongly pH-dependent. Spectra recorded on films adjusted at the same pH, at 243 or 277 K, dry or wet showed similar features. The D115A and T90V FTIR spectra were closer to WT, showing minor structural differences. The band at 1734 cm^{-1} of the deconvoluted FTIR spectrum, corresponding to the carboxylate of Asp115 was absent in all mutants. In conclusion, Thr90 plays a critical role in maintaining the operative location and structure of helix C, through three complementary interactions: an interhelical hydrogen bond with Asp115, an intrahelical hydrogen bond with the peptide carbonyl oxygen of Trp86, and a steric contact with the retinal. The interactions established by Thr90 emerge as a general feature of archaeal rhodopsin proteins.

IV.1. Introduction

The purple membrane patches of Halobacterium salinarum cells contain a single protein, bacteriorhodopsin (BR) which translocates protons from the interior to the exterior of the cell upon photon absorption by a retinal molecule **(1)**. The native structure of bacteriorhodopsin consists of a seven α-helical bundle densely packed forming a para-crystalline arrangement of BR trimers **(2-8)**. Protein-protein, lipid-protein interactions and the lateral pressure exerted by the lipid chains on the protein molecules have an important role in this arrangement **(9-11)**. Because of the high BR density, the protein in turn should accomplish some characteristics to allow the formation of the hexameric arrangement. Helix-helix interactions as well as retinal-protein interactions are important elements involved in the BR compactness. When a relaxation of the protein structure occurs, the hexagonal arrangement appears impaired. One example refers to the bleached membrane, where the retinal absence compels the helices to lose several interactions **(12, 13)**. Another case corresponds to the triple or the quadruple mutants E9Q/E194Q/E204Q and E9Q/E74Q/E194Q/E204Q, that exhibit a more relaxed conformation as compared to WT **(14, 15)**.

The mutant T90A shows some characteristics indicative of a certain degree of softening of both the para-crystalline arrangement and the interactions within the seven-helical bundle. This is demonstrated by the decreased cooperativity and temperature of the differential scanning calorimetry pre-transition, as well as by a decreased temperature of the main transition **(16)**. Because Thr90 most probably does not form part of the proton transport chain **(6, 7)**, it is likely that its importance relies on structural aspects. An earlier work already demonstrated the inability of the iodoacetic acid-derivatized T90C to fold normally in detergent/phospholipid micelles **(17)**, indicating that the –OH function and/or the side chain bulkiness is an important structural feature. According to the high-resolution BR structures, Thr90 (helix C) and Asp115 (helix D) form a hydrogen bond (**6, 7**; see **Fig. IV.1**). These two amino acids, which are conserved among various archaeobacterial strains **(18, 19)**, may be important in structural terms. Another significant structural interaction may be the hydrogen bond formed by

the –OH group of Thr90 with the peptide carbonyl oxygen of Trp86, as bends and twists in transmembrane helices are induced by Thr through formation of an hydrogen bond with the backbone **(20, 21)**. The BR structural models effectively show a kink in helix C at this level **(Fig. IV.1)**. On the other hand, Pro residues are known as helix-breaking residues, and thus the adjacent Pro91 may contribute to bend the helix. Again, sequence comparison shows that Pro91 is conserved **(18)**. Finally, there are van der Waals contacts between the methyl group of Thr90 and the retinal chain that may also be important for the correct location of retinal.

In this work, we analyze in detail the behavior of the T90A, T90V and D115A mutants, in order to determine the structural and functional consequences of the disruption of the interactions involving the Thr90 side chain. In the T90A mutant, we describe a chromoprotein with very different properties as compared to wild type BR, including a decrease in the efficiency of the proton transport, and some critical alterations in the photocycle. Besides, the D115A and T90V mutations provide further knowledge about the role of the set of interactions involving Thr90.

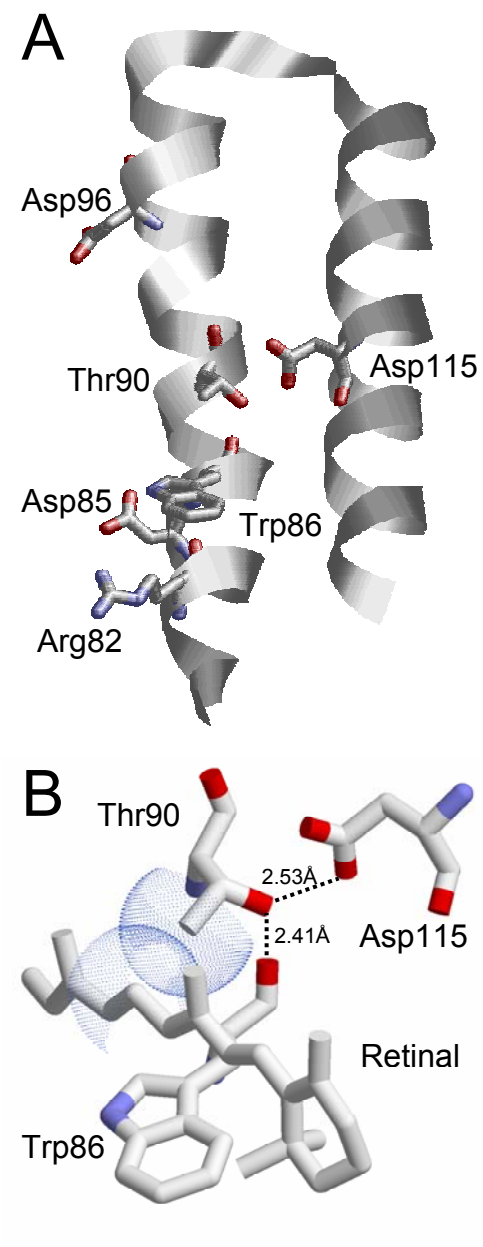

Fig. IV.1. Structure of helices C and D of bacteriorhodopsin. The structure was taken from the PDB entry 1kgb. (A) Locations and orientations of key residues of helices C and D. (B) Detail of the hydrogen bonds formed by the –OH group of Thr90 with Asp115 and with the carbonyl oxygen of Trp86. The steric interaction of the methyl group of Thr90 with the C11-C13 of the retinal is also shown.

IV.2. Material and Methods

The construction and expression of T90A and D115A mutants in Halobacterium salinarum was carried out as described **(14)**. The mutant T90V was a generous gift from Dr. J.K. Lanyi.

UV-Vis spectra of dark- or light-adapted purple membrane suspensions ($1.5 \cdot 10^{-5}$ M, $3.5 \cdot 10^{-5}$ M in the case of T90A) were recorded with a Cary Bio3 spectrophotometer, using an integrating sphere when necessary. The difference spectra were obtained by subtracting light-adapted minus dark-adapted samples.

Flash-induced transient absorbance changes were monitored using a LKS50 instrument from Applied Photophysics. A Q-switched Nd:YAG laser (Spectron Laser Systems, UK; pulse width ca. 9 ns; E=5 mJ/pulse/cm^2; repetition frequency 0.5 Hz) at 532 nm was used for light excitation. Transient pH changes in the bulk medium were followed by measuring the absorbance changes of 50 μM pyranine at 460 nm in a purple membrane suspension, in 1M KCl pH 7.0 **(22)**. To obtain the net absorbance changes of pyranine, the traces of samples in the absence of the dye were subtracted from those in its presence. The negative signal of $\Delta\Delta A$ indicates the release of protons by BR (pyranine protonation), whereas the positive signal indicates BR proton uptake. Photocycle reactions of PM suspensions of T90A and D115A mutants in 1M KCl were followed by the acquisition of absorbance spectra at 410, 555 and 660 nm as a function of time, at pH 6.5 and pH 10.0.

Infrared experiments were performed at 277 K and 243 K with wet and dry samples. The temperature was controlled and maintained using a homemade cell holder and a cryostat. Membrane samples were suspended in 150 mM KCl and either 3 mM carbonate-bicarbonate for pH 10.0 or 3 mM sodium phosphate for pH 7.0. Preparation of membrane films and spectra acquisition were done as described **(23)** with a Bio-Rad FTS6000 spectrometer at 2 cm^{-1} resolution. At least 3 cycles of 350 scans were averaged (i.e. at least 1050 interferograms were accumulated per spectrum). Difference spectra were calculated by subtracting unphotolyzed BR from the corresponding photointermediate. Absorption spectra were Fourier self-deconvoluted using the Kauppinnen algorithm **(24)**, with a Lorentzian band shape, a full width at half height of 10 cm^{-1} and a band narrowing factor k of 2.0. When necessary, films were illuminated with blue light to drive any remaining intermediate back to BR.

Differential scanning calorimetry (DSC) experiments were performed as described previously **(16)**.

IV.3. Results

Light-dark Adaptation— Light-dark adaptation was found to be abnormal in T90A. **Fig. IV.2** shows the absorbance and difference spectra (light-adapted minus dark-adapted) in water, 150 mM KCl, and 1 M KCl (pH 7.0, room temperature). In H_2O, a decrease of the extinction coefficient and virtually no shift of the maximum upon illumination are observed. When the ionic strength is increased, a more normal behavior is observed (increase of the extinction coefficient and red-shift upon light adaptation), due probably to the partial recovering of the normal isomer ratio in dark-adapted form. Under the conditions presented in **Fig. IV.2**, dark adaptation is very slow, taking at least 1 month to complete. In contrast, T90V and D115A show a normal dark adaptation, although all mutants present a shifted absorbance maxima as compared to WT (see **Table IV.1**).

Photocycle Reactions and Proton Uptake and Release— **Fig. IV.3A** shows kinetic traces of the light-induced absorption changes for T90A, T90V, D115A and WT, in 1M KCl, pH 6.5 (room temperature), normalized to the M amplitude. All mutants present a faster M rise and a slower M decay than WT (see **Table IV.1**). **Fig. IV.3A** also shows that D115A presents a higher amount of O intermediate than T90A, T90V or wild type, and that T90A and T90V exhibit a longer-living O intermediate. At pH 10, like at neutral pH, the M rise of T90A and of T90V is faster and the M decay slower than those of the WT, while D115A has a faster M decay (**Fig. IV.3B** and **Table IV.1**). On the other hand, at neutral or at alkaline pH both the amplitude of M intermediate

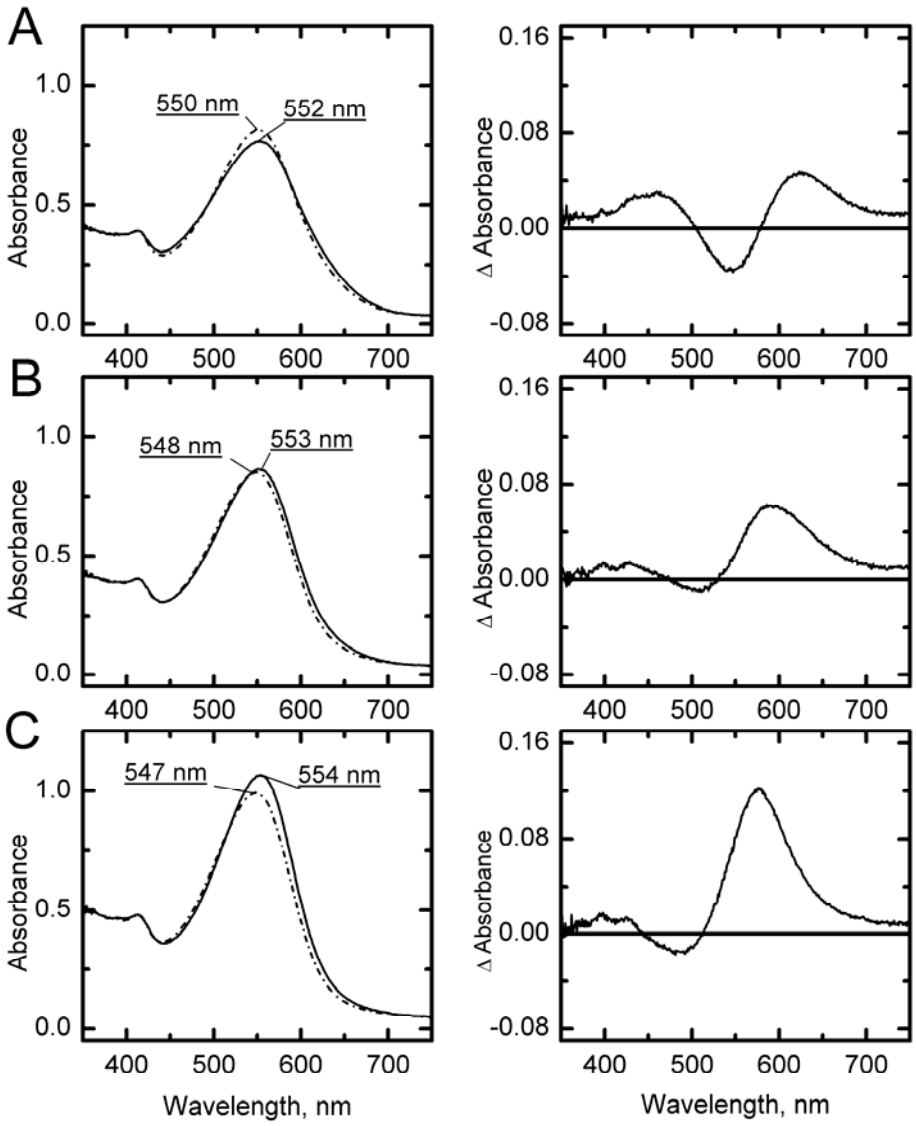

Fig. IV.2. Light-dark absorption spectra of T90A. Left column: absorption spectra of dark-adapted (dash-dot line) and light-adapted (solid line) membrane suspensions of T90A, at pH 7.0. (A) in water; (B) in 150 mM KCl; (C) in 1 M KCl. Right column: Difference spectra obtained by subtracting light- minus dark-adapted spectra.

Table IV.1

Time constants of M rise and decay obtained by fitting the absorption changes at 410 nm from Fig. 3 (1 M KCl, pH 6.5 or 10.0, 293 K) to a biexponential function. In parentheses, the corresponding fraction amplitude. Maximum absorbance values at 150 mM KCl, pH 7.0 are also shown.

	WT	D115A	T90V	T90A
Max. Abs. DA	558 nm	551 nm	545 nm	548 nm
Max. Abs. LA	568 nm	557 nm	551 nm	553 nm
M rise pH 6.5	4.1 μs (0.10)	8.2 μs (0.30)	4.5 μs (0.50)	1.5 μs (0.70)
	70 μs (0.90)	50 μs (0.70)	40 μs (0.50)	60 μs (0.30)
M rise pH 10.0	3 μs (0.80)	2.1 μs (0.75)	1.5 μs (0.65)	2.1 μs (0.90)
	20 μs(0.20)	80 μs (0.25)	20 μs (0.35)	50 μs (0.10)
M decay pH 6.5	3 ms (1.0)	7.2 ms (0.90)	4.5 ms (0.80)	9 ms (0.70)
		70 ms (0.10)	70 ms (0.20)	93 ms (0.30)
M decay pH 10.0	3 ms (0.50)	5 ms (0.40)	5.7 ms (0.45)	21 ms (0.40)
	80 ms (0.50)	51 ms (0.60)	155 ms (0.55)	235 ms (0.60)

(maximal signal at 410 nm) and the signal at the λ_{max} of 555 nm (disappearance of the BR form) of T90A are about a 20% of the WT signal, whereas they are about 40% for T90V and about 50% for D115A. At pH 4.0, no signal was detected for T90A at any of the wavelengths analyzed, indicating the absence of photocycle intermediates under these conditions, while both T90V and D115A showed small signals (data not shown).

Fig. IV.4 shows the pyranine signal for T90A, T90V, D115A and WT at pH 7.0. As it is apparent, a weak signal is obtained for T90A and T90V, amounting to about 10% of the WT signal for T90A and about 20% for T90V. This is in keeping with the low accumulation of M intermediate obtained at neutral pH and with the decreased pumping efficiency of T90A incorporated into liposomes, which was found to be less than 20% **(16)**. The signal of D115A also appears decreased, to about 50% of the WT signal, again in accordance with the amplitude of the M intermediate for this mutant.

Fourier Transform Infrared Spectra— A general characteristic of the infrared difference spectra of T90A films, obtained by continuous illumination, is their low intensity, in accordance with the small signal obtained in flash photolysis experiments. On the other hand, we have found that the difference spectra depend mainly on the pH. As shown in **Fig. IV.5A**, the spectra taken at pH 10.0, at either 243 or 277 K, dry or wet, are similar to each other and relatively similar to the WT M_1 intermediate spectrum **(25)**. Asp85 appears protonated (band at 1762-1763 cm^{-1}), and a small negative band appears at 1747 cm^{-1}, not present in the WT difference spectrum. The amide I is also somewhat changed in comparison to the WT M_1 intermediate.

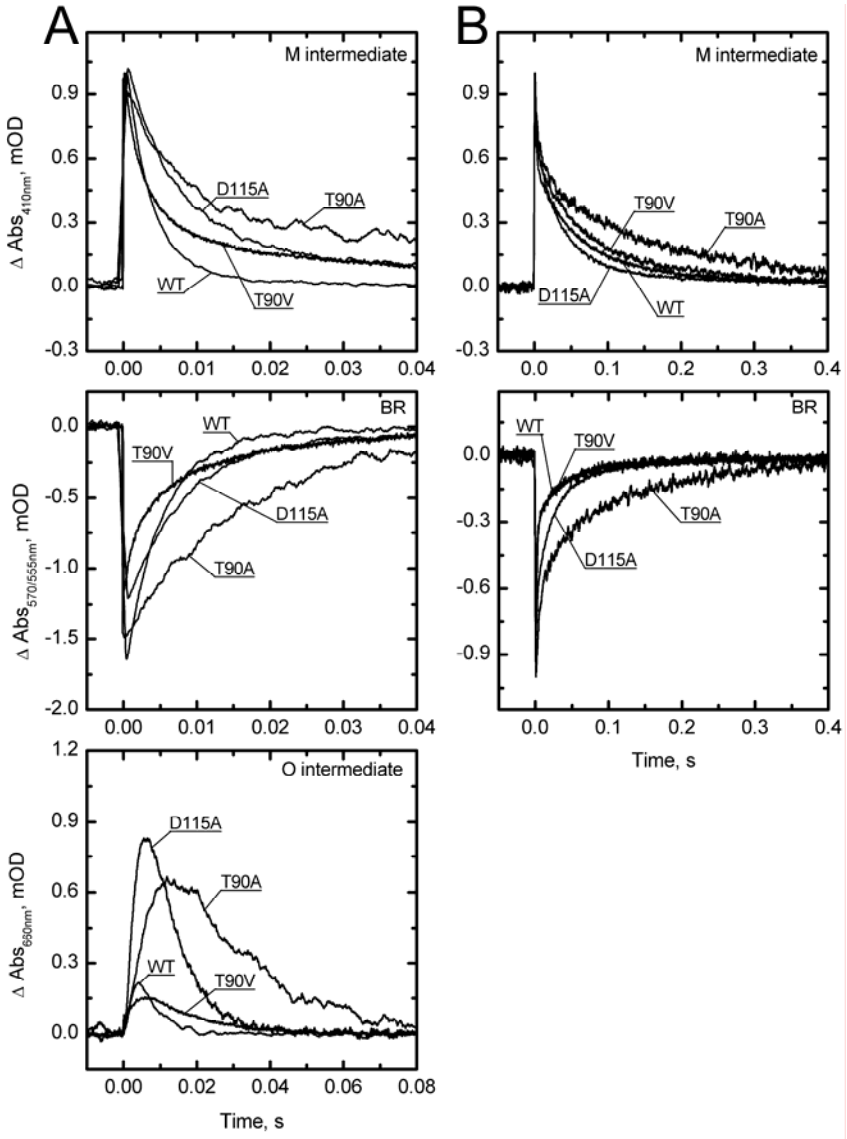

Fig. IV.3. Kinetics of photocycle intermediates. The traces show the absorption changes corresponding to the M intermediate (410 nm, top), BR depletion and recovery (555 nm for T90A, T90V and D115A; 570 nm for WT, middle) and O intermediate (660 nm, bottom). Column (A), pH 6.5, 1 M KCl, 293 K. Column (B), pH 10.0, 1 M KCl, 293 K. The absorption changes at 410, 660 and 570/555 nm, were normalized to the amplitude of the M intermediate for each pigment at the respective pH.

The pair of bands at 1640 cm^{-1} (negative) and at 1624 cm^{-1} (positive) indicate the presence of a protonated Schiff base in the unphotolyzed pigment and a deprotonated Schiff base in the M_1-like intermediate. In the amide II, the C=C stretching band appears at 1530 cm^{-1}, in keeping with the known inverse relationship with the λ_{max} of the visible absorption spectrum, which is 550 nm at pH 10. On the other hand, the retinal negative peaks at 1201 and 1167 cm^{-1} indicate that the retinal is in the all-trans configuration in the unphotolyzed state **(26)**. It is interesting to note that the small negative peak at 1276 cm^{-1} is not

present, indicating that the conformational changes of the T90A photocycle do not affect Tyr185 **(27)**.

At pH 7.0 **(Fig. 5B)**, the difference spectra depend more on the particular conditions, especially on the water content. The carboxylate band of Asp85 is less evident and shifted to 1764-1768 cm^{-1}, depending on the temperature and the state of the sample. The negative band at 1698 cm^{-1}, particularly evident in the wet samples, corresponds probably to the band at 1692 cm^{-1} in WT and T90A at pH 10.0. This shift may indicate that the corresponding reverse turns of the unphotolyzed protein have a different structure in wet samples at pH 7.0 from those at pH 10.0. The positive band at 1509 cm^{-1} is also mainly seen in wet samples **(Fig. 5B)**. It may be reminiscent of the band at 1506 cm^{-1}, seen in the O difference spectra **(28)**. The most striking feature observed at pH 7.0 is the positive 1222 cm^{-1} peak, which again is more intense in wet samples and is accompanied by a low intensity of the 1200 cm^{-1} band.

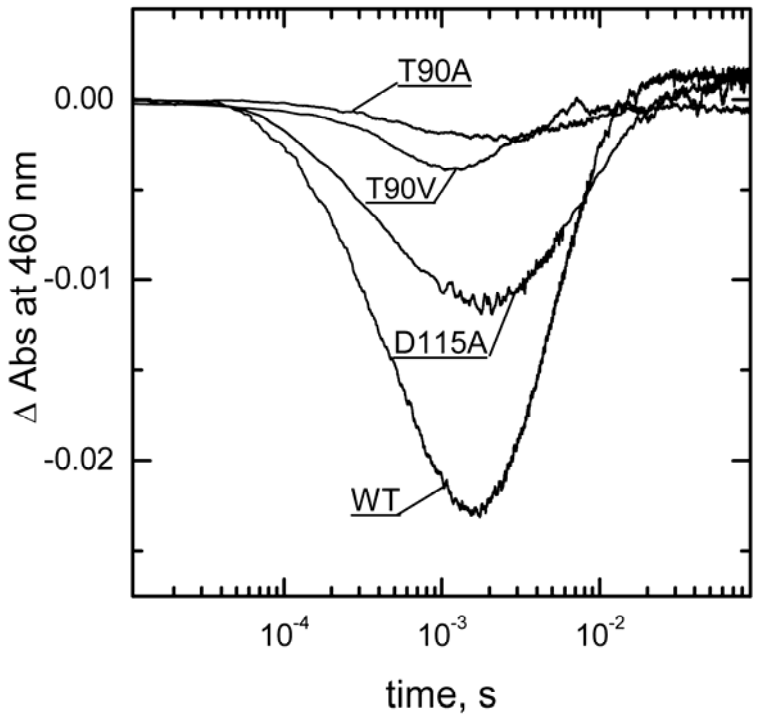

Fig. IV.4. Light-induced pyranine signals. Pyranine absorption changes were measured at 460 nm in suspensions of T90A, T90V, D115A and WT, in 150 mM KCl (pH 7.0) at 293 K. Proton uptake from BR causes an increase of absorbance, while proton release causes a decrease. Protein concentration, $1.5 \cdot 10^{-5}$ M.

These features indicate that at neutral pH the retinal adopts a distorted configuration in T90A as compared to WT. Difference spectra for D115A and T90V were more similar to WT, with only some deviation appearing in the amide I and in the fingerprinting region of the retinal (data not shown).

Fig. IV.6A presents FTIR difference spectra collected under conditions of N intermediate. D115A shows an N-like intermediate, whereas the main feature of T90A and T90V is an M-like intermediate (compare with the spectrum of WT). In D115A, the peak of protonated Asp85 is shifted to a more M-like position (1761 cm^{-1}) and the 1650 cm^{-1} peak corresponding to helical conformational changes is absent, as in T90A. The T90V mutant shows an M-like spectrum, although as in D115A, a small positive band at 1186 cm^{-1} (characteristic of N) is present. **Fig. 6B** shows the absorbance FTIR spectra of WT, T90A, T90V and D115A films at pH 7.0 in the carboxylate region after band narrowing by deconvolution. Two bands can be seen in the WT sample at 1734 and 1740 cm^{-1}, which are assigned to Asp115 and Asp96, respectively **(29)**. In the mutants, the band at 1734 cm^{-1} is missing, whereas the band at 1740 cm^{-1} keeps its position in T90A, and shifts to 1741 cm^{-1} in T90V and D115A. Similar spectra were found at pH 10 (data not shown). This indicates that in T90A and T90V, the –COOH group of Asp115 does not contribute to the carboxylate region and thus is most likely deprotonated at neutral or alkaline pH.

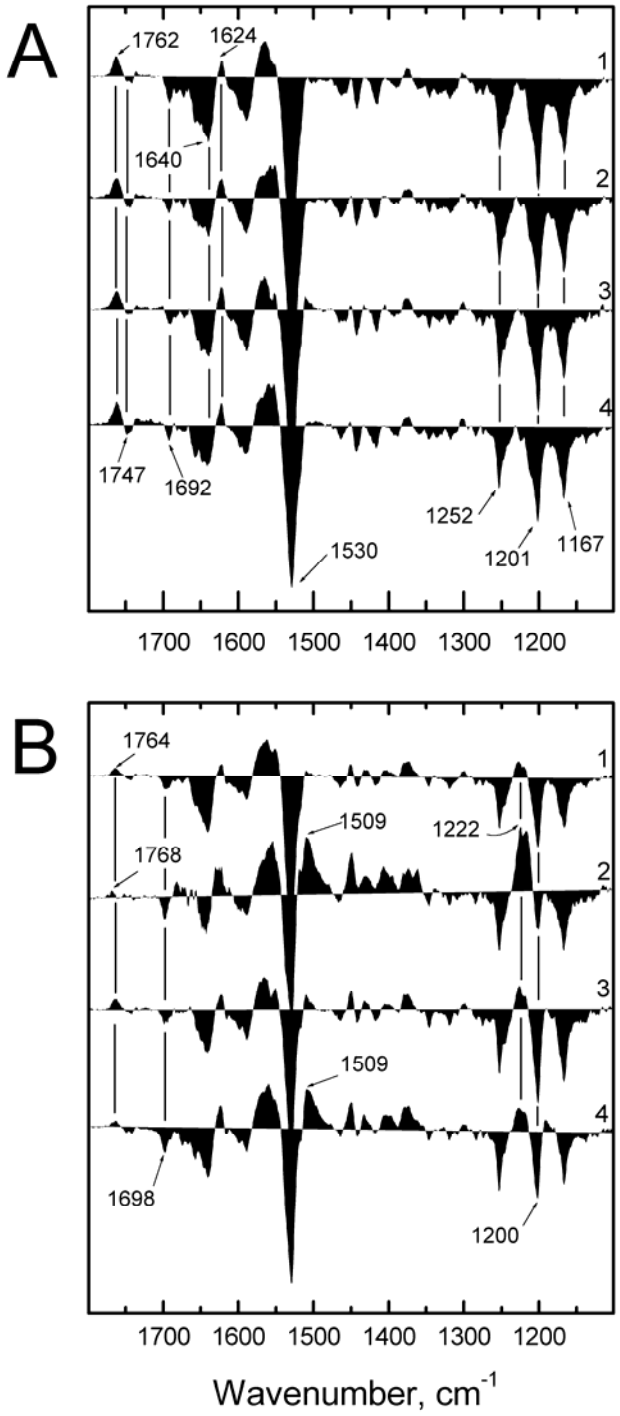

Fig. IV.5. FTIR-Difference spectra of T90A. The films were prepared from suspensions in 150 mM KCl at pH 10.0 (A) and pH 7.0 (B). Conditions: (1) dry sample at 277 K; (2) wet sample at 277 K; (3) dry sample at 243 K; (4) wet sample at 243 K. The spectra are scaled so that all of them have the same intensity.

Thermal stability— DSC experiments were performed on wild type and mutant BR to determine the influence of the mutations on the structural stability. **Fig. IV.7** shows the DSC scans after baseline subtraction. As is known, the WT purple membrane presents two transitions: the pre-transition that is assigned to the

reversible disorganization of the para-crystalline arrangement, and the main transition, due to the irreversible (partial) protein denaturation. The figure shows that the mutations induce a clear destabilization. As described previously **(16)**, T90A has the main transition at 83 ºC and a decreased area of the transition curve, thus presenting a dramatic decrease in conformational stability as compared to WT (main transition at 98 ºC). T90V and D115A show an intermediate behavior. They have the same main transition temperature (92ºC), but T90V shows a lower cooperativity. The mutations affect even more the pre-transition. As compared to WT, there is a decrease in the temperature of the pre-transition of 12 ºC for D115A, 20 ºC for T90V and about 30 ºC for T90A. Additionally, an important decrease in cooperativity is observed, especially for T90V and T90A. Overall, these data indicate a more relaxed structure of the BR mutants, giving rise in turn to a decreased stability of the para-crystalline arrangement.

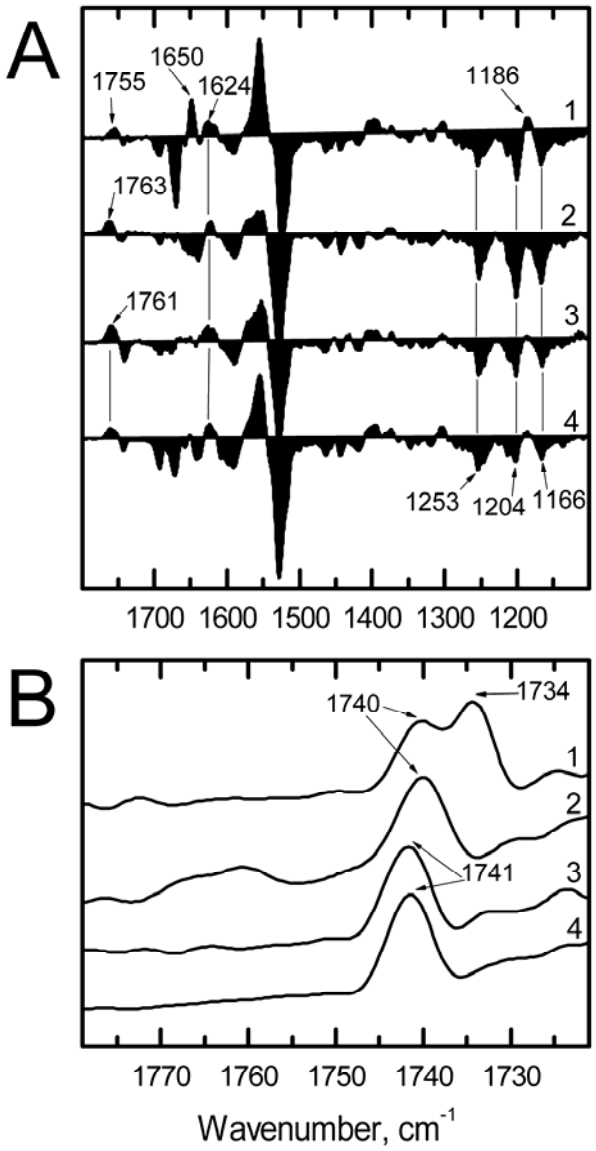

Fig. IV.6. N-like FTIR difference spectra and carboxylic region of the FTIR deconvoluted spectra of T90A, T90V, D115A and WT. A, comparison of T90A, T90V, D115A and WT FTIR difference spectra under conditions for WT to yield the N intermediate (pH 10.0, wet sample, at 277 K). (1) WT; (2) T90A; (3) T90V; (4) D115A. B, Carboxylic region of the deconvoluted spectra of purple membrane dry films at 293 K obtained from membrane suspensions in 150 mM KCl, pH 7.0. (1) WT; (2) T90A; (3) T90V; D115A. The parameters used for deconvolution are a full bandwidth at half height of 10 cm^{-1} and a narrowing factor k of 2.

IV.4. Discussion

The study of the BR mutants T90A, T90V and D115A presented in this paper provides the means to evaluate the scope of the three interactions held by the Thr90 side chain: the steric interaction with the retinal at the level of C_{11}-C_{13}, and the hydrogen bonds established with Asp115 and with the carbonyl oxygen of Trp86. The results reveal Thr90 as a key element in the structure of BR, in accordance with our previous conclusions **(16)**. Focusing on proton pumping, mutagenesis on Thr90 yields a protein with a clear decrease in the proton pumping ability. Thus, substitution of Thr90 with Ala, that avoids all the interactions of the residue 90, decreases the pumping efficiency to only about 10% of the pyranine signal in comparison with WT. Similarly, substitution of Thr90 with Val, that keeps the steric interaction with the retinal but loses the hydrogen bonds, shows a proton pumping about a 20% of that of WT. In accordance with this trend, the D115A mutant, that only loses the hydrogen bonding of Thr90 with Asp115, shows a proton pumping of about a 50% as compared to WT. Previous data on T90V expressed in E. coli and reconstituted into liposomes also showed a somewhat decreased proton pumping activity, although not as important as in our case (about 70%, ref. **30**), whereas T90C showed similar proton pumping as WT **(17)**. This discrepancy may be due to a more relaxed conformation of the protein in the monomeric state that is obtained by reconstitution, as compared to the crystalline lattice of purple membrane.

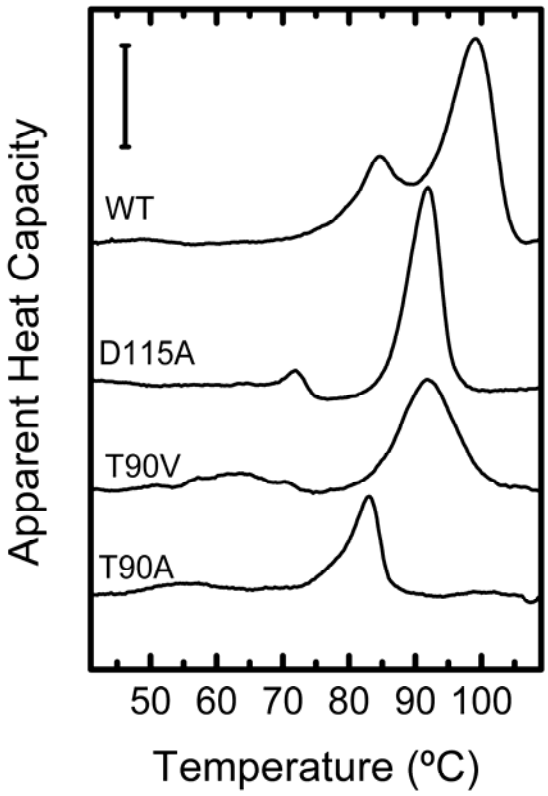

Fig. IV.7. DSC-thermograms of wild type and mutants D115A, T90V and T90A. Purple membrane patches were suspended in H_2O at a concentration of 2.0 mg/ml, pH 7.0. The curves were corrected with the instrumental and chemical baselines. Scans were taken at 1.5 K/min. Scale bar represents an apparent heat capacity of 5.10^{-4} cal/ºC.

The kinetics and yield of the photocycle intermediates constitute a valuable appraisal of the disruption of the function of BR produced by the mutations. First of all, the amount of M intermediate is much decreased in T90A compared to WT, and decreased to half of the value of WT in T90V and D115A, suggesting a back-reaction to the purple form from one of the intermediates preceding M. On the other hand, the M rise is faster than WT in all mutants, at neutral or alkaline pH, whereas the M decay is slower in all mutants at both pH conditions, except for D115A, which shows faster M decay kinetics at alkaline pH. This indicates that the deprotonated state of the Schiff base, i.e., the M intermediate, is favored in T90A and T90V, in agreement with FTIR data (see **Fig. IV.6A**). On the other hand, the absorbance maximum and dark-light adaptation properties give information on the environment of the retinal chromophore. As described in the Results section, all three mutants show shifted absorbance maxima, but only T90A has abnormal dark-light adaptation kinetics. This means that the steric interaction between the methyl group of Thr90 and the retinal participates in the dark-light adaptation process. Anomalous percentage of the all-trans and 13-cis isomers in the mutant, as was described for T90V expressed in E. coli and reconstituted into liposomes **(30)** can be another expression of this altered environment of the retinal chromophore.

FTIR difference spectra on T90A reinforce the idea of a strong distortion of the photocycle due to the mutation and depending essentially on the pH. The fact that a dry sample at 243 K gives rise to a spectrum nearly identical to that of a wet sample at 277 K, both at the same pH (see **Fig. IV.5**), is a clear demonstration of the insensitivity of T90A on hydration level and temperature. On the other hand, under the experimental conditions for which the WT films produce an almost pure N intermediate, D115A gives rise to an N-like intermediate with some alterations, T90V yields a mixture of M and N intermediates, whereas T90A does not show any N-like intermediate. At neutral pH, T90A appears to behave even in a more abnormal manner, detected especially through the positive retinal band at 1222 cm^{-1}, which at pH 4.0 is still present as almost the unique perceptible band (data not shown). Hence, the entire FTIR data such as the Asp85 protonation intensity, the retinal bands in the fingerprinting region or the amide region, are in keeping with the photocycle

measurements showing that T90A behavior appears more alike to WT as the pH is increased. This strong pH dependence of T90A suggests that, on pH decrease, protonation of one or more groups abolishes the essential structural design of the protein characteristic of WT. Because this effect does not occur in WT neither in D115A, nor in T90V the clear and dominant effect of pH must be due to a change in the pK_a of one or more side chains due to the changed conformation in the mutant.

In order to check if the altered functional behavior of the mutants has any correspondence with their conformational properties in the resting state, we have performed DSC experiments. In parallel to the decrease in proton pumping efficiency, the mutations studied give rise to a decrease in the protein stability. T90A, that has lost all interactions created by Thr90, shows a remarkable decrease of thermal stability **(16)**. The intermediate behavior of T90V and D115A as compared to WT and T90A is in keeping with the maintenance of some of the interactions held by Thr90 in the WT. Both T90V and D115A have lost the hydrogen bond established between Thr90 and Asp115, and both show the same decrease in the temperature of the main transition, although D115A has a more cooperative transition. On the other hand, T90A has lost the interaction with the retinal as compared to T90V, and it is certainly less stable. Therefore, we are tempting to deduce that both the hydrogen bond between Thr90 and Asp115, and the steric interaction of Thr90 with the retinal contribute similarly to the BR conformational stability. However, this is a very simple description of the effects of the mutations, as other factors such as the volume occupied by the side chains, changes in the hydrophobic effect or in the side chain conformational entropy will also contribute to the final structural stability. Denaturation experiments using aliphatic alcohols already revealed the importance of polar interactions for the formation of the tertiary structure of BR **(31)**. Therefore, although a variety of forces and interactions contribute to achieve the seven-helical functional bundle **(32-36)**, polar interactions seem prominent. On the other hand, it appears that the para-crystalline arrangement of BR trimers in the membrane depends in a more subtle way on the interactions formed by Thr90, as indicated by the gradual decrease of the pre-transition temperature among the mutants studied (see the Results). Thus, it seems that the formation of the hexameric structure requires

not only the presence of protein-protein and lipid-protein interactions, but also a BR compact structure that some mutations are not able to preserve, giving rise to a less stable para-crystalline arrangement.

The importance of Thr90 in assuring the correct location of key amino acid side chains of helix C involved in proton transport provides a basis for discussing the role of the central part of helix C. Two nearby side chains, Pro91 and Trp86, which are fully conserved among 25 archaeal rhodopsins **(18)**, may also contribute to the precise location of helix C. Previous data obtained in detergent/phospholipid micelles showed that Pro91 mutation alter several photocycle and proton pumping properties **(37, 38)**, indicating that it is important for the proton-pumping function. Therefore, it is plausible that the three conserved residues at positions 86, 90 and 91 contribute through different ways to the same structural purpose, that is, to provide the correct location of the functional side chains located on helix C as well as that of the retinal. It is interesting to point out that Trp86 and Pro91 are conserved not only among the 25 archaeal rhodopsins (bacteriorhodopsins, halorhodopsins and sensory rhodopsins), but also in 5 fungal chaperones and in proteorhodopsin, while Thr90 is conserved only among archaeal rhodopsins **(18, 19)**. Although Trp86 forms part of the retinal environment, it may have as well other more general structural functions, as Pro91, related to the formation of the seven-helical bundle. Thr90, in contrast, may be necessary especially for retinal-containing transmembrane proteins. For example, in halorhodopsin Asp141 (homologous to Asp115) is also within hydrogen-bonding distance of Thr116 (homologous to Thr90) **(39)** indicating the same possible function as in BR.

The importance of Thr90 may come from the necessity of accurate conformational changes affecting helix C during the photochemical cycle, linked to the retinal movements. Such subtle conformational changes have been described recently in the K to L transition, in which a local bending of helix C towards the proton translocation channel is anticipated to play a central role in setting the stage for proton transfer **(40)**.

IV.5. References

1. Oesterhelt, D., and Stoeckenius, W. (1973) Proc. Natl. Acad. Sci. USA 70, 2853-2857
2. Henderson, R., and Unwin, P. N. (1975) Nature 257, 28-32
3. Grigorieff, N., Ceska, T. A., Downing, K. H., Baldwin, J. M., and Henderson, R. (1996) J. Mol. Biol. 259, 393-421
4. Pebay-Peyroula, E., Rummel, G., Rosenbusch, J. P., and Landau, E. M. (1997) Science 277, 1676-1681
5. Luecke, H., Richter, H. T., and Lanyi, J. K. (1998) Science 280, 1934-1937
6. Luecke, H., Schobert, B., Richter, H. T., Cartailler, J. P., and Lanyi, J. K. (1999) J. Mol. Biol. 291, 899-911
7. Facciotti, M. T., Rouhani, S., Burkard, F. T., Betancourt, F. M., Downing, K. H., Rose, R. B., McDermott, G., and Glaeser, R. M. (2001) Biophys. J. 81, 3442-3455
8. Neutze, R., Pebay-Peyroula, E., Edman, K., Royant, A., Navarro J., and Landau E. M. (2002) Biochim. Biophys. Acta 1565, 144-167
9. Curran, A. R., Templer, R. H., and Booth, P. J. (1999) Biochemistry 38, 9328-9336
10. Weik, M., Patzelt, H., Zaccai, G., and Oesterhelt, D. (1998) Mol. Cell 1, 411-419
11. Heyes, C. D., and El-Sayed, M. A. (2002) J. Biol. Chem. 277, 29437-29443
12. Cladera, J., Galisteo, M. L., Sabés, M., Mateo, P. L., and Padrós, E. (1992) Eur. J. Biochem. 207, 581-585
13. Moller, C., Buldt, G., Dencher, N. A., Engel, A., and Muller, D. J. (2000) J. Mol. Biol. 301, 869-879
14. Sanz, C., Lazarova, T., Sepulcre, F., González-Moreno, R., Bourdelande, J. L., Querol, E., and Padrós, E. (1999) FEBS Lett. 456, 191-195
15. Padrós, E., Sanz, C., Lazarova, T., Márquez, M., Sepulcre, F., Trapote, X., Muñoz, F.-X., González-Moreno, R., Bourdelande, J. L., and Querol, E. (2001) in Bioelectronic Applications of Photochromic Pigments, eds. Dér, A. and Keszthelyi, L., Vol. 335, pp. 120-136
16. Perálvarez, A., Barnadas, R., Sabés, M., Querol, E., and Padrós, E. (2001) FEBS Lett. 508, 399-402
17. Flitsch, S. L., and Khorana, H. G. (1989) Biochemistry 28, 7800-7805
18. Ihara, K., Umemura, T., Katagiri, I., Kitajima-Ihara, T., Sugiyama, Y., Kimura, Y., and Mukohata, Y. (1999) J. Mol. Biol. 285, 163-174
19. Zhai, Y., Heijne, W. H., Smith, D. W., and Saier, M. H., Jr. (2001) Biochim. Biophys. Acta 1511, 206-223
20. Gray, T. M., and Matthews, B. W. (1984) J. Mol. Biol. 175, 75-81
21. Ballesteros, J. A., Shi, L., and Javitch, J. A. (2001) Mol. Pharmacol. 60, 1-19
22. Grzesiek, S., and Dencher, N. A. (1986) FEBS Lett. 208, 337-342
23. Lazarova, T., & Padrós, E. (1996) Biochemistry 35, 8354-8358

24. Kauppinnen, J.K., Moffatt, D.J., Mantsch, H.H., and Cameron, D.G. (1981) Anal. Chem. 53, 1454-1457
25. Braiman, M.S., Ahl, P.L., and Rothschild, K.J. (1987) Proc. Natl. Acad. Sci. USA 84, 5221-5225
26. Maeda, A., Sasaki, J., Pfefferle, J. M., Shichida, Y., and Yoshizawa, T. (1991) Photochem. Photobiol. 54, 911-921
27. He, Y., Krebs, M. P., Fischer, W. B., Khorana, H. G., and Rothschild, K. J. (1993) Biochemistry 32, 2282-2290
28. Zscherp, C., and Heberle, J. (1997) J. Phys. Chem. B 101, 10542-10547
29. Sasaki, J., Lanyi, J. K., Needleman, R., Yoshizawa, T., and Maeda, A. (1994) Biochemistry 33, 3178-3184
30. Marti, T., Otto, H., Mogi, T., Roesselet, S. J., Heyn, M. P., and Khorana, H. G. (1991) J. Biol. Chem. 266, 6919-6927
31. Mitaku, S., Suzuki, K., Odashima, S., Ikuta, K., Suwa, M., Kukita, F., Ishikawa, M., and Itoh, H. (1995) Proteins 22, 350-362
32. Javadpour, M. M., Eilers, M., Groesbeek, M., and Smith, S. O. (1999) Biophys. J. 77, 1609-1618
33. Fleming, K. G., and Engelman, D. M. (2001) Proc. Natl. Acad. Sci. USA 98, 14340-1434
34. Langosch, D., and Heringa, J. (1998) Proteins 31, 150-159
35. Kahn, T. W., Sturtevant, J. M., and Engelman, D. M. (1992) Biochemistry 31, 8829-8839
36. Azuaga, A. I., Sepulcre, F., Padrós, E., and Mateo, P. L. (1996) Biochemistry 35, 16328-16335
37. Mogi, T., Stern, L. J., Chao, B. H., and Khorana, H. G. (1989) J. Biol. Chem. 264, 14192-14196
38. Zhang, Y. N., El Sayed, M. A., Stern, L. J., Marti, T., Mogi, T., and Khorana, H. G. (1993) Photochem. Photobiol. 57, 1027-1031
39. Kolbe, M., Besir, H., Essen, L. O., and Oesterhelt, D. (2000) Science 288, 1390-1396
40. Edman, K., Royant, A., Larsson, G., Jacobson, F, Taylor, T., van der Spoel, D., Landau, E.M., Pebay-Peyroula, E., and Neutze, R. (2004) J. Biol. Chem. 279, 2147-2158

Hay un silencio que mata
Una escalera que sube
Y una duda que me baja
Y una cabeza en las nubes

Estopa

CHAPTER V.

ON THE DYNAMIC ROLE OF PROLINE RESIDUES IN TRANSMEMBRANE HELICES: THE CASE OF BACTERIORHODOPSIN

Abstract

Proline residues in transmembrane helices have been bound to have important roles in the functioning of membrane proteins. Moreover, Pro residues occur with high frequency in transmembrane α-helices, as compared to α-helices for soluble proteins. Here, we report several properties of the bacteriorhodopsin mutants P50A (helix B), P91A (helix C) and P186A (helix F). Compared to wild type, strongly perturbed behaviour has been found for these mutants. In the resting state, hydroxylamine accessibility, Asp-85 pK_a and light-dark adaptation were severely altered. On light activation, hydroxylamine accessibility, proton transport activity, M formation kinetics and FTIR difference spectra of M and N intermediates showed clear distortions. Besides, distances from the peptidyl N of the mutated Ala to the oxygen of the i-4 or i-3 residue of the crystal structures allow only the formation of hydrogen bonds for P50A and P186A. Based on a) severe alterations of a number of protein properties in both the resting state and in the light-activated states; and b) the similarity of the crystalline structures of mutants with that of wild type, we conclude that the transmembrane proline residues of bacteriorhodopsin fulfill a structural dynamic role in both the resting and the light-activated states. In this last case, they may serve as transmission elements of conformational changes during the transport process. We propose that these concepts can be extended to other transmembrane proteins.

V.1. Introduction

The role of prolines in transmembrane α helices has been a challenge for a long time **[1-4]**. Proline side chains are relatively frequent in transmembrane helices, where they are involved usually in a change of the orientation of the helix **[5-7]**. Pro at residue *i* introduces an steric clash with the *i-4* residue and the loss of a backbone hydrogen bond, which implies the kink or bend of the helix **[8]**. This introduces some anisotropic flexibility avoiding undesired conformations of the helix **[8-11] (Fig. V.1)**. In this way, Pro residues can help the helix to adopt the optimal disposition to establish important helix-helix packing interactions **[12]**. Derived from the steric clash, proline is able to make non-conventional C–H· · ·O hydrogen bonds involving the ring C_δ–H group with the i-3 and/or i-4 residues **[13]**. The protons of this Cδ have a more positive charge due to its proximity to the N atom of the proline ring, providing a more electrostatic interaction for the Cδ-H···O bond **[14]**. This feature may compensate for the lack of a conventional hydrogen bond, and may play a significant role in the transmission of conformational changes along the helix. Another possible role of Pro side chains may come from the *cis-trans* isomerization of the peptidyl prolyl bonds, facilitating the movement of a part of the helix **[15]**. Thus, proline can act as a hinge, changing the path of the transmembrane helix, and becoming an efficient mechanism in switching the conformation in transport proteins. However, at present there is still no definite answer about the relative importance of the different structural/functional roles in which Pro residues in transmembrane helices can participate: static or dynamical or both? Conflicting reports have been published in this respect. According to Nilsson et al. **[16]**, proline residues appear to have no gross conformational effects when placed centrally in the transmembrane helix. Other works emphasize a role for helix–helix interactions **[17, 18]**, or give importance to

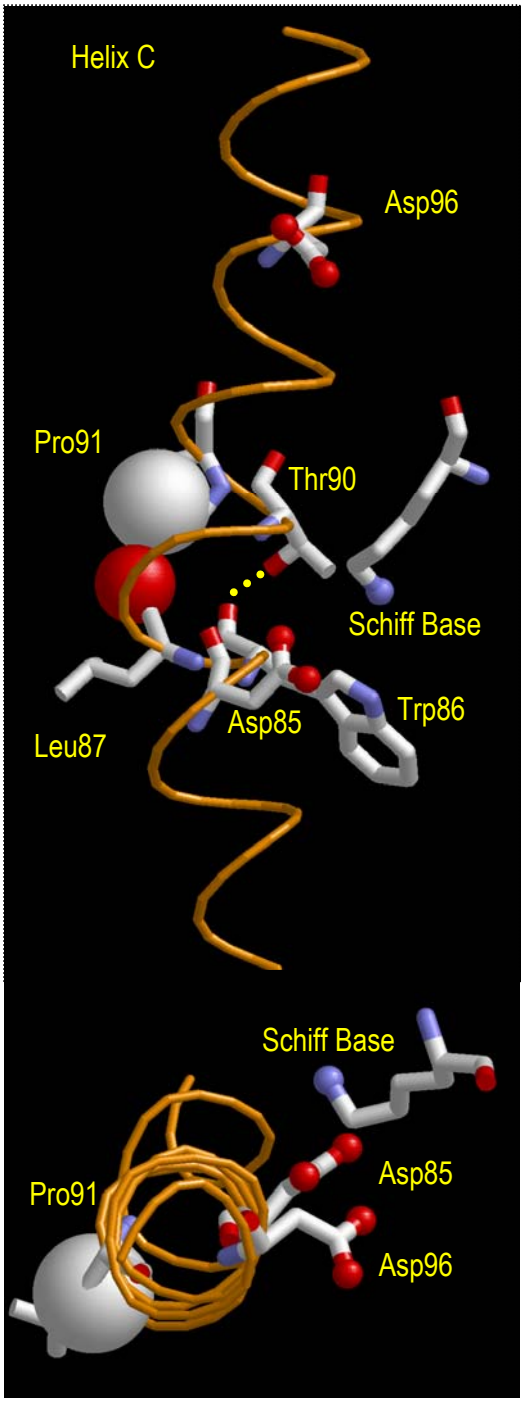

Fig. V.1. Diagram of the helix C. *Up*, plot of the steric clash induced by Pro91 and Leu87. Proton pumping related groups are displayed. Thr90 and Trp86 hydrogen bond enhances the kink in Helix C. *Down*, The clash prevents Asp85 and Asp96 from moving further away the Schiff Base (PDB coordinates from 1M0L).

the particular nature of the side chain **[19, 20]**. Recently, studies have revealed the modulation of proline kinks in α helices through Ser and Thr side chains, enhancing or attenuating the bend of the helix **[21]**.

Bacteriorhodopsin (BR) constitutes a suitable model for the analysis of the role of transmembrane proline residues for several reasons, but especially because the 3D structures of wild type and several mutants are known **[20, 22]** and it is possible to perform structural and functional analyses under native conditions (purple membrane). To provide experimental evidence about the role of Pro side chains we analyze the structural and functional consequences of changing separately each of the three transmembrane Pro residues of BR to Ala. As shown in **Fig. V.2**, these residues are located in helix B (Pro-50), helix C (Pro-91) and helix F (Pro-186) and may act as hinges, permitting changes in the accessibility of regions of the protein and so facilitate the transit of the proton. Pro-91 and Pro-186 are fully conserved among the 25 known archaeal rhodopsins **[23]**. Interestingly, a high degree of conservation of the α-helix embedded prolines has been demonstrated among BR and the hepta-helical G-protein coupled receptors **[24]** if sequential ordering of the helical domains is ignored, suggesting an important structural role for these prolines. Some reports have already appeared studying the proline residues of BR in particular **[25-31]**. Movements have been detected in the helices where these prolines are embedded **[32-34]** and conformational changes during the photocycle involving prolines have been described **[35, 36]**. Folding experiments **[17]** suggest that all three prolines participate in the formation of the retinal binding pocket, as deduced from altered regeneration dynamics of the apoprotein with retinal. Mutagenesis studies on *E.coli*-reconstituted systems showed altered proton pumping rates, particularly for Pro-186 mutants **[27, 30]**. Even though this system has been recognized to yield results that are not reproducible in the native system **[37]**, these data already suggested a contribution of transmembrane prolines to bacteriorhodopsin structure and/or function. By using the BR mutants expressed in the homologous organism we now extend the earlier studies made on the *E. coli* system **[26, 27, 29, 30]**. We show that Pro to Ala mutations induce strong reduction of transport and cause other important alterations, pointing toward a dynamic role of proline residues in transmembrane helices of BR.

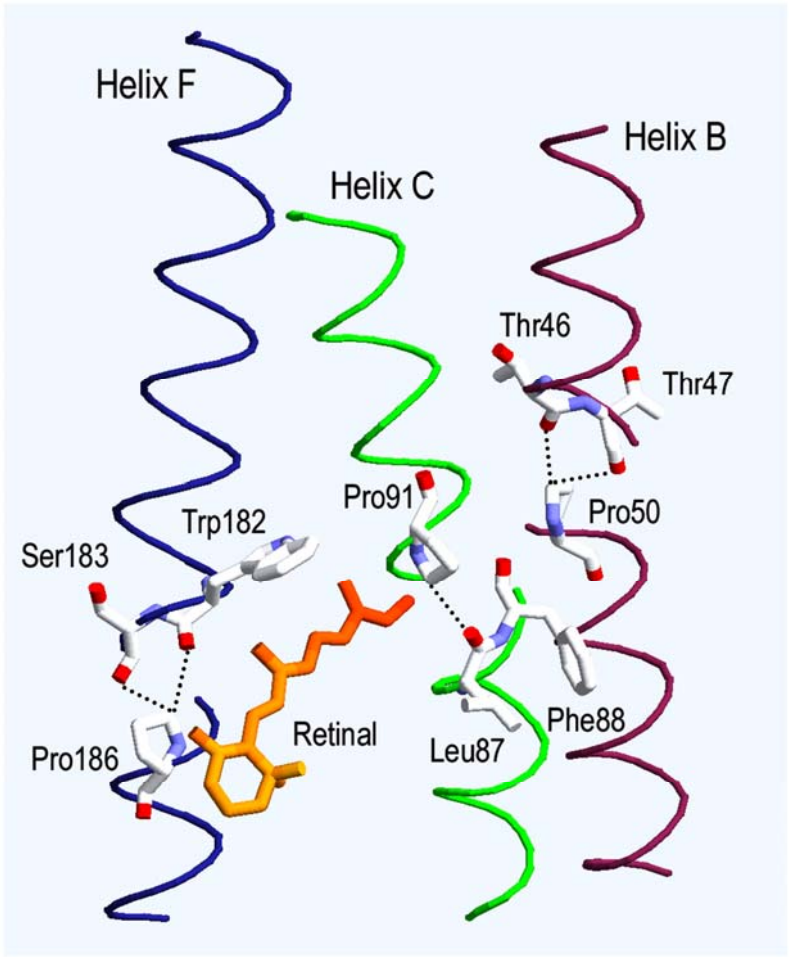

Fig. V.2. Location of transmembrane prolines in bacteriorhodopsin wild type structure (PDB code 1PY6). The C_δ-H···O hydrogen bonds involving Pro residues are plotted taking into account the relative distances shown in Table V.2.

V.2. Materials and Methods

The construction of BR mutants P50A, P91A and P186A was performed through transformation of the plasmid pXL-NovR containing the mutated bop gene in the L33 strain of *Halobacterium salinarum* **[38]**. The expression and isolation of the WT and mutant proteins were done as described in Oesterhelt et al. **[39]**.

pH titrations to obtain pK_a values were carried out by adding micro-volumes of HCl or NaOH solutions to membrane suspensions ($1.5 \cdot 10^{-5}$ M BR). Absorption spectra were taken using an integrative sphere device (to minimize the lose of signal caused by light scattering) placed in a Varian Cary 3 spectrophotometer.

Absorbance changes at 615 nm as a function of pH were used to monitor the purple-to-blue transition. Experimental data were normalized to the largest value at 615 nm and fitted to the Henderson-Hasselbach equation.
Membrane suspensions ($1.5 \cdot 10^{-5}$ M BR) were reacted with 1 M hydroxylamine in a medium containing 150 mM sodium phosphate (pH 7.0). Reactions under light were done using white light of 300 lux of luminance.

Liposome preparation was done as described **[40]**. Proton pumping pH measurements were done by stabilization of the sample at under red dim light at room temperature. The sample was illuminated with yellow-filtered light of a luminance of about $8 \cdot 10^4$ lux on the sample. The initial rate of proton pumping was determined by a linear fit of the pH changes within the first 15 s of illumination.

Dark-light adaptation spectra of purple membrane suspensions ($1.5 \cdot 10^{-5}$ M) were recorded with a Cary Bio3 spectrophotometer, using an integrating sphere when necessary. The difference spectra were obtained by subtracting light-adapted minus dark-adapted samples.

Flash Photolysis transient pH changes in the bulk medium were followed by measuring the absorbance changes of 50 µM pyranine at 460 nm in a purple membrane suspension, in 1M KCl pH 7.0. To obtain the net absorbance changes of pyranine, the traces of samples in the absence of the dye were subtracted from those in its presence. The negative signal of $\Delta\Delta A$ indicates the release of protons by BR (pyranine protonation), whereas the positive signal indicates BR proton uptake. M kinetics of PM suspensions of Pro→Ala mutants in 1M KCl were followed by the acquisition of absorbance spectra at 410nm as a function of time, at pH 6.5 and pH 10.0. Time constants of M rise (τ_{ave}) were obtained from the fitting of the M rise kinetics to a single or a double exponential.

FTIR experiments were performed at 277 K and 243 K with wet and dry samples. The temperature was controlled and maintained using a homemade cell holder and a cryostat. Membrane samples were suspended in 150 mM KCl and either 3 mM carbonate-bicarbonate for pH 10.0 or 3 mM sodium phosphate for pH 7.0. Preparation of membrane films and spectra acquisition was done as described **[41]** with a Bio-Rad FTS6000 spectrometer at 2 cm^{-1} resolution. At least 3 cycles of 350 scans were averaged (i.e. at least 1050 interferograms

were accumulated per spectrum). Difference spectra were calculated by subtracting unphotolyzed BR from the corresponding photointermediate.

C_δ-H···O hydrogen bonding distances were determined for the crystal structures indicated in the Tables using the RasTop software (http://www.geneinfinity.org/rastop).

V.3. Results

Initial Dark State of Bacteriorhodopsin

To monitor the dynamic initial state and possible alterations of the retinal environment in bacteriorhodopsin, we compared the behaviour of the visible spectrum of mutants and their pH dependence (the purple-to-blue transition) with regards to WT. Absorbance maxima of the three Pro mutants in the light or dark-adapted are somewhat shifted (see **Table V.1**), and show altered light-dark adaptation. Upon light adaptation, P50A shows an increase of its absorption coefficient of about 8%, whereas P186A shows 12% increase. The light-dark adaptation of P91A depends on ionic strength as evidenced by the increase of the absorption coefficient, ranging from 0% in water to about 12% in 1 M KCl. This behavior parallels that described for the T90A mutant **[42]**.

The Asp85 pK_a, obtained from the purple-to-blue transition, is altered by an amount depending on the mutant and on the ionic strength (**Table V.1**). In 150 mM KCl, the P186A mutation exerts the most pronounced modification of the Asp85 pK_a, 1.3 pH units, while there is an increase of one pH unit for P50A and only an increase of 0.4 pH units for P91A.

As a means to evaluate changes in dynamics of the path leading to the Schiff base of BR, hydroxylamine accessibility to the Schiff base was measured in the dark. It was found to be greatly increased (see **Fig. V.3A** and **Table V.1**). Both P91A and P50A show a fast reaction with a $t_{1/2}$ of 1.3 and 3 hours, respectively, whereas P186A has a $t_{1/2}$ of 8 hours and WT 160 hours. Therefore, a flexibility increase in the initial state leading to enhanced hydroxylamine accessibility is induced by the substitutions of Pro residues, especially for P50A and P91A, although P186A also shows higher accessibility.

Table V.1 Spectral features of bacteriorhodopsin WT and proline mutants.

	WT	P50A	P91A	P186A
Max. Abs. DA (nm)	558	557	560	563
Max. Abs. LA (nm)	568	564	563	576
pK_a H_2O*	3.2	5.3	3.9	4.5
pK_a 150 mM KCl*	2.7	3.7	3.1	4.0
$t_{1/2}$ NH_2OH Light† (min)	180	1.2/27	0.8/35	46
$t_{1/2}$ NH_2OH Dark (h)†	160	3	1.3	8

*Apparent pK_a of Asp85 values were obtained from the plot of absorption changes as a function of pH.
†Rate of the hydroxylamine reactions were obtained from the exponential fitting to the experimental curves. P50A and P91A, under illumination, show a biexponential fitting, indicating the presence of two components.

To consider the interactions that can be affected upon Pro mutation, we took into account that Pro side chains can establish an alternative kind of hydrogen bond to the oxygen atoms of the i-3 and/or i-4 residues through its C_δ **[13, 14]**. At the same time, a steric clash between the Pro ring and these same carbonyls prevent movements of the Pro towards the i-3 or i-4 residues. In helix C, the steric clash induced by Pro91 is somewhat enhanced, since Trp86 (*i-5*) is also within hydrogen bonding distance. According to the distances in **Table V.2**, Ala50 in P50A may establish a backbone hydrogen bond with Thr46 **[22]**, and Ala186 of P186A may form a 3_{10} helix turn through a hydrogen bond with the i-3 residue. Thus, from a structural point of view, mutation of Pro to Ala does not seem to recover a regular α-helix, but will instead change the local interactions in a helix-dependent manner.

The Light-Activated Bacteriorhodopsin

The accessibility of hydroxylamine to the SB was monitored under light-induced conditions (**Fig. V.3B**, **Table V.1**). Upon illumination, P50A shows a $t_{1/2}$ of 27 min, P91A 35 min and P186A 46 min, as compared to WT that has a $t_{1/2}$ of 180 min. Therefore, Pro mutations increase hydroxylamine accessibility under illumination, as was observed in darkness.

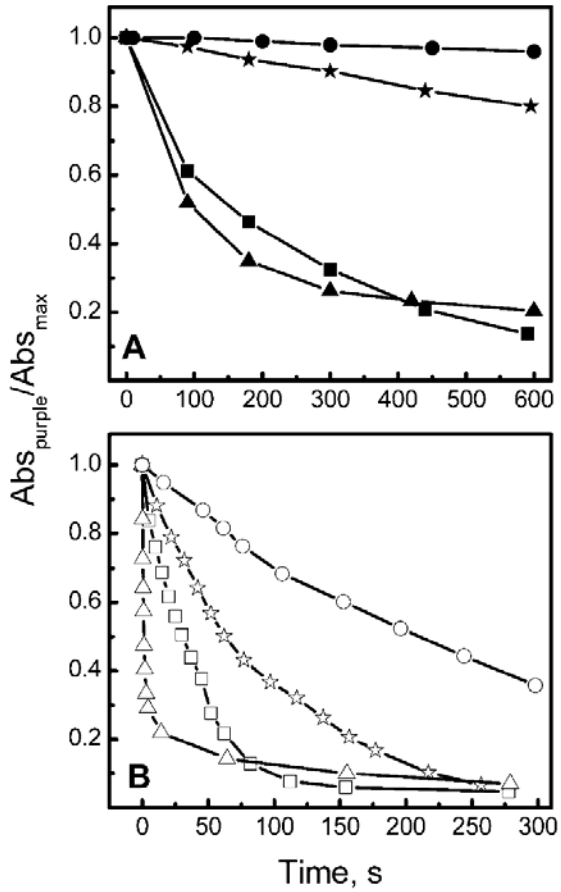

Fig. V.3. Hydroxylamine reactions. (A) Rates of Schiff base accessibility to hydroxylamine in the absence of light recorded for WT (●) and mutants P50A (■), P91A (▲) and P186A (★). (B) Rates of Schiff base accessibility performed under illumination for WT (○), P50A (□), P91A (△) and P186A (☆), using a light of 300 lux of luminance.

To determine possible alterations of the photocycle of the BR Pro mutants, M rise and decay kinetics were acquired by flash photolysis, at pH 6.5, 1 M KCl and room temperature. In all three mutants a rate of M formation higher than WT is apparent (**Fig. V.4**), indicating a faster Schiff base deprotonation. This is in keeping with the reported increase of the rate of light-induced Schiff base

deprotonation for these mutants expressed in *E. coli* and reconstituted into liposomes **[30]**. Virtually no changes were observed for the M decay kinetics.

Table V.2. Distances in Å between $C_{\delta i}$ of Pro (50, 91 and 186) and the peptidyl O of the i-3, i-4 and i-5 residues of bacteriorhodopsin.
The values indicated are the average between the distances of chains A and B of the crystal structure.

		$C\delta_{Pro50}$			**$C\delta_{Pro91}$**			**$C\delta_{Pro186}$**		
Protein	PDB code	O_{Ile46}	O_{Thr46}	O_{Thr47}	O_{Trp86}	O_{Leu87}	O_{Phe88}	O_{Leu181}	O_{Trp182}	O_{Ser183}
WT	1PY6	5.35	2.88	3.06	3.59	3.11	3.54	5.80	3.16	3.16
P50A	1PXR	5.31*	3.26*	3.35*						
P91A	1Q5J				4.25*	4.19*	3.63*			
P186A	1Q5I							5.92*	3.89*	3.17*

*In the case of Pro→Ala mutants, the distance between peptidyl N of Ala and the peptidyl O of i-3, i-4 and i-5 (only for Ala91) residue was measured.

Proton uptake and release upon illumination of WT and mutant pigments in membrane sheets was estimated by using the pH indicator pyranine. **Fig. V.5** shows the pyranine signal obtained at pH 7.2, after a laser flash. Compared to the WT a decrease in the release and uptake for all the three Pro mutants is apparent. P186A is the most affected mutant having about 20% of the amount of proton release and uptake compared to WT, whereas P91A shows about 35% and P50A about 70% (see **Table V.3**).

To monitor the proton pumping activity, purple membrane patches were reconstituted into liposomes **[27, 40]** and the variation of pH in the medium was recorded while illuminating the liposome suspension. Proton pumping activity is altered by the substitution of transmembrane embedded prolines (see **Table V.3** and **Fig. V.6**). The relative proton pumping activity values agree well with pyranine experiments, except in the case of P186A where the pyranine value is about half of that obtained for the liposomes. Irrespective of the causes that

may explain this difference, it is clear that the substitution of the proline side chains at the 91 or 186 positions decrease significantly the proton pumping capacity to less than 45% of WT, as measured by both pyranine and light-induced pH changes.

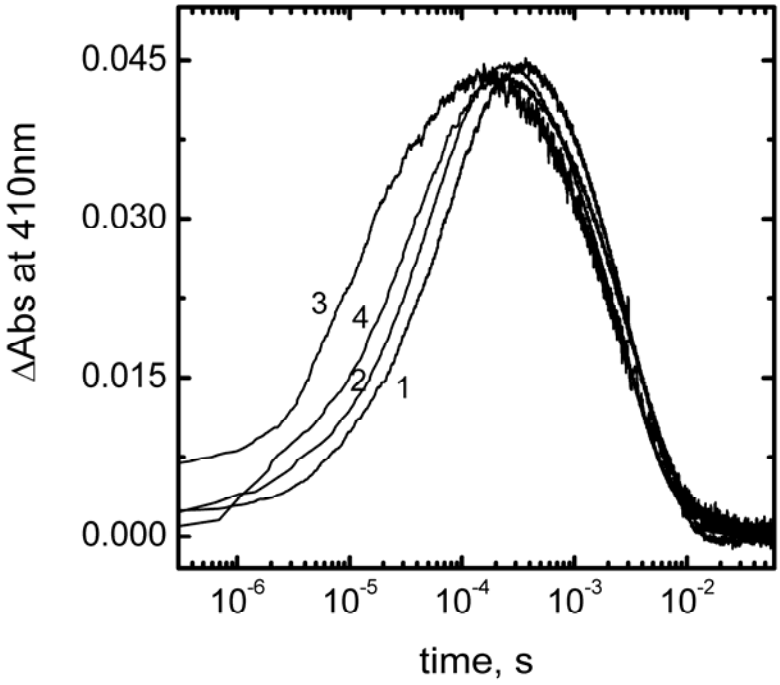

Fig. V.4. Kinetics of M photointermediate. Changes in absorbance at 410 nm of WT (1), P50A (2), P91A (3) and P186A (4) suspensions in 1M KCl, pH 6.5 at room temperature were averaged to determine the time constants of M rise. τ_{ave} were: WT 60 μs, P50A 45 μs, P91A 7 μs and P186A 35 μs.

We used FTIR spectroscopy to determine differences in conformational changes at the level of the photocycle intermediates that could clarify the role of Pro residues in proton transport. To this end, we analyzed the light-induced difference spectra of membrane films under conditions that are known to drive the WT protein to M intermediate (243 K dry film, pH 10), or to N intermediate (277 K, wet film, pH 10). All three mutants showed diverse alterations in the difference spectra obtained under these conditions, as compared to WT pigment.

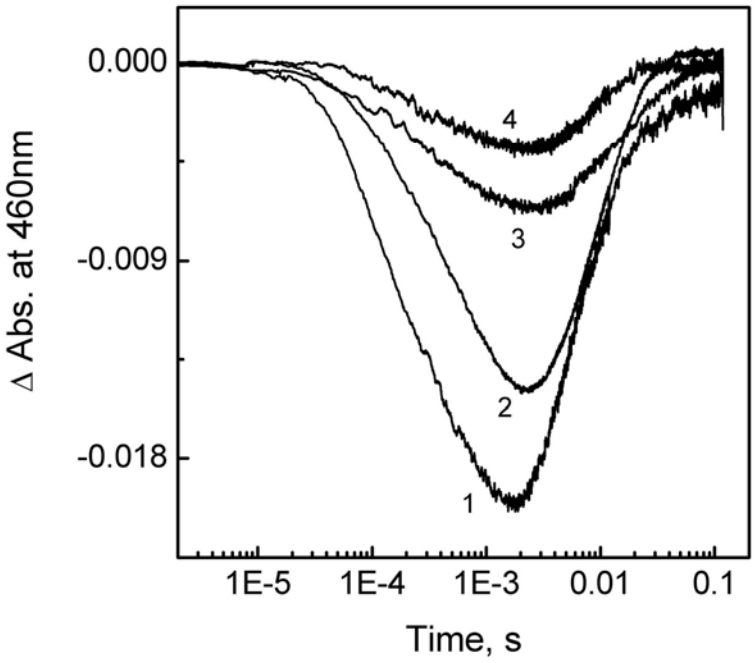

Fig. V.5. Light-induced proton changes as measured with the pH dye pyranine signals. Pyranine absorption changes were measured at 460 nm in suspensions of WT (1), P50A (2), P91A (3) and P186A (4) in 1M KCl (pH 7.2) at 298 K. Proton uptake from BR causes an increase of absorbance, while proton release causes a decrease. Protein concentration, $1.5 \cdot 10^{-5}$ M.

Fig. V.7A presents spectra obtained at 243 K, dry film, pH 10. The WT protein shows a difference spectrum between BR and the M intermediate; M is characterized, among other features, by the positive peak at 1762 cm^{-1} due to Asp85 protonation and by a vibration of retinal at 1186 cm^{-1} below the baseline [43]. Although all three Pro mutants also showed the peak at 1761-1763 cm^{-1} of protonated Asp85, several differences were observed in the rest of the spectrum, compared to WT.

P50A shows changes in the secondary structure, as indicated by changed peaks in the amide region **(Fig. V.7A)**. New positive peaks at 1679 and at 1662 cm^{-1} appear and a broad negative peak at 1649 cm^{-1} replaces the peaks at 1658 and 1641 cm^{-1}. In the amide II region, new peaks appear at 1548 and 1511 cm^{-1}. These differences indicate several variations in the conformational changes accompanying formation of the M intermediate. In the retinal fingerprint region **(Fig. V.7A)**, a small positive band at 1193 cm^{-1} is seen, whereas the negative peak at 1167 cm^{-1}, corresponding to M intermediate C-C stretching vibration of retinal, is absent. Compared to WT, these changes are indicative of a severely altered retinal pocket, which in turn affects the retinal structure.

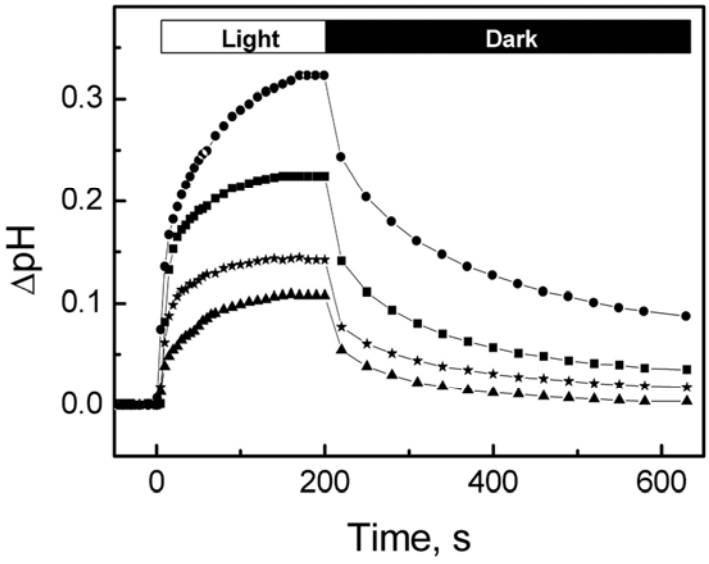

Fig. V.6. Light-induced pH changes of BR-incorporated liposomes as a function of time. WT (●), P50A (■), P91A (▲) and P186A (★). Initial pH, 6.5, in KCl 150 mM.

Table V.3. Bacteriorhodopsin relative proton pumping activity
The values corresponding to the initial rate were obtained by a linear fitting of the first 15 seconds of illumination. The values presented are the average of at least three independent experiments.

	Proton Pumping		
	Liposomes		Pyranine
	Initial Rate	Steady State	
WT	1.00	1.00	1.00
P50A	0.75	0.70	0.70
P91A	0.35	0.35	0.35
P186A	0.40	0.45	0.20

The mutant P91A shows, in the amide region, a positive peak at 1650 cm^{-1} and a more prominent peak at 1554 cm^{-1}, indicative of alterations in α helices. In the retinal region, several major changes are evident. The C_{14}-C_{15} *all trans* vibration at 1201 cm^{-1} is significantly decreased, the peak at 1186 cm^{-1} is

slightly positioned above the baseline, and the peak at 1254 cm^{-1} appears distorted. These alterations demonstrate an altered retinal pocket. Together with the variations observed in the amide region, they indicate a changed conformation of the protein in this intermediate.

In P186A, the negative peaks at 1658 and 1641 cm^{-1} have less intensity, suggesting a lesser amount of protein conformational changes in this M-like intermediate, as compared to WT. The retinal region shows the three peaks at 1254, 1201 and 1167 cm^{-1} with similar intensities among them, whereas for the WT these peaks have very different intensities. This indicates the presence of distortions in the retinal pocket.

Under conditions yielding N intermediate (wet film, 297 K, pH 10) all four spectra show an overall pattern corresponding to N-like intermediate: the Asp85 peak at 1755 cm^{-1} and a positive peak of retinal at 1186 cm^{-1} **(Fig. V.7A)**. Like for the M intermediate, the mutants show several alterations.

P50A presents the most similar spectrum to WT, although it has the negative band of Asp96 at 1744 cm^{-1} and the 1738 cm^{-1} band of Asp115 are more intense. In the amide region, a peak at 1657 cm^{-1} is seen. The retinal region shows only minor changes as compared to WT.

The spectrum of P91A shows the absence of the positive band at 1737cm^{-1}, corresponding to Asp115. In the amide I, the bands at 1626 cm^{-1} corresponding to β sheets and at 1615 cm^{-1} of Pro side chains **[36]** appear slightly changed. The band at 1404 cm^{-1} that is decreased or absent, is of more difficult assignment. It can correspond to symmetric -COO^- stretching vibrations of Asp96 **[44]** or to Pro side chains **[36]**. In the retinal region, a clearly decreased 1201 cm^{-1} negative band and changed 1186 and 1253 cm^{-1} bands indicate a strongly distorted retinal environment. As a whole, these changes point to the presence of variations in the protein structure.

In the carboxylic region, P186A presents a shape very similar to WT. In the amide region, an extra peak at 1658 cm^{-1} is evident, indicating abnormal changes of helices in this intermediate. P186A also shows an increased negative peak at 1640 cm^{-1}. This band has been reported as corresponding in the major part to the C=N stretching vibration of protonated Schiff base **[45]**. As for P91A, the peak at 1404 cm^{-1} is absent in P186A. The retinal fingerprint

region shows that, like for the M intermediate, the three retinal peaks have similar intensity, indicating some distortions of the retinal environment.

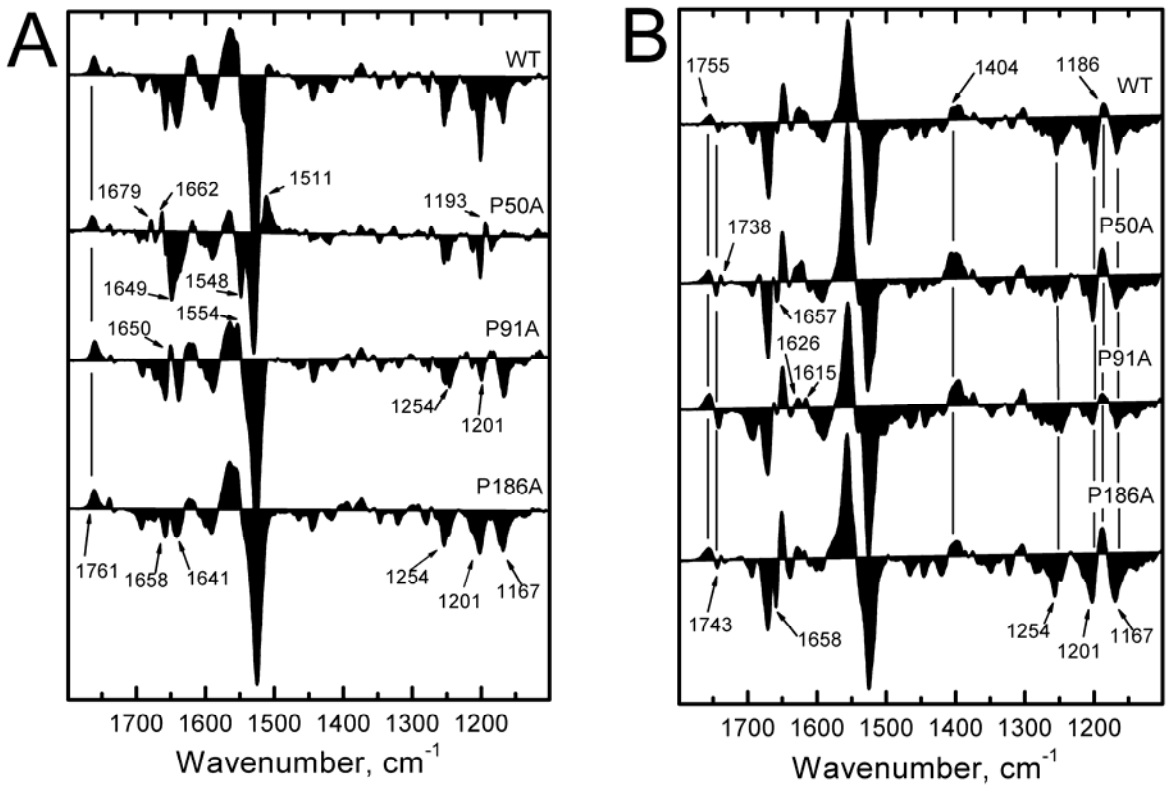

Fig. V.7. A. Fourier transform infrared difference spectra corresponding to BR-M state. Spectra for WT, P50A, P91A and P186A were collected under M-yielding conditions (dry film, pH 10, 243 K). B. Fourier transform infrared difference spectra corresponding to BR-N state. Spectra for WT, P50A, P91A and P186A were collected under N-yielding conditions (wet film, pH 10, 277 K).

V.4. Discussion

The availability of crystal structures of the Ala mutants of the three intra-helical prolines of BR (P50A **[20]**, P91A and P186A **[22]**) provides a unique opportunity of gaining insight into the role, static or dynamic, for transmembrane prolines. As shown by Yohannan et al. **[22]** from a comparison of the $N_{i+4}\cdots O_i$ distance plots of the corresponding crystal structures, mutation of these prolines has little structural consequences. Using the Prokink program **[46]** with the crystal structures **[20, 22, 47]** we have confirmed the presence of only small changes in either the bend angle, the wobble or the face shift of the

corresponding helices among the Pro mutants and the WT (not shown). Therefore, mutation of any of the three transmembrane prolines does not eliminate the bending of the helices, neither induces noticeable conformational changes in the BR resting state. However, our results demonstrate that replacement of these proline residues results in severe alterations of a number of protein properties in both the resting state and in the light-activated states.

Initial-Dark State of Bacteriorhodopsin

In contrast to crystal structures, our experimental results provide a dynamic perspective of the resting state of the protein. All three mutated proteins have a different behaviour in the resting state compared to WT. Hydroxylamine experiments performed in the dark argue for an increased accessibility of the protein, especially for P50A and P91A. Additionally, pK_a and dark-light adaptation appear altered in the mutants. How can these differences be explained in spite of the almost unchanged structures revealed by the crystals? The answer must rely on the conformational dynamics which, in turn, will depend on the set of interactions established by each amino acid.

As is known, Pro side chains can act as hinges that decouples the pre- and post-proline portions of the helix, due to the lack of a regular hydrogen bond. The resulting flexibility is higher than that of a standard helix, but it shows a preferred direction for bending motions because of the necessity to avoid the steric clash with the backbone carbonyl at the i-4 position. In an isolated helix, mutation to Ala will decrease the overall flexibility, but will increase it in the unfavourable direction. It is likely that this same effect is present in helices B, C and F of BR even that a modulation will be exerted by helix-helix interactions. This effect may be important especially for helix C because Pro91 is oriented in such a way that its substitution with Ala will allow motions of the helix away from the proton pathway. This will result in higher accessibility to the solvent molecules and improper location of key side chains of helix C.

Thus, the experimental results can be explained by differences in mobility created by the peculiar behaviour of proline. The inability of crystallography to detect these changes is related to the fact that crystallography yields information on the mean structures of the crystal.

The Light-Activated Bacteriorhodopsin

The decrease of proton transport efficiency argues for strong alterations of the conformational changes associated with the transport process. This is in keeping with the increase in the hydroxylamine accessibility that occurs under illumination, which demonstrates a destabilization of the protein structure during the photocycle.

To get more precise information on the effects of Pro mutations on the photocycle, we analyzed the FTIR difference spectra at the level of the M- and the N-like intermediates. Protonation of Asp85 (band at 1762 cm^{-1}) was found to behave in a near-normal way for both intermediates, as was the case for the Asp96 band at 1742 cm^{-1} in N. Hence, the two principal protein groups directly involved in the transport mechanism have behaviour near to that of WT in this part of the photocycle. Focusing on Asp115, it appears somewhat altered in P91A mutant. This may be explained by the fact that Thr90 makes a hydrogen bond with Asp115 **[48]**. In the amide I region of M intermediate of P50A, an helix alteration is seen agreeing with movements associated to Helix B described in Solid State NMR studies **[31, 49]**.By contrast, the retinal fingerprint region shows significant alterations in all three mutants. This observation, along with other discrete changes observed in the amide region and around 1400 cm^{-1}, indicates that the mutated Pro residues affect principally the protein structural changes at the level of the retinal pocket. On the other hand, the influence of Pro side chains on the dynamics of the retinal pocket and thus on the transport depends on their location in relation to the retinal: Pro91 produces the largest effect whereas Pro50, which is farther, has the least effect. Therefore, the results presented here lead us to conclude that the three Pro residues have a role in allowing the required conformational changes involving the retinal pocket during the photocycle. What is more, it is conceivable that Pro residues, especially Pro91 and Pro186 are mainly responsible for transmitting the conformational changes from the retinal to the rest of the protein. Generally speaking, the absence of the transmembrane Pro can cause futile photocycles, in which the coupling between the retinal changes and proton transport is decreased, and thus the transport efficiency is also decreased.

Concluding remarks

The immediate consequence of our results, when considering the absence of significant structural changes in the resting state of the BR mutants as compared to WT, is that proline residues in transmembrane helices have a dynamic role. It is generally accepted that a Pro located in the middle of a transmembrane helix increases the helix flexibility because the normal hydrogen bonds cannot form **[2, 7]**. On the other hand, Proline is an anisotropic amino acid that avoids certain movements of the helix by the steric clash between Cγ of Pro and the peptydil O of the i-4 residue **[8]**. This hindrance disappears when Pro is substituted to Ala, and the dynamic behaviour of the helix is somewhat shifted, permitting additional movements in the helix. This explains the increase in hydroxilamine accessibility and other altered properties in the resting state. The increased effect on function and stability exerted by P91A mutation may arise not only because this allows movements of the helix toward the exterior of the protein, but also from the fact that Ala91 is unable to establish a hydrogen bond to recover the structure of an average α-helix; this leaves an i-4 free residue, with no typical nor alternative hydrogen bond.

This mobility increase disturbs the correct helical local interactions during the photocycle **[17, 27, 29, 30, 50]**, giving rise to the altered conformational changes of the retinal pocket observed by FTIR and to a decrease in the proton pumping efficiency. A dynamic role for Pro-186, serving as a hinge residue, has been anticipated on the basis of infrared **[51]**, electron diffraction **[34]** and ^{13}C NMR experiments **[49]**. With regards to Pro-91, it is worthwhile to consider the important role of the preceding residue in the helix, Thr-90, in BR function **[40, 42]**. According to these studies, T90A has about 10% of proton pumping activity of WT and there are significant alterations in other properties as the infrared difference spectra. The results about Thr-90 and Pro-91 mutants taken together emphasize the essential contribution of the middle of helix C, in terms of its precise location and flexibility, to the function and dynamics of BR. Thr90-Pro91 motif in Helix C results in a more restrictive steric clash directed to increase the anisotropy of the helix movements. This will allow to respond to the requirements of proton pumping, but avoiding at the same time, detrimental

conformations of the helix such as the induced by Ala mutation in both cases **(FIG. V.1)**. According to crystallographic studies, the deformation of helix C in the L intermediate seems to play a central role in setting the stage for proton transfer **[33]**. In this case, mutation of Pro91 may avoid this conformational change, as mutation of Thr90, decreasing the proton pumping efficiency.

An important role of transmembrane Pro residues has also been proposed for the family of hepta-helical G-protein coupled receptors, implicating these residues in the functional mechanism of signal transduction **[9, 52, 53]**. Specifically, experiments and molecular dynamics simulations revealed conformational changes that are important for receptor activation, produced by a change in the kink of the helix 6 at the level of the conserved Pro **[52, 54-56]**. As is known, direct alignment of BR sequence with those of GPCR gives a poor match **[57, 58]**. However, if the sequential ordering of the helical domains is ignored **[56]**, the three BR transmembrane prolines correspond to conserved GPCR prolines in helices 6, 5 and 4 **[24]**. Therefore, our results give strong support to the important role of Pro residues in this receptor family. As for the BR function, the involvement of Pro side chains in the dynamics of the protein segments defining the substrate pocket can be essential.

More generally, considering a protein as a dynamic system in which the major part of interactions are transient in nature, the relevance of a proline located in a transmembrane helix will not be given by the kink it induces in the resting state, but by its environment. That is, a Pro side chain present in a non-kinked transmembrane helix may develop its dynamic role during the conformational changes involved in the function, without the need of a kink to be observed in the resting state. The proline will act as a singular point in the helix facilitating the flexibility needed for a correct function.-

An important corollary of this work that can be extended to other membrane proteins containing Pro residues in their transmembrane helices is that even that crystal structures of wild type and mutated proteins appear the same, caution should be taken in deriving conclusions about their function. That is, the mutation can alter helix flexibility or the capacity to establish transient interactions, but still have the same structure in the initial state. We fully agree that it is essential not to overlook the importance of dynamical fluctuations about the crystallographic structure **[33]**.

Therefore, direct information about function and structural dynamics should be gained to assess if a Pro replacement leads to functional impairment or not.

V.5. References

1. Bywater, R.P., D. Thomas, and G. Vriend, *A sequence and structural study of transmembrane helices.* J Comput Aided Mol Des, 2001. **15**(6): p. 533-52.
2. Slepkov, E.R., et al., *Proline residues in transmembrane segment IV are critical for activity, expression and targeting of the Na+/H+ exchanger isoform 1.* Biochem J, 2004. **379**(Pt 1): p. 31-8.
3. Deber, C.M. and A.G. Therien, *Putting the beta-breaks on membrane protein misfolding.* Nat Struct Biol, 2002. **9**(5): p. 318-9.
4. Ballesteros, J.A. and H. Weinstein, *Analysis and refinement of criteria for predicting the structure and relative orientations of transmembranal helical domains.* Biophys J, 1992. **62**(1): p. 107-9.
5. Woolfson, D.N. and D.H. Williams, *The influence of proline residues on alpha-helical structure.* FEBS Lett, 1990. **277**(1-2): p. 185-8.
6. Woolfson, D.N., R.J. Mortishire-Smith, and D.H. Williams, *Conserved positioning of proline residues in membrane-spanning helices of ion-channel proteins.* Biochem Biophys Res Commun, 1991. **175**(3): p. 733-7.
7. Cordes, F.S., J.N. Bright, and M.S. Sansom, *Proline-induced distortions of transmembrane helices.* J Mol Biol, 2002. **323**(5): p. 951-60.
8. Bright, J.N. and M.S.P. Sansom, *The flexing/twirling helix: Exploring the flexibility about molecular hinges formed by proline and glycine motifs in transmembrane helices.* Journal of Physical Chemistry B, 2003. **107**(2): p. 627-636.
9. Sansom, M.S. and H. Weinstein, *Hinges, swivels and switches: the role of prolines in signalling via transmembrane alpha-helices.* Trends Pharmacol Sci, 2000. **21**(11): p. 445-51.
10. von Heijne, G., *Proline kinks in transmembrane alpha-helices.* J Mol Biol, 1991. **218**(3): p. 499-503.
11. Reiersen, H. and A.R. Rees, *The hunchback and its neighbours: proline as an environmental modulator.* Trends Biochem Sci, 2001. **26**(11): p. 679-84.
12. Orzáez, M., et al., *Influence of proline residues in transmembrane helix packing.* J Mol Biol, 2004. **335**(2): p. 631-40.
13. Chakrabarti, P. and S. Chakrabarti, *C--H.O hydrogen bond involving proline residues in alpha-helices.* J Mol Biol, 1998. **284**(4): p. 867-73.
14. Bhattacharyya, R. and P. Chakrabarti, *Stereospecific interactions of proline residues in protein structures and complexes.* J Mol Biol, 2003. **331**(4): p. 925-40.
15. Bruns, K., et al., *Structural characterization of the HIV-1 Vpr N terminus: evidence of cis/trans-proline isomerism.* J Biol Chem, 2003. **278**(44): p. 43188-201.
16. Nilsson, I., et al., *Proline-induced disruption of a transmembrane alpha-helix in its natural environment.* J Mol Biol, 1998. **284**(4): p. 1165-75.
17. Lu, H., T. Marti, and P.J. Booth, *Proline residues in transmembrane alpha helices affect the folding of bacteriorhodopsin.* J Mol Biol, 2001. **308**(2): p. 437-46.

18. Curran, A.R. and D.M. Engelman, *Sequence motifs, polar interactions and conformational changes in helical membrane proteins.* Curr Opin Struct Biol, 2003. **13**(4): p. 412-7.
19. Agah, S., J.D. Larson, and M.T. Henzl, *Impact of proline residues on parvalbumin stability.* Biochemistry, 2003. **42**(37): p. 10886-95.
20. Faham, S., et al., *Side-chain contributions to membrane protein structure and stability.* J Mol Biol, 2004. **335**(1): p. 297-305.
21. Deupi, X., et al., *Ser and Thr residues modulate the conformation of pro-kinked transmembrane alpha-helices.* Biophys J, 2004. **86**(1 Pt 1): p. 105-15.
22. Yohannan, S., et al., *The evolution of transmembrane helix kinks and the structural diversity of G protein-coupled receptors.* Proc Natl Acad Sci U S A, 2004. **101**(4): p. 959-63.
23. Ihara, K., et al., *Evolution of the archaeal rhodopsins: evolution rate changes by gene duplication and functional differentiation.* J Mol Biol, 1999. **285**(1): p. 163-74.
24. Metzger, T.G., et al., *An analysis of the conserved residues between halobacterial retinal proteins and G-protein coupled receptors: implications for GPCR modeling.* J Chem Inf Comput Sci, 1996. **36**(4): p. 857-61.
25. Deber, C.M., B.J. Sorrell, and G.Y. Xu, *Conformation of proline residues in bacteriorhodopsin.* Biochem Biophys Res Commun, 1990. **172**(2): p. 862-9.
26. Ahl, P.L., et al., *Effects of amino acid substitutions in the F helix of bacteriorhodopsin. Low temperature ultraviolet/visible difference spectroscopy.* J Biol Chem, 1988. **263**(27): p. 13594-601.
27. Mogi, T., et al., *Structure-function studies on bacteriorhodopsin. VIII. Substitutions of the membrane-embedded prolines 50, 91, and 186: the effects are determined by the substituting amino acids.* J Biol Chem, 1989. **264**(24): p. 14192-6.
28. Engelhard, M., et al., *Solid-state 13C-NMR of [(3-13C)Pro]bacteriorhodopsin and [(4-13C)Pro]bacteriorhodopsin: evidence for a flexible segment of the C-terminal tail.* Eur J Biochem, 1996. **235**(3): p. 526-33.
29. Rothschild, K.J., et al., *Vibrational spectroscopy of bacteriorhodopsin mutants: evidence for the interaction of proline-186 with the retinylidene chromophore.* Biochemistry, 1990. **29**(25): p. 5954-60.
30. Zhang, Y.N., et al., *Effects of mutagenetic substitution of prolines on the rate of deprotonation and reprotonation of the Schiff base during the photocycle of bacteriorhodopsin.* Photochem Photobiol, 1993. **57**(6): p. 1027-31.
31. Lansing, J.C., et al., *Solid-state NMR investigation of the buried X-proline peptide bonds of bacteriorhodopsin.* Biochemistry, 2003. **42**(12): p. 3586-93.
32. Kouyama, T., et al., *Crystal structure of the L intermediate of bacteriorhodopsin: evidence for vertical translocation of a water molecule during the proton pumping cycle.* J Mol Biol, 2004. **335**(2): p. 531-46.
33. Edman, K., et al., *Deformation of helix C in the low temperature L-intermediate of bacteriorhodopsin.* J Biol Chem, 2004. **279**(3): p. 2147-58.

34. Subramaniam, S. and R. Henderson, *Molecular mechanism of vectorial proton translocation by bacteriorhodopsin.* Nature, 2000. **406**(6796): p. 653-7.
35. Rothschild, K.J., et al., *Fourier transform infrared evidence for proline structural changes during the bacteriorhodopsin photocycle.* Proc Natl Acad Sci U S A, 1989. **86**(24): p. 9832-5.
36. Gerwert, K., B. Hess, and M. Engelhard, *Proline residues undergo structural changes during proton pumping in bacteriorhodopsin.* FEBS Lett, 1990. **261**(2): p. 449-454.
37. Needleman, R., et al., *Properties of Asp212----Asn bacteriorhodopsin suggest that Asp212 and Asp85 both participate in a counterion and proton acceptor complex near the Schiff base.* J Biol Chem, 1991. **266**(18): p. 11478-84.
38. Sanz, C., et al., *Opening the Schiff base moiety of bacteriorhodopsin by mutation of the four extracellular Glu side chains.* FEBS Lett, 1999. **456**(1): p. 191-5.
39. Oesterhelt, D. and W. Stoeckenius, *Isolation of the cell membrane of Halobacterium halobium and its fractionation into red and purple membrane.* Methods Enzymol, 1974. **31**: p. 667-78.
40. Perálvarez, A., et al., *Thr90 is a key residue of the bacteriorhodopsin proton pumping mechanism.* FEBS Lett, 2001. **508**(3): p. 399-402.
41. Lazarova, T. and E. Padros, *Helical and reverse turn changes in the BR->N transition of bacteriorhodopsin.* Biochemistry, 1996. **35**(25): p. 8354-8.
42. Perálvarez-Marín, A., et al., *Thr-90 plays a vital role in the structure and function of bacteriorhodopsin.* J Biol Chem, 2004. **279**(16): p. 16403-9.
43. Braiman, M.S., P.L. Ahl, and K.J. Rothschild, *Millisecond Fourier-transform infrared difference spectra of bacteriorhodopsin's M412 photoproduct.* Proc Natl Acad Sci U S A, 1987. **84**(15): p. 5221-5.
44. Dioumaev, A.K., et al., *Coupling of the reisomerization of the retinal, proton uptake, and reprotonation of Asp-96 in the N photointermediate of bacteriorhodopsin.* Biochemistry, 2001. **40**(38): p. 11308-17.
45. Earnest, T.N., J. Herzfeld, and K.J. Rothschild, *Polarized Fourier transform infrared spectroscopy of bacteriorhodopsin. Transmembrane alpha helices are resistant to hydrogen/deuterium exchange.* Biophys J, 1990. **58**(6): p. 1539-46.
46. Visiers, I., B.B. Braunheim, and H. Weinstein, *Prokink: a protocol for numerical evaluation of helix distortions by proline.* Protein Eng, 2000. **13**(9): p. 603-6.
47. Faham, S. and J.U. Bowie, *Bicelle crystallization: a new method for crystallizing membrane proteins yields a monomeric bacteriorhodopsin structure.* J Mol Biol, 2002. **316**(1): p. 1-6.
48. Luecke, H., et al., *Structure of bacteriorhodopsin at 1.55 A resolution.* J Mol Biol, 1999. **291**(4): p. 899-911.
49. Kira, A., et al., *Significance of low-frequency local fluctuation motions in the transmembrane B and C alpha-helices of bacteriorhodopsin, to facilitate efficient proton uptake from the cytoplasmic surface, as revealed by site-directed solid-state (13)C NMR.* Eur Biophys J, 2004.

50. Rothschild, K.J., et al., *Conserved amino acids in F-helix of bacteriorhodopsin form part of a retinal binding pocket.* FEBS Lett, 1989. **250**(2): p. 448-52.
51. Ludlam, C.F., et al., *Site-directed isotope labeling and ATR-FTIR difference spectroscopy of bacteriorhodopsin: the peptide carbonyl group of Tyr 185 is structurally active during the bR-->N transition.* Biochemistry, 1995. **34**(1): p. 2-6.
52. Gether, U., *Uncovering molecular mechanisms involved in activation of G protein-coupled receptors.* Endocr Rev, 2000. **21**(1): p. 90-113.
53. Stitham, J., K.A. Martin, and J. Hwa, *The critical role of transmembrane prolines in human prostacyclin receptor activation.* Mol Pharmacol, 2002. **61**(5): p. 1202-10.
54. Chen, S., et al., *Mutation of a single TMVI residue, Phe(282), in the beta(2)-adrenergic receptor results in structurally distinct activated receptor conformations.* Biochemistry, 2002. **41**(19): p. 6045-53.
55. Jensen, A.D., et al., *Agonist-induced conformational changes at the cytoplasmic side of transmembrane segment 6 in the beta 2 adrenergic receptor mapped by site-selective fluorescent labeling.* J Biol Chem, 2001. **276**(12): p. 9279-90.
56. Pardo, L., et al., *On the use of the transmembrane domain of bacteriorhodopsin as a template for modeling the three-dimensional structure of guanine nucleotide-binding regulatory protein-coupled receptors.* Proc Natl Acad Sci U S A, 1992. **89**(9): p. 4009-12.
57. Hibert, M.F., et al., *Three-dimensional models of neurotransmitter G-binding protein-coupled receptors.* Mol Pharmacol, 1991. **40**(1): p. 8-15.
58. Trumpp-Kallmeyer, S., et al., *Modeling of G-protein-coupled receptors: application to dopamine, adrenaline, serotonin, acetylcholine, and mammalian opsin receptors.* J Med Chem, 1992. **35**(19): p. 3448-62.

So where do we go? And what should we do?
And why is the table set for two?
Is the answer in the question?
I need some more suggestions
MxPx

CHAPTER VI.

Analyzing the contribution of Helix-embedded Prolines to the stability of Bacteriorhodopsin.

Abstract

Denaturation experiments have been long used for determining protein structure properties. Simulation studies and experimental methods are used here for analyzing the thermal stability of Bacteriorhodopsin. A comparison of the native protein against mutants of transmembrane prolines has been performed to gain additional information on the role of prolines in transmembrane helices.

Floppy Inclusion and Rigid Substructure Topography simulations provide a good approach when complemented with experimental data to identify regions relevant for the structure of the protein. Simulation and experimental techniques agrees in a less stable structure for P186A mutant. From UV-Vis thermal denaturation experiments, a dependence on the pH is found for P91A, showing a less stable structure at acid pH than the native protein. In the case of P50A, no significant differences with the native protein are found either in simulation studies or in experimental data.

VI.1. Introduction

The structure of a protein is a relevant aspect directly related to its function. Folding is the process that derives in a functional structure. Therefore, unfolding (reversible) and denaturing (irreversible) are processes that yield structural information on the process of losing the structure. As a matter of fact, unfolding and denaturing of protein are techniques often more used than folding, because they are easier to be traced experimentally and they are also guessed to predict folding **(*1*)**. The study of transmembrane proteins is in this aspect even more difficult. To perform folding studies, even some denaturing conditions may occur, as solubilizing the protein to remove lipids to later on try to incorporate it in model membranes containing lipids that does not fit the natural environment where the protein resides and performs its function **(*2-5*)**. By this, unfolding and/or denaturing experiments have become a suitable alternative to study the structural behaviour of a protein, and the relevant residues and domains involved both in folding and in keeping the structure. In addition, the development of biological processes simulation tools and molecular dynamics has open a new field of study to identify the residues of the primary sequence that are more relevant for the fully functional structure of a protein. In this way, the unfolding of Rhodopsin has been simulated recently **(*6*)** by the Floppy Inclusion and Rigid Substructure Topography (FIRST) method applied to the crystal structure of this protein (PDB code 1L9H). By this, they have identified amino acids that contribute to the structural stability core of the protein.

In the case of Bacteriorhodopsin, several experimental data on folding/unfolding and denaturing are available **(*7-16*)**. Nevertheless, biophysical techniques do not provide a high resolution image of the atomic events occurring during the denaturing process. As an approach, we pretend to relate the results of the simulation of a thermal denaturation of the protein in the crystal structure with experimental denaturation of the protein in suspension. Summing up experimental evidences with simulation studies may yield some information on how the losing of some interactions or some alterations of the native structure such as mutations may affect local domains. The FIRST

analysis may also be a useful tool for determining subtle differences among similar crystal structures and even for validating the quality of the structure.

Here, a comparison between experimental thermal denaturation and simulated protein unfolding of Bacteriorhodopsin WT and transmembrane proline mutants is presented. In addition we present a comparison of the crystal structure of the native protein against single proline mutants recently published (***17, 18***). In this way, we try to gain information about the structural alterations induced by mutation of these Pro side chains.

VI.2. Materials & Methods

Expression of protein samples

The construction of BR mutants P50A, P91A and P186A and the expression and purification of the Purple Membrane in *Halobacterium salinarum* was carried out as described (***19***).

UV-Vis Thermal Stability

Analysis of thermal stability of dark-adapted Purple membrane samples in H_2O ($0.75 \cdot 10^{-5}$ M) at pH 4.0 and 7.0 was carried out by recording absorption spectra in the UV-visible range during thermal ramps of 5ºC steps, from 20 to 105ºC in a Cary Bio3 spectrophotometer. Samples were allowed to stabilize for 8 min at each temperature. The absorbance changes at 560 nm are observed to monitor the denaturation of the chromoprotein through the release of retinal although other species appear before (see Results). The disappearance of the retinal-protein associated form fits with a sigmoid function **Fig. VI.1a**. This fitting provides a T_m for the reaction that corresponds to a transition state when 50% of the molecules have the retinal linked and 50% have the retinal bleached. The first derivative of this sigmoid yields a one peak (transition) curve corresponding to the T_m of the reaction **Fig VI.1b**.

Simulated Thermal Denaturation

FIRST (Floppy Inclusion and Rigid Substructure Topography) is a software developed to predict and analyze protein flexibility (***6, 20-22***) upon hydrogen-

bond breaking. This algorithm counts and identifies the bond-rotational degrees of freedom in a directed graph (PDB file), whose vertices represent protein atoms and whose edges represent covalent and non-covalent (hydrogen-bond and hydrophobic) constraints within the protein. This software focus on flexible regions (underconstrained) and rigid clusters. FIRST defines a rigid cluster as a collection of interlocked bonds in which no relative motion can be achieved without a cost in energy. On one hand, a rigid cluster that does not contain redundant bond constraints is minimally rigid (isostatic). On the other hand, a rigid cluster that contains redundant bond constraints (overconstrained) introduces stress in this region, which becomes more stable than an isostatic one. An overconstrained cluster remains rigid despite one bond breaks. FIRST detect collective motions, which are associated to a couple of rotable bonds, and occur within a particular flexible region. Thus, this software analyzes and quantifies the rigidity or flexibility of a protein using a graphic model (PDB atomic coordinates). The WEB version of this software at http://flexweb.asu.edu/firstweb/firstweb_index.html provides the chance to run the software on PDB crystal structures online. We submitted the chain A of the structures for WT (1PY6), P50A (1PXR), P91A (1Q5J) and P186A (1Q5I) mutants of BR after preprocessing the coordinates as follows:

- Addition of hydrogen atoms by Whatif software **(*23*)**.
- Removing exposed water molecules determined by PROACT **(*24*)**.

Once the molecule is processed, the submission involves setting certain parameters as the Energy cutoff and the Radius of the hydrophobic function. The values of -0.1 Kcal/mol for Energy Cutoff (hydrogen bonding energy) and 0.5 Å of Radius in Function 2 (hydrophobicity) were used **(*25*)**.

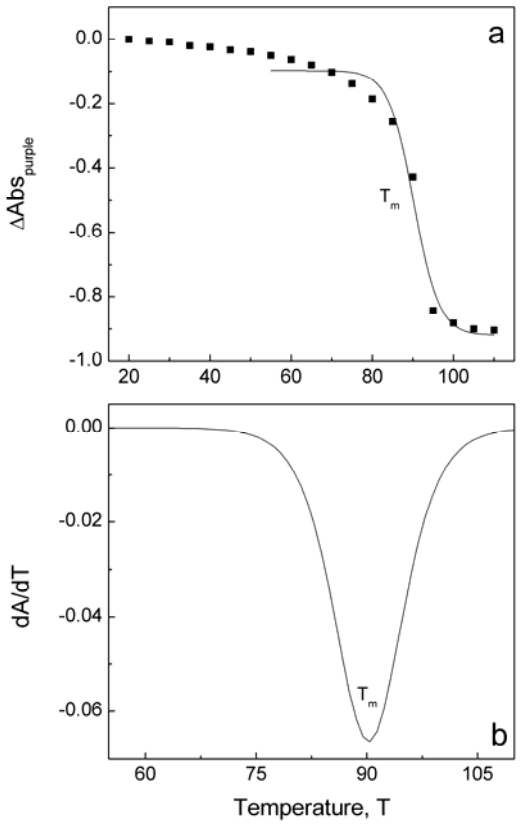

FIG VI.1. (a) Plot of the ΔAbs at 560nm as a function of temperature for WT Bacteriorhodopsin. The fitting to a sigmoid function is also displayed. The T_m corresponds to the inflexion point of the function. (b) The first derivative of the sigmoid function in (a) is represented. It yields a one peak curve corresponding to the T_m of the reaction.

This software generates a set of output data; the following plots are taken into account:

- Representation of the order parameter **Fig. VI.2a**: The fraction of the number of atoms participating in the largest cluster, X_c as a function of the mean coordination, <r>, i.e., the average number of neighbors for each atom. This plot determines the most relevant steps in simulating the denaturation process, defined as the Native state, Transition state and Denaturated state.
- The plot of the 2nd derivative of the number of floppy modes (the available degrees of freedom) with respect to <r>, is also used as a specific heat-like curve to relate it to transition state in experimental data **Fig. VI.2a**.

- Hydrogen bonding dilution plot: determines which residues remain rigid along a specific heat-like curve. It is used for the representation of the remaining rigid cluster during the protein denaturation.

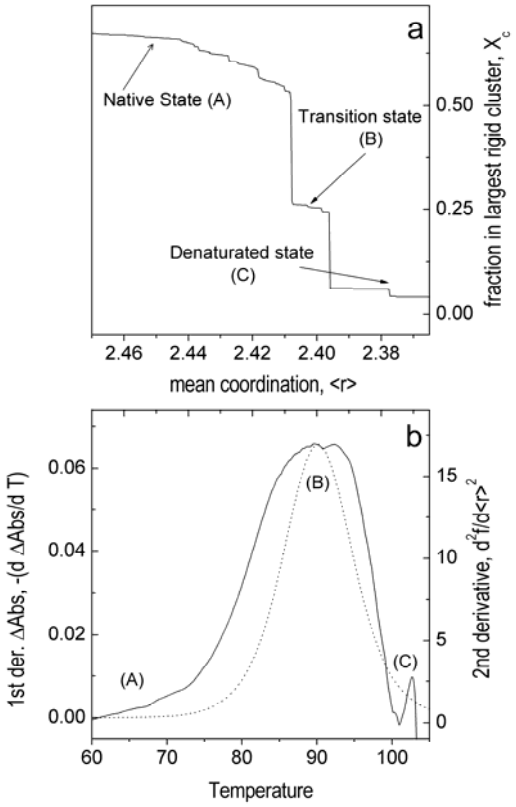

Fig VI.2. (a) Order parameter of the denaturation simulation of Bacteriorhodopsin. It corresponds to the fraction of the number of atoms participating in the largest cluster (X_c) as a function of the mean coordination number <r>. (b) Composite graph of the negative of the 1st derivative of ΔAbs at 560nm (Y, left) as a function of the temperature (X, bottom) and the 2nd derivative of the number of floppy modes (Y, right) with respect to <r> (X, top). Both the order parameter and the 2nd derivative serves as indicators of the different states occurring during the denaturation of BR. It should be pointed out that no correspondence between the particular values of temperature and <r> is proposed in this plot; it is used solely to suggest that some sort of relationship is likely to exist between both magnitudes when considering the denaturation process of a protein.

VI.3. Results & Discussion

UV-Vis Thermal stability

Spectral changes in the visible absorption band of the chromoprotein give information about protein conformational changes that finally gives rise to denaturation of the retinal binding pocket resulting in retinal release. When

membrane suspensions are gradually heated, the structural dynamics of the protein varies a set of events occur prior to the denaturation of the protein. The rising and fading of different species is represented in UV-Vis difference spectra by the increase or decrease the absorbance at certain wavelengths **Fig. VI.3**.Thermal stability experiments at pH 7.0 shows at 630 nm the blue form appearance as a function of temperature at about 50ºC. This form comes from the release of cations and the subsequent partial protonation of Asp85 due to a change in its pK_a (***26***). At about 70ºC appears the red form (460 nm). Finally, at about 80ºC, the protein begins to denaturate and the free retinal absorption band (380 nm) appears. At about 100ºC, the protein appears fully denaturated. Focusing on P91A mutant, it is remarkable the absence of the blue form, indicating a distortion of Asp85 environment or the absence of bound cations. At pH 4.0, it is remarkable the fact that all proline substituted mutants present an absence of the blue form (630 nm) arguing for altered Asp85 surroundings induced by mutation (data not shown). Working at pH 4.0 implies that in the mutants the experiments are performed at or below the Asp85 pKa, while for WT the experiment is done over the pKa of Asp85 (see **Table V.1**).

TABLE VI.1.

Identification of the three main states during simulated denaturation. T_m for the experimental transition state.

	WT	P50A	P91A	P186A
T_m[a] pH 7.0	90.5ºC	91.5ºC	88.4ºC	85.1ºC
T_m[a] pH 4.0	68.1ºC	71.1ºC	53.5ºC	71.7ºC
Native State[b]	2.45	2.45	2.45	2.45
Transition State[b]	2.401	2.398	2.396	2.399
Denaturated State[b]	2.374	2.373	2.374	2.371
Energy related to Transition State[c] (Kcal/mol)	-3.31	-3.05	-3.05	-2.64

[a] T_m value obtained from the sigmoid fitting of the experimental data.
[b] The three main states are identified by the order parameter and the 2nd derivative of the floppy modes as a function of the mean coordination.
[c] Energy of the broken hydrogen bond corresponding to the Transition state, displayed in the 2nd column of the dilution plot Fig. VI.4.

When the T_m for the denaturation of the WT protein and the mutants at pH 7.0 are compared **Table VI.1, Fig. VI.4c**, no severe alterations are found for P50A, P91A is slightly decreased and P186A presents a decrease of 4ºC. However, at pH 4.0 where the protein is less stable, the most affected sample is P91A, with a decrease of about 15ºC while P50A and P186A are somewhat increased. This may be explained by the Asp85 pK_a, because at this pH Asp85 is partially protonated and the distorted environment of this residue (the Schiff Base counter-ion) in this mutant, may favour the release of retinal, decreasing severely the thermal stability of the P91A protein.

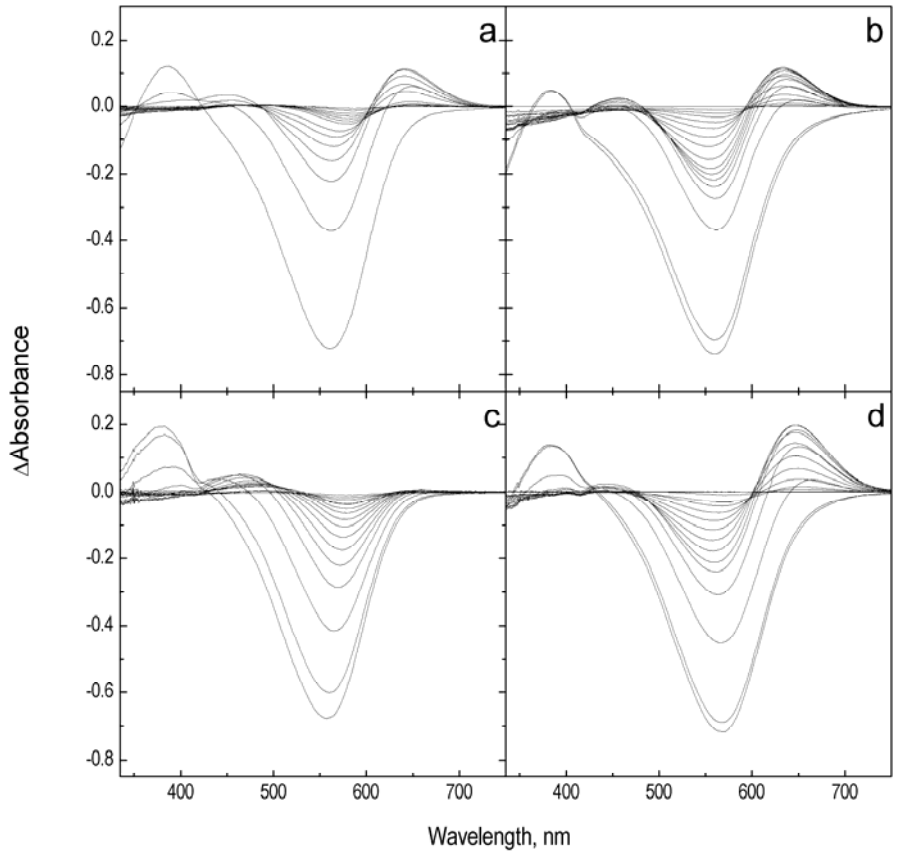

Fig. VI.3. Difference spectra of the UV-Vis thermal denaturation of BR. (a) WT; (b) P50A; (c) P91A; (d) P186A. Gradual heating of PM samples at pH 7.0 was performed. The curves correspond to the difference of absorbance spectra taken at each temperature step minus 20ºC one.

Simulated Thermal Denaturation

FIRST simulates a thermal denaturation by breaking hydrogen bonds one by one in a protein and evaluating the consequences in terms of flexibility/rigidity induced by this breaking (***6, 20-22***) . It assumes the system as a protein bond

network consisting of covalent bonds, hydrogen bonds, and hydrophobic interactions. As a main output, it generates a hydrogen bond dilution plot consisting of colored regions (***6, 21***). The colored regions display rigid clusters and the thin black lines represent flexible ones along the protein sequence as the denaturation process occurs **FIG VI.4**.

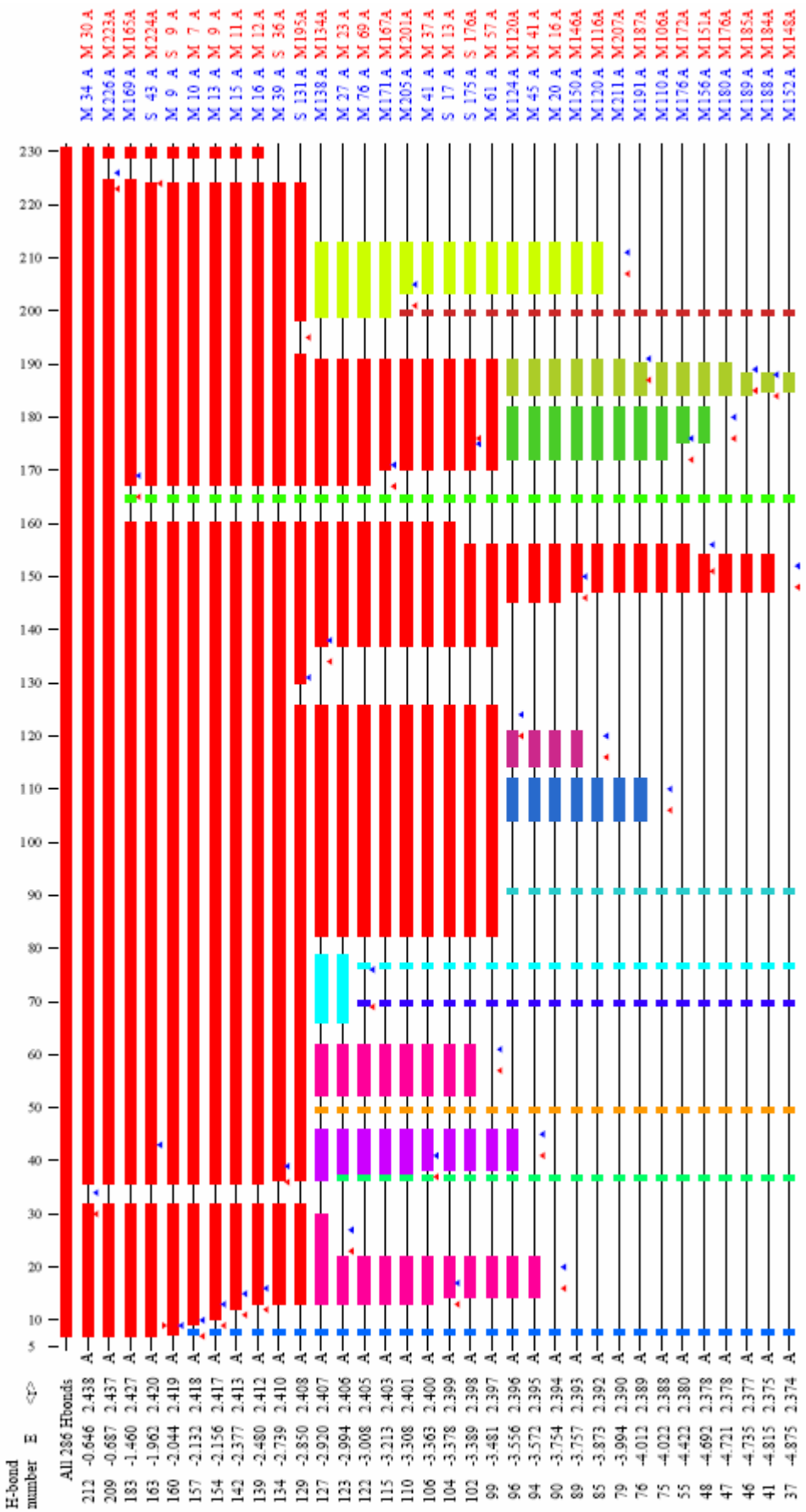

Fig. VI.4. Hydrogen dilution plot for chain A of the crystal structure of WT Bacteriorhodopsin (1py6). From left to right, in the first column the number of hydrogen bonds remaining in the structure is displayed. The Energy of the removed hydrogen bond is in the 2nd column. The 3rd column displays the average number of atom neighbours for the atoms involved in the hydrogen bond. The following item, the dilution plot, is a linear representation of the protein structure, divided in rigid (thick colored) and flexible regions (thin black lines). The two last colums represent the donor (blue) and acceptor (red) of the broken hydrogen bond at each dilution step. Taking into account if the atoms involved are from the main chain (backbone) or from the side chain of the amino acid, a M or a S is respectively written. To easily identify where the residues are located, small red and blue arrows are plotted in the dilution plot.

Once the thermal denaturation is performed, the three main states can be assigned by means of the dilution plot by considering the mean coordination <r>, which is taken as a measure of the average number of neighbors for each atom **Fig. VI.5a, b**. Then, the mean coordination assigned for each state in each mutant is shown in **Table VI.1**. The native state has been previously defined as 2.45 (***21***). No significant differences are seen for Transition neither for Denaturation state.

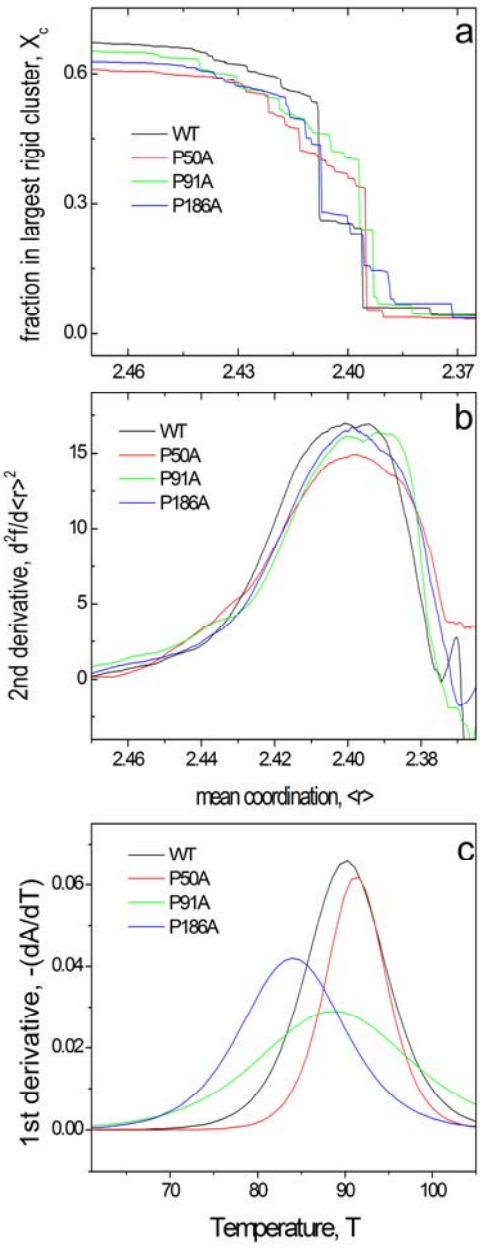

Fig. VI.5. (a) Order parameter (see legend to Fig VI.2.) of the PDB structures of WT (1py6), P50A (1pxr), P91A (1q5j) and P186A (1q5i). (b) 2nd derivative of the floppy modes for the indicated structures. Related to the order parameter by the mean coordination, the values for the main states of the simulation of each structure are represented in Table VI.1. (c) The T_m for the UV-Vis Thermal denaturation are displayed for WT and mutant proteins.

For each state, the Energy of the hydrogen bond recently broken is shown (**Fig. VI.4**). In the case of the transition state the Energy assigned for the broken hydrogen bond at this point reveal subtle differences for P50A (1pxr) and P91A (1q5j) when comparing with the crystal structure of WT BR (1py6) (**Table VI.1**). In the case of P186A (1q5i) a higher difference is observable indicating a less stable structure.

Simulated vs. UV-Vis Thermal Denaturation

In **Fig. VI.6** the dilution plots corresponding to the transition state for the Bacteriorhodopsin structures are represented. The fraction of rigid structure remaining in this state indicates that, compared to WT (fraction of 0.61), the mutants present almost no difference, P50A (0.67), P91A (0.67) and P186A (0.57). Thus, the differences in simulated thermal denaturation are more qualitative than quantitative, i.e. the distribution of the hydrogen bond and the hydrophobic interactions breaking in the 3D structures may play a critical role. **Fig VI.6** shows that there are differences in the rigid clusters remaining in the transition state. For example, P186A retains a small cluster of about 5 amino acids in helix G. This may be related to the lower thermal stability of the retinal pocket of this mutant (**Fig. VI.5c** and **Table VI.1**). The lower energy assigned to the hydrogen bond just broken to yield the Transition state in P186A mutant, may be related with a less stable structure coinciding with a lower T_m in UV-Vis experiments at pH 7.0 (see **Table VI.1**). On the other hand, the shape of the experimental thermal transition of the mutants **Fig. VI.5c** indicates differences in the cooperativity of the transition. In this way, the case of P91A is somewhat significant, because despite having a slightly lower T_m, however it shows a less cooperative or a slower denaturation, fact that can be related with apparent no quantitative changes in the simulation. It is remarkable the fact that both experimental and simulation results, argues for a less stable structure for P186A.

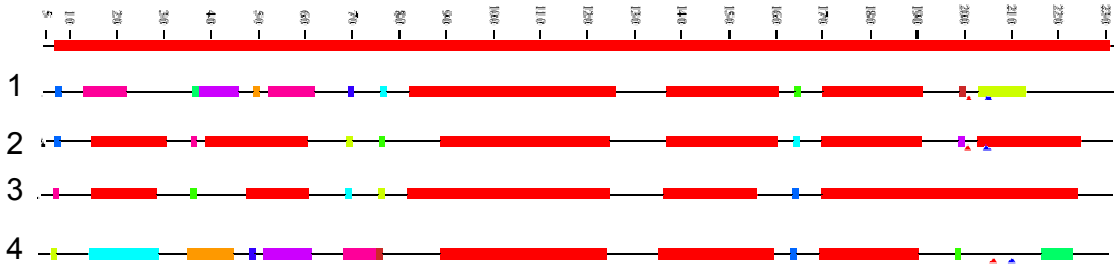

Fig. VI.6. Remaining rigid structure in the transition state obtained by simulated denaturation. (1) WT; (2) P50A; (3) P91A; (4) P186A. The thick colored regions correspond to rigid clusters and the thin black lines represent flexible ones. This linear representations are extracted from the respective hydrogen dilution plot (see Fig. VI.4)

In **Fig. VI.7**, the 3D display of each main state tries to emulate what happens in experimental conditions. Nevertheless, is known from FTIR thermal denaturation experiments **(*9*)**, that despite reaching the denaturation of the protein, the major part of the α-helical architecture is not lost in this state. So, the almost random coil assigned for the simulation of the denaturated state indicates the difficulty in relating the experimental data to the theoretical estimations. In this case, the main obstacle appears when one tries to link the temperature of the sample with the mean coordination <r>. It might be that the denaturated final state of the simulation may correspond to a temperature far over 100ºC. On the other hand, it is obvious that the FIRST analysis takes into account only the crystal structure of the protein in the crystal state, without considering the influence of the paracrystalline arrangement of BR molecules in the native membrane. Is in the case of the transition state where more information can be related to experimental transition state. In the case of P186A **Fig. VI.7**, a more affected or open structure is observable, going in the same direction of experimental results. Evidenced in **Fig. VI.6** and **Fig. VI.7**, appears the relevance of the C-D loop, which in the transition state still remains rigid. This fact goes in the same direction as the motif Thr90-Pro91 may play in the correct placing of Helix C **(CHAPTER V)**. C-D loop due to its short length (only 1 residue) may be an additional mechanism to avoid detrimental dynamics of Helix C, and preventing the misplacing of relevant residues in the proton pumping function of the protein (i.e. Asp85, Asp96 and Arg82). This loop is also evidenced as determinant by the impossibility of expressing mutant which possesses a longer loop at this position (data not shown).

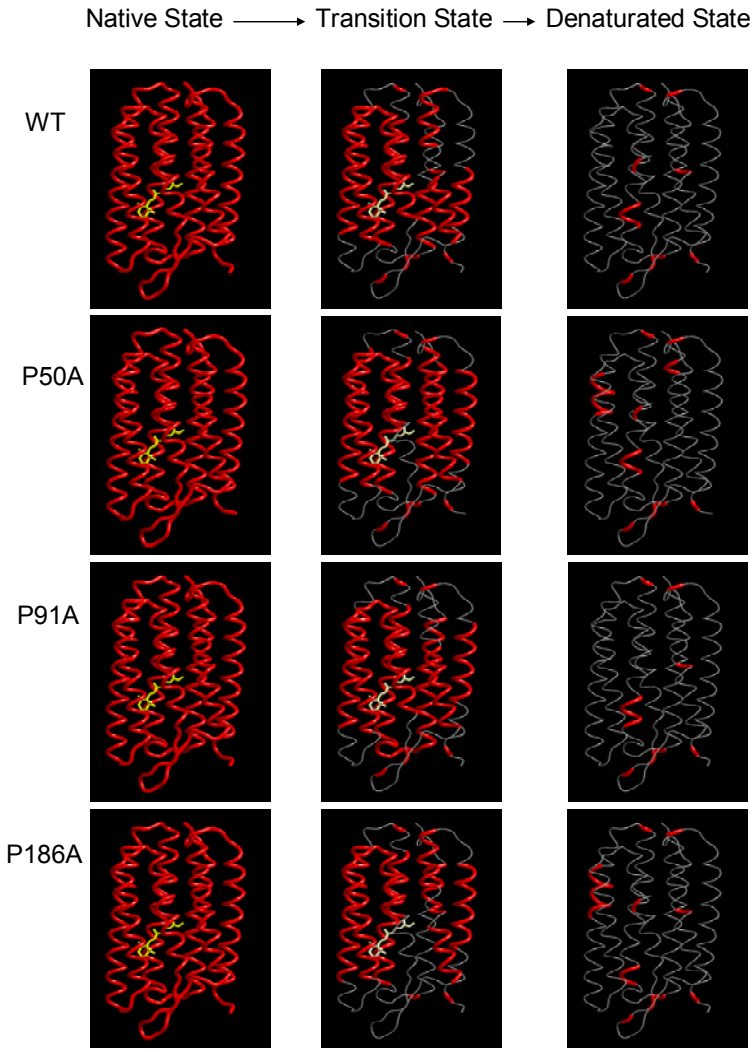

Fig. VI.7. Evolution of the simulated thermal denaturation in the 3D structure. The red thick structures display rigid regions while the grey thin ones represent denatured structures. Retinal is displayed in yellow in the native state, light-yellow in transition state and no represented in denaturation state. This figuration of retinal presence is done to relate the simulation with what happens in UV-Vis experiments. In the case of the denaturated state (not solely on Bacteriorhodopsin structure), it must be emphasized that all the prolines are present. This limitation of the FIRST algorithm comes from the fact that Pro is always considered as rigid. Furthermore, in the case of some Heteroatoms (with no O, N or S atoms) present in the structure (i.e. retinal), the only interactions are the hydrophobic ones, not taking into account low energy hydrogen bonds.

VI.4. References

1. Finkelstein, A. V. (1997) Can protein unfolding simulate protein folding? *Protein Eng 10*, 843-845.
2. Booth, P. J., and Curran, A. R. (1999) Membrane protein folding. *Curr Opin Struct Biol 9*, 115-121.
3. Booth, P. J., Templer, R. H., Curran, A. R., and Allen, S. J. (2001) Can we identify the forces that drive the folding of integral membrane proteins? *Biochem Soc Trans 29*, 408-413.
4. Booth, P. J., Templer, R. H., Meijberg, W., Allen, S. J., Curran, A. R., and Lorch, M. (2001) In vitro studies of membrane protein folding. *Crit Rev Biochem Mol Biol 36*, 501-603.
5. White, S. H., and Wimley, W. C. (1999) Membrane protein folding and stability: physical principles. *Annu Rev Biophys Biomol Struct 28*, 319-365.
6. Rader, A. J., Anderson, G., Isin, B., Khorana, H. G., Bahar, I., and Klein-Seetharaman, J. (2004) Identification of core amino acids stabilizing rhodopsin. *Proc Natl Acad Sci U S A 101*, 7246-7251.
7. Heyes, C. D., Wang, J., Sanii, L. S., and El-Sayed, M. A. (2002) Fourier transform infrared study of the effect of different cations on bacteriorhodopsin protein thermal stability. *Biophys J 82*, 1598-1606.
8. Shnyrov, V. L., and Mateo, P. L. (1993) Thermal transitions in the purple membrane from Halobacterium halobium. *FEBS Lett 324*, 237-240.
9. Cladera, J., Galisteo, M. L., Sabes, M., Mateo, P. L., and Padros, E. (1992) The role of retinal in the thermal stability of the purple membrane. *Eur J Biochem 207*, 581-585.
10. Brouillette, C. G., McMichens, R. B., Stern, L. J., and Khorana, H. G. (1989) Structure and thermal stability of monomeric bacteriorhodopsin in mixed phospholipid/detergent micelles. *Proteins 5*, 38-46.
11. Brouillette, C. G., Muccio, D. D., and Finney, T. K. (1987) pH dependence of bacteriorhodopsin thermal unfolding. *Biochemistry 26*, 7431-7438.
12. Lu, H., Marti, T., and Booth, P. J. (2001) Proline residues in transmembrane alpha helices affect the folding of bacteriorhodopsin. *J Mol Biol 308*, 437-446.
13. Allen, S. J., Kim, J. M., Khorana, H. G., Lu, H., and Booth, P. J. (2001) Structure and function in bacteriorhodopsin: the effect of the interhelical loops on the protein folding kinetics. *J Mol Biol 308*, 423-435.
14. Kim, J. M., Booth, P. J., Allen, S. J., and Khorana, H. G. (2001) Structure and function in bacteriorhodopsin: the role of the interhelical loops in the folding and stability of bacteriorhodopsin. *J Mol Biol 308*, 409-422.
15. Chen, G. Q., and Gouaux, E. (1999) Probing the folding and unfolding of wild-type and mutant forms of bacteriorhodopsin in micellar solutions: evaluation of reversible unfolding conditions. *Biochemistry 38*, 15380-15387.
16. Booth, P. J. (2000) Unravelling the folding of bacteriorhodopsin. *Biochim Biophys Acta 1460*, 4-14.
17. Yohannan, S., Faham, S., Yang, D., Whitelegge, J. P., and Bowie, J. U. (2004) The evolution of transmembrane helix kinks and the structural

diversity of G protein-coupled receptors. *Proc Natl Acad Sci U S A 101*, 959-963.
18. Faham, S., Yang, D., Bare, E., Yohannan, S., Whitelegge, J. P., and Bowie, J. U. (2004) Side-chain contributions to membrane protein structure and stability. *J Mol Biol 335*, 297-305.
19. Sanz, C., Lazarova, T., Sepulcre, F., Gonzalez-Moreno, R., Bourdelande, J. L., Querol, E., and Padros, E. (1999) Opening the Schiff base moiety of bacteriorhodopsin by mutation of the four extracellular Glu side chains. *FEBS Lett 456*, 191-195.
20. Hespenheide, B. M., Rader, A. J., Thorpe, M. F., and Kuhn, L. A. (2002) Identifying protein folding cores from the evolution of flexible regions during unfolding. *J Mol Graph Model 21*, 195-207.
21. Rader, A. J., Hespenheide, B. M., Kuhn, L. A., and Thorpe, M. F. (2002) Protein unfolding: rigidity lost. *Proc Natl Acad Sci U S A 99*, 3540-3545.
22. Thorpe, M. F., Lei, M., Rader, A. J., Jacobs, D. J., and Kuhn, L. A. (2001) Protein flexibility and dynamics using constraint theory. *J Mol Graph Model 19*, 60-69.
23. Vriend, G. (1990) WHAT IF: a molecular modeling and drug design program. *J Mol Graph 8*, 52-56, 29.
24. Williams, M. A., Goodfellow, J. M., and Thornton, J. M. (1994) Buried waters and internal cavities in monomeric proteins. *Protein Sci 3*, 1224-1235.
25. Zavodszky, M. I., Lei, M., Thorpe, M. F., Day, A. R., and Kuhn, L. A. (2004) Modeling correlated main-chain motions in proteins for flexible molecular recognition. *Proteins 57*, 243-261.
26. Sanz, C., Marquez, M., Peralvarez, A., Elouatik, S., Sepulcre, F., Querol, E., Lazarova, T., and Padros, E. (2001) Contribution of extracellular Glu residues to the structure and function of bacteriorhodopsin. Presence of specific cation-binding sites. *J Biol Chem 276*, 40788-40794.

I've exposed your lies, baby
The underneath's no big surprise
Now it's time for changing
And cleansing everything

Muse.

CHAPTER VII.

GENERAL DISCUSSION

VII. GENERAL DISCUSSION

BR consists in a set of amino acids synergized to drive a function, proton pumping. The protons that participate have a road to walk, from the inner to the outer side of the cell, and the transport does not consist in a single step. The programmed stops that the protons do are, besides the Schiff Base, several amino acids and water molecules. The two residues involved directly in proton pumping (Asp96 and Asp85) are located in Helix C of this transmembrane protein. Arg82 that has a crucial role in the proton release mechanism is also located in Helix C. Remembering the questions concerning Helix C proposed in chapter I.6.:

- Is it important to maintain a correct position of these residues and to which extent?
- Must they be located precisely around the SB all along the photocycle?
- Does this helix need to change the conformation to distinguish between the extracellular and the cytoplasmic events during the photocycle?

The answer then was supposed to be a strong “yes”. The experimental evidences presented in this work permit to give a more detailed and argued answer.

Helix-embedded prolines of BR (50, 91 and 186) have been also studied **(Chapter V)**. Whether these prolines perform a static and/or dynamic role has been a challenge since the beginning, and several studies **[1-8]** tried to solve this question. All these studies were performed with protein expressed in *E.coli*, and until 2004 no study appeared using protein expressed in its native environment, when crystal structures of mutants P50A, P91A and P186A have been published **[9, 10]**. Results obtained from experimental data in relation to these structures have been discussed **(Chapter V)** and, in this section, an attempt to give a comprehensive overview is made.

VII.1 Thr90

Chapter III and **IV**, provide an insight on how important is this residue in Helix C. In fact, it is highly conserved, fully in archaea (**Fig. I.16**). The first approach taken in **Chapter III**, result in an incomplete answer to the proposed questions. Distortion on the Asp85 and Schiff Base environment is evidenced by alterations in the spectroscopic features of the mutated protein T90A (see **Chapter III.3**). Hydroxylamine reactions and thermal stability show that the mutation favours accessibility to SB in conditions of stress (chemical or thermal). This looser structure of the mutant is confirmed by DSC experiments. The fact that both the main thermal transition and the pre-transition appear at decreased temperatures demonstrates that the interactions exerted by Thr90 are important not only for the interactions between helices including retinal, but also for the maintenance of the para-crystalline arrangement (see **Chapter III.3**). And last but not the least, why such a severe decrease of proton pumping is induced by the mutation? Thr90 does not participates directly in proton transport, but may be a key point in maintaining the correct positioning of the residues involved directly to proton pumping. All these results argue for a relevant role of Thr90 in BR; nevertheless, there is no clear idea of how this role was exerted. Speculations on the possible role of the intra or inter-helical interactions arise; the steric contact with retinal through the C_γ of Thr90 becomes also a possibility. These new set of questions are answered in **Chapter IV**. Further details on T90A and new mutations were studied (T90V and D115A) in order to solve the questions stated in **Chapter III**.

The new perspective taken in **Chapter IV** in addition to the information obtained in **Chapter III**, pretend to be a mean to determine which one of the interactions established by Thr90 (hydrogen bond with Asp115 and Trp86 and steric contact with retinal) is more relevant or even whether a synergy between the interactions is necessary. A new approach (indirect one) to estimate the proton pumping is taken (see **Chapter IV.3**), and again T90A shows an altered proton release and uptake activity, which is related to proton pumping, with a pyranine signal of about a 10% compared to WT. The mutants T90V and D115A showed a pyranine signal of 20% and 50% respectively, indicating also

a decreased proton pumping efficiency. In fact, as more interactions are affected, larger is the effect (T90A>T90V>D115A>WT).

Flash Photolysis and FTIR experiments were applied to study the photocycle (see **Chapter IV.3**). Through Flash Photolysis, the kinetics and yield of M intermediate is evaluated, thus an appraisal of the disruption of the function of BR produced by the mutations is obtained. The M intermediate is the only one of the photocycle with a deprotonated SB. It is a key intermediate because the first step of transport, the proton transfer from th SB to Asp85, occurs during M intermediate rise. In this case, the quantum yield and the kinetics of the mutants are affected in comparison with WT. Again, the more affected mutant is T90A. FTIR studies confirm the results obtained by Flash Photolysis, evidencing a more altered photocycle for T90A. Deconvolution of absorbance spectra of the WT and mutant proteins in the carboxylic region is an evidence of the absence of the 90-115 hydrogen bond.

Experiments of Dark-Light adaptation (see **Chapter IV.3**) reinforce the idea of a SB altered environment in T90A stated in **Chapter III**. The abnormal dark-light adaptation of T90A, but not for T90V or D115A strengthen the fact that C_γ of Thr90 contact with retinal is necessary for the correct retinal accommodation. Despite that T90V pretends to mimic this interaction, the fact that Thr is so highly conserved **[11] (see Fig. I.15)** in this position in retinal containing proteins argues for a dependence on this amino acid to exert a determined function.

Further DSC experiments with T90V and D115A mutants, show an intermediate behaviour of these mutants compared to WT and T90A, in the T_m of the main transition. Nevertheless, T90V shows a less cooperative transition than D115A. This is in keeping with the fact that perhaps Valine does not mimic exactly the contact with retinal exerted by Threonine. Focusing on the pre-transition, T90V show a more decreased temperature than D115A indicating a more relaxed para-crystalline arrangement, i.e. a less compacted trimer structure, but never so affected as T90A. This comes from the fact that T90A has completely lost the interaction with retinal. Derived from these DSC experiments, some relevance is emphasized on both the hydrogen bond between 90 and 115 and the steric contact. Nevertheless, other factors can contribute to the final structural stability (see **Chapter IV.4**).

As a summary, a synergetic effect of the interactions exerted by Thr90 can be deduced. Taking into account that more perturbing the mutation, larger the effect, when residue 90 loses all its related interactions in T90A, a severe effect both in the resting state and in the dynamic structure and of course in the function of the protein is produced. When a “softer” mutation is introduced, the function and the structure get partially over. By this it can be inferred that Thr90 in BR assumes a key role not only in maintaining the correct location of the Helix C residues, indispensable for the function of the protein; Thr90 also assumes an important paper in the stability of the para-crystalline arrangement, needed for the disposition of the trimers.

It is feasible that the steric interaction between Thr90 and retinal plays a significant role in the positioning of the retinal in the retinal binding pocket. The hydrogen bond established by the -OH group of Thr90 with the peptidyl O of Trp86 (removed in T90V and T90A) and the hydrogen bond between Thr90 and Asp115 side chain (removed in T90A, T90V and D115A) suggests a dynamic role of Thr90 (by its double possibility of hydrogen bonding) becoming a crucial point in certain steps of the photocycle. As the result of changing the hydrogen bond from one residue to another, Thr90 can change the orientation of the pre-Thr and post-Thr segments of the helix C to favor the proton transport. Taking into account that the switch of accessibility of the SB towards extracellullar or cytoplasmic side plays an important role in the photocycle, Thr90 can be hypothesized as a key amino acid in the extracellular-to-cytoplasmic change between M1 and M2 intermediates **(see Fig. I.6.A)** also supported by the movements of helix C monitored in X-ray diffraction data **[12]**.

The importance of the central region of helix C is also highlighted by the preceding residue, Thr89, whose relationship with Asp85 has been widely discussed **[13-15]**. Thr89 when compared to Thr90 has a more local effect. Thr89 establishes a hydrogen bond through its side-chain with Asp85 side-chain, keeping the proper environment between the counter-ion and the Schiff Base. Thus, Thr89 participates indirectly in the proton pumping through its interaction with Ap85, although it has been implicated in the proton transfer step from the SB to Asp85 **[14]**. Meanwhile Thr90 has more general role by participating in the dynamics of helix C (see also **Section VII.3**).

VII.2. Pro91

Three prolines are embedded in transmembrane helices in Bacteriorhodopsin. This has been used as an advantage to carry out the study of Pro91 in comparison with "similar" environments (i.e. Pro50 and Pro186) in the same protein.

In **Chapter V**, a study on transmembrane Prolines has been driven in order to find out what the role of embedded prolines of BR is. This study pretends also to gain insight into the general function performed by prolines in transmembrane proteins.

Although transmembrane prolines have been already studied in the system of *E.coli* **[1, 4, 5]**, the study reported here provides a more detailed perspective of these residues in BR. The results obtained summed up with the X-ray crystallographic data **[10]**, yield information on the role of these prolines in BR. Different studies have been carried out on Pro91 of BR **[1, 4]**, as a residue supposed to fulfil a particular role as an α-helix breaking residue. Most of them are carried out in *E.coli*, meanwhile expressing mutant proteins in *H.salinarum,* as we have done, has the advantage of the native environment and native membrane composition without denaturing conditions to reconstitute the protein. In order to determine whether a structural and/or functional role should be assigned to this Proline the studies presented in **Chapter V** have been performed. In addition, the recent 3D structure of the mutant **[9]** provides an additional insight on the alterations of the resting state induced by the mutation. The structure of P91A has little structural alterations compared to WT as detailed in **Fig I.15**.

Studies based on the resting state of P91A result on a structure more accessible for solvent molecules than for the WT, despite the crystallographic structures does not show significant differences. Hydroxylamine accessibility, Asp85 pK_a and Dark-Light adaptation appear somewhat altered in P91A, indicating that they are not so similar to the native structure. The experimental results provide a dynamic perspective of the structure versus the static perspective of a crystal. As discussed in **Chapter V.4**, the lost interactions exerted by C_δ of Pro when residue 91 is mutated to Ala alter the dynamics of the protein even in non-light-induced states, despite of not being detected in the crystal structure. Furthermore, UV-Vis denaturation studies (see **Chapter VI**) on dark-

adapted P91A, argue for a distorted environment of the Asp85 and the retinal binding pocket. Indeed, the structural stability of the protein at acid pH is severely decreased, emphasizing even more the dynamic role contrasting with the static crystal structure showing no changes.

In light-stimulated BR, the most remarkable result is the decrease in the proton pumping rate of P91A to about 35% of the WT activity, both in liposomes (direct) and pyranine (indirect) experiments (see **Chapter V.3**). Hydroxylamine under light experiments, in keeping with FTIR and Flash Photolysis data show a destabilization of the structure of the protein during the photocycle.

FTIR experiments on P91A mutant show an altered retinal environment indicating that in M and N the retinal is not well accommodated in order to perform the conformational changes and the charge movements needed to pump the proton **[16]**. In addition, the Asp96 band is somewhat shifted in the N-intermediate of this mutant (see **Fig. V.7**). If the environment of this residue is affected during its reprotonation this yields a less efficient photocycle deriving in a worst proton pumping. Also Asp115 band is distorted in the N-photointermediate of this mutant. This is understandable from the point of view that Asp115 interacts through a direct hydrogen bond with Thr90 (neighbour residue of Pro91) and with a water mediated hydrogen bond with Leu87 (Cδ partner of Pro91). Thus, the mutation Ala91 may difficult these interactions distorting the environment of Asp115, and what is more, avoiding relevant Helix C-Helix D interactions that can be important for the protein function.

Pro91 in Helix C is assumed to maintain the correct position and flexibility of the helix during the steps of the photocycle. As a dynamic element, Pro may permit the movements of pre- and post-proline segments through the necessary conformational steps to correctly place both the Asp96 (post-proline segment) and the Asp85 and Arg82 (pre-proline segment) near or far to the SB **(Fig. VII.1)**. Assuming the extracellular-to-cytoplasmic switch of the Schiff Base in the photocycle **(Fig. I.6.A)**, Pro91 (joining forces with Thr90) could be in charge of this conformational switch in M_2. Focusing on the movement of the helix C monitored on the L-intermediate **[12]**, Pro91 may be the key point that permits the motion of the helix, thus inverting the donor/acceptor relationship between Asp85/SB, allowing then Asp85 to accept the proton coming from the Schiff Base. It is observable in the L intermediate crystallographic data **[12]** that the

local bending of Helix C plays a central role in setting the stage for proton transfer, changing the electrostatic environment of the retinal in this photointermediate. Mutation of Pro91 to Ala, may avoid this deformation, and consequently altering the proton pumping activity of this mutant. These alterations may give rise to changes in the retinal environment seen by FTIR and in the kinetics of M rise in the photocycle (see **Chapter V.3**).

As a final consideration, it is important the high conservation degree for Pro91 in type 1 rhodopsins **[11]** and the studies that acknowledge the conservation of this proline also in GPCRs **[17]**. This again strengthens the fact that this proline has an special relevance at this position.

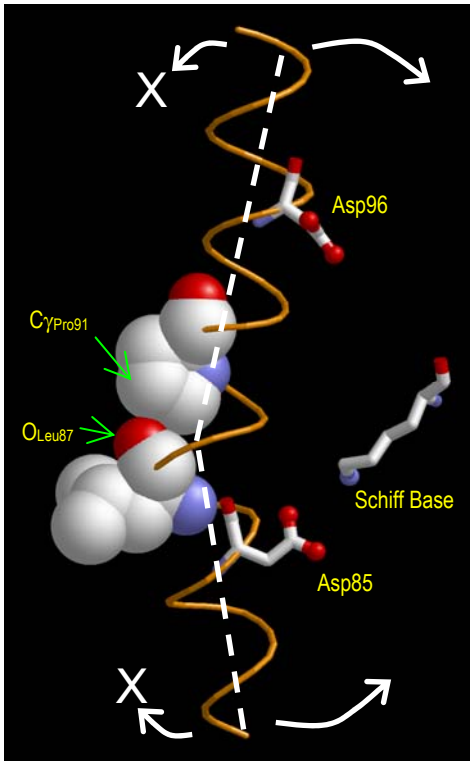

Fig. VII.1. Diagram of Helix C of Bacteriorhodopsin. Disposition of Asp85 and Asp96 respect to the Schiff Base is represented. The steric clash induced between Leu87 and Pro91 is displayed in order to show the division of the helix in two segments (dotted white line). Arrow are quantitative, indicating the degree of bending that the egments may reach by each side. X indicates restriction of movement induced by the steric clash.Atomic coordinates are from 1M0L from the Protein Data Bank (PDB).

VII.3 Thr90-Pro91 motif

Derived from the results, the importance of the motif Thr90-Pro91 in assuring the correct location of key amino acid side chains of Helix C involved

in proton transport is beyond any doubt. The effect exerted by Thr90 is somewhat enhanced by Pro91, acting as a dynamic turning point for this helix to assume the conformational changes all along the photocycle, in order to drive the proton pumping function properly. All the interactions exerted by this motif **(FIG. I.12 and FIG. VII.2)** conduces to a strong control of this region. Pro divides the whole helix in two subunits or segments that may act independently, dividing the photocycle events in cytoplasmic and extracellular. Furthermore, this motif also contributes to the correct placing of the retinal in the retinal binding pocket.

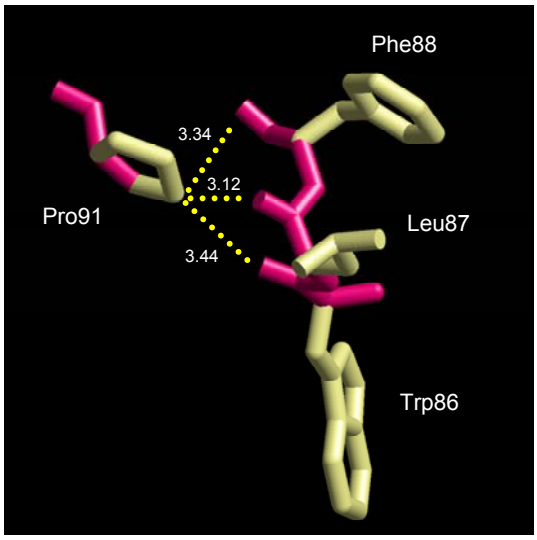

Fig. VII.2. Distances from the Cδ of Pro91 to the i-5, i-4 and i-3 residues. In this PDB coordinates of the ground state of BR (1M0L), Pro91 is prone to form hydrogen bonds with 3 residues. Taking into account that Pro can perform from none to 2 hydrogen bonds, this yields the chance of 2^N-1 possibilities of hydrogen bonding, where N is the number of residues which are in the immediate environment of Pro (least than 3.7Å).

The steric clash **(Fig VII.1)** induced by Cγ of Pro91 (*i*) with the peptydil O of Leu87 (*i-4*), avoids a bending of the helix towards a direction that may drive away proton pumping involved residues (Asp85, Asp96) from the SB.

On the other hand, Pro specific ability to perform hydrogen bonding through its Cδ could explain how this check point in the middle of helix C acts. Pro specific hydrogen bonds may be easily formed or broken (due to its lower energy with respect to average hydrogen bonds) all the way along the conformational events that take place in the protein, either in the photocycle or in the resting state. Focusing on Pro91, in front of Pro50 and Pro186, the fact

that an additional hydrogen bond can be established (type 5/4/3) should be relevant. Motif Thr90-Pro91 strengthens the bending of this helix **[18]**, providing an extra flexibility. This kind of flexibility is anisotropic, i.e. only in determined directions **(Fig. VII.3)**. This ability may confer to this Thr90-Pro91 motif an extra degree of freedom to perform its dynamic role, acting even more as hinge than the similar environments of Pro50 and Pro186, which do not contain the modulation of Thr90.

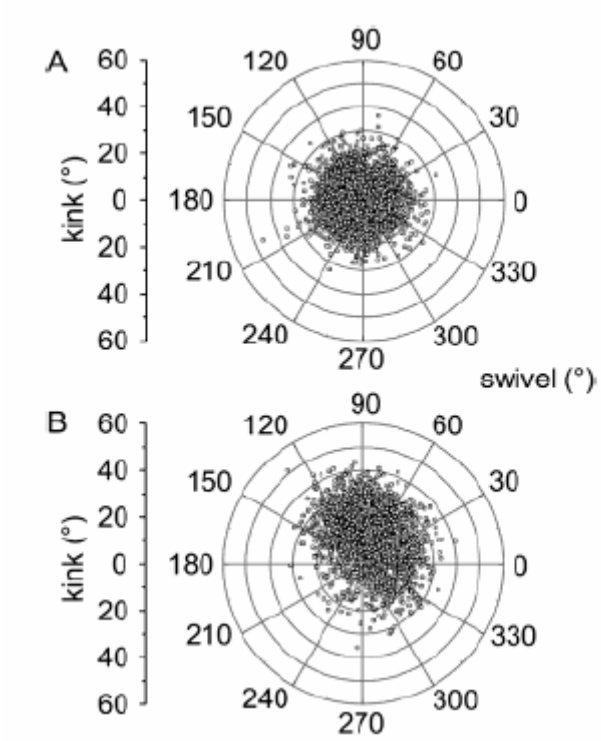

Fig. VII.3. Plot of a simulation for a poly-Alanine helix (A) and for a poly-Alanine helix with one single Pro at the center of the helix (B). The kink angle (bending) vs. the swivel angle is represented. An homogeneous distribution is shown for poly-ala meanwhile for Pro-containing helix, certain angles are restricted. This restriction comes from the steric clash induced by Pro [19].

Despite of the local changes induced by the mutation in the environment of the residue, taking a broader point of view, Pro should be considered as a residue that adds valuable degrees of freedom to proteins (in this case transmembrane proteins) in order to perform movements and conformational changes directed to drive their functions. This may explain why the presence of Pro-embedded in transmembrane α-helices have a high frequency **(Fig. VII.4)**.

Answering the questions relative to Helix C in BR, its remarkable how a versatile and efficient mechanism is present in this Helix for regulating the protein function (proton pumping), and this mechanism is the motif Thr90-Pro91.

Additionally, another subtle mechanism seems to act over the positioning of Helix C. The relevance of the short C-D loop (only 1 amino acid) has been tested by increasing the length of this loop and no expression was achieved (data not shown).

VII.5. Helix-embedded prolines Pro50 and Pro186

In principle, mutation of Pro to Ala could recover a typical α-helical disposition of the backbone. Thus, when residue 50 or 186 is an Ala, Helix is supposed to lose the bending. However, the crystal structure **[10]** reveals that the bending remains, so Pro50 or Pro186 are not supposed to be the main factor that bend the helix, or at least to maintain the kink. Maybe Pro allows the kinking, and other interactions (polar, hydrophobic…) all along the helix are the responsible of keeping the helix kinked.

-Pro50

The results shown in **Chapter V.3 and Chapter VI.3** for P50A, argue for an altered structure and function, both in the resting (hydroxylamine and UV-Vis Thermal Denaturation) and the light-induced state (Hydroxylamine, FTIR, Flash Photolysis and Proton Pumping) despite that the mutation doesn't affect the bending in Helix B. This suggests that Pro50 is a dynamic hinge. Likely in the case of Pro91 in helix C, Pro50 favours a set of conformational movements that may occur all along the photocycle and even in the resting state. If Pro is not present at this position, the helix is not disposed in the proper place, thus, the function is not performed correctly; the retinal is more accessible and the photocycle is somewhat distorted. In this sense, Solid State Nuclear Magnetic Resonance (NMR) studies on BR **[6, 7]** show fluctuations of Helix B at the level of Pro50. The contact of Val49 with Lys216 (Schiff Base) present in the WT and P50A crystal structures (PDB code 1PY6 and 1PXR respectively) may be lost when Pro50 is mutated to Ala, during some conformational steps.

Thr46 interacts both with Pro50 (Cδ-H···O) and Asp96 (average hydrogen bond). When Pro50 is mutated to Ala, the inter-helical hydrogen bond between Asp96 (Helix C) and Thr46 (Helix B) may affect the environment of Asp96. This is evidenced by FTIR N intermediate spectrum showing an Asp96 distorted environment (see **Fig. V.7B**).

Another aspect that should be considered is the motif Thr-Thr-X-X-Pro **[18]** present in this helix. Thr47 and even Thr46 may modulate the role exerted by Pro50, which establishes hydrogen bonds with Thr46 and Thr47 through the Cδ. In keeping with what happens with Pro91 (see **Section VII.2** and **VII.3**), the dynamic ability of Helix B may be significantly reduced due to the lost interactions.

-Pro186

Pro186 is a residue included in the Retinal Binding Pocket **[2, 3]** and as Pro91 is highly conserved in archaeal rhodopsins **[11]** (see **Fig. I.15.**).

Besides being part of the RBP, Pro186 is supposed to be related to the movements of Helix F and G during the photocycle that open the cytoplasmic channel to permit the entrance of water molecules to reprotonate Asp96 after its deprotonation in N-intermediate. This opening seems to occur in the late M intermediate **[20, 21]**.

Comparing the structure of the WT (1PY6) and P186A (1Q5I), Yohannan et al. **[9]** show that there are no significant differences between both structures. Nevertheless, the distances measured in **Chapter V.3** demonstrate that a 3_{10} turn could form in Helix F in P186A mutant.

Experimental evidences **(Chapter V.3 and Chapter VI.3)** argue for an altered environment of the protein in the resting state. Hydroxylamine reactions show 20-fold increased accessibility, denoting the existence of an altered dynamics in the mutant. Also Asp85 pK_a, and light-dark adaptation goes in the same direction, demonstrating that he retinal and the counter-ion (Asp85) environments are distorted. In addition, thermal denaturation strengthen the fact that the resting structure is somewhat affected, by less stability in front of heating. This mutant is also affected when light-induced changes are provoked, as shown by photocycle alterations, detected by FTIR and Flash Photolysis. FTIR N intermediate shows an altered amide I (**Chapter V** and **Fig. V.7A**). This

may indicate a changed helix F and G disposition in the photocycle corresponding to less efficient proton transport when observed by pyranine (20%) or by proton pumping in liposomes (45%).

The results obtained in **Chapter V** provide an insight on the environment of Helix F of BR. This helix contains conserved residues **[3]** (Trp182, Tyr185, Pro186 and Trp189) which contribute to the correct location of the retinal (these residues are members of the RBP see **Fig.I.6A**). Among them, Trp182 is at distance from Pro186 able to perform a Cδ hydrogen bond (see **Chapter V.3**). When 186 is mutated to Ala, the possibility of performing thisinteraction is restricted. In fact, the only possibility derived from the comparison of the structures is the formation of a 3_{10} turn in this helix. This means that 2 residues of the RBP (186 and 182) are not placed were they are supposed to be, not only in the resting state but all along the photocycle. Therefore, the dynamics of the protein are distorted both in the resting state and in the light-stimulated state. This final consequence is also applicable to the other couple of mutants (P50A and P91A).

As in the case of Pro50, the kink of helix F exerted by Pro186 can be also modulated by Ser183 residue in the i-3 position **[18]**. This modulation is lost in the mutant, because Ser183 cannot exert its role without a Pro to be regulated.

-Embedded-Prolines in Bacteriorhodopsin

As a general feature, all the Pro→Ala mutants present a distortion of the environment of the retinal, and a set of results indicating helix alteration evidenced by:

-Increased accessibility to hydroxylamine.

-Retinal environment distorted: -DA-LA adaptation.
-FTIR.

-Helical distortion→ FTIR amide I bands.

-Altered photocycle→ Flash Photolysis (**Chapter V** and **[1]**)
and FTIR data.

-Altered proton pumping function→ Liposomes (**Chapter V** and **[4]**) and Pyranine signal.

-Contribution of Pro91 and Pro186 to the structural stability (not for Pro50) by SDS unfolding experiments **[9, 10]**.

-Relevant for the folding of the protein **[5]** (Pro50 and Pro91) and for the locking of the retinal in the RBP **[2, 5]** (Pro186).

Against all these experimental evidences, the crystalline structures argue for no significant differences among WT and mutants. Where do the differences obtained experimentally come from? Thinking on the crystal structure as a picture of a state, where no fluctuations can be observed, it is easy to remember the statement that some crystallographers have settled recently **[12]**, pointing towards the tendency to overlook dynamic fluctuations about the crystallographic structures [22].

VII.6. Role of Prolines in Transmembrane Helices

What conclusions can be derived from the experimental results in Chapter V that can be extended to Transmembrane helices?

Transmembrane proteins perform a wide variety of functions, mostly all to communicate an outer medium with an inner one or vice versa. Ion channels and G-protein-coupled receptors (GPCRs) are a clear example of this transmembrane signaling **[23]**. Archaeal rhodopsins, bovine or human Rhodopsin, bovine or human Na^+/H^+ exchanger (8 isoforms), receptors for serotonin, adrenergic receptors, ATP/ADP mitochondrial carriers, and a large set of transmembrane proteins, despite being ion channels, GPCRs, eukaryotic or prokaryotic, all of them have at least a common feature: they present Helix-embedded Prolines.

The high frequency presence of prolines in the middle of an α-helix (see **Fig. VI.5** from Cordes et *al.* 2002) in addition to the fact that they are also highly conserved **[17, 24]** argues for a relevant role of Pro at this position furthermore when summed up with experimental data.

Pro is a very controversial residue. It cannot establish the average interactions that other residues can **[23]**; it has a pyrrolidine ring that permits a cis-trans isomerization **[23]**; it is an anisotropic amino acid **(Fig. VII.3)** that restricts

certain positions when placed in an α-helix orienting helices in a preferent way; this induces an alternative way of interacting (Cδ-H···O, see **Fig. VII.5**) **[26, 27]** and this alternative interactions are derived from an steric clash that avoid determined conformations that may move further away relevant residues from the active site of the protein **[19, 28]**.

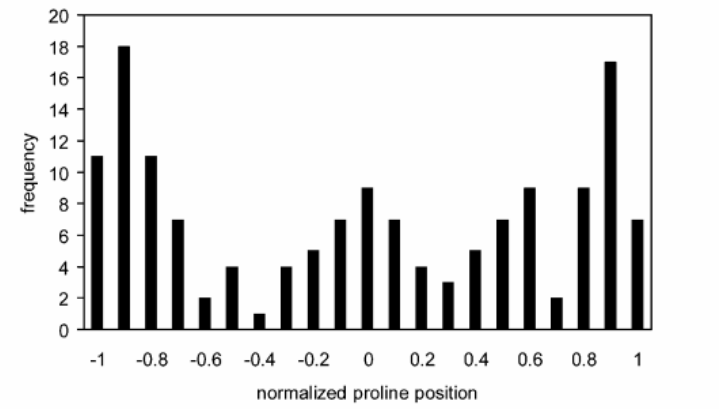

Fig. VII.4.Proline positions along Transmembrane helices. The frequency of proline residues is shown as a function of normalised proline position (where -1 corresponds to the N terminus and +1 corresponds to the C terminus of a Transmembrane helix, so that 0 is the centre of the helix) [25].

In summary, Pro is a specific amino acid that confers flexibility and functionality to both pre-proline and post-proline segments of an α-helix. These dynamic features (as commented in **Section V.3**) increases the degrees of freedom that an α-helix has in order to drive their function, that in a simplistic way, is to separate two mediums or communicate them.

Certainly, the results obtained in **Chapter V** do not pretend to become the definitive answer, but all the discussed information in **Section IV.5** should yield some knowledge on the function of Pro embedded in α-helices.

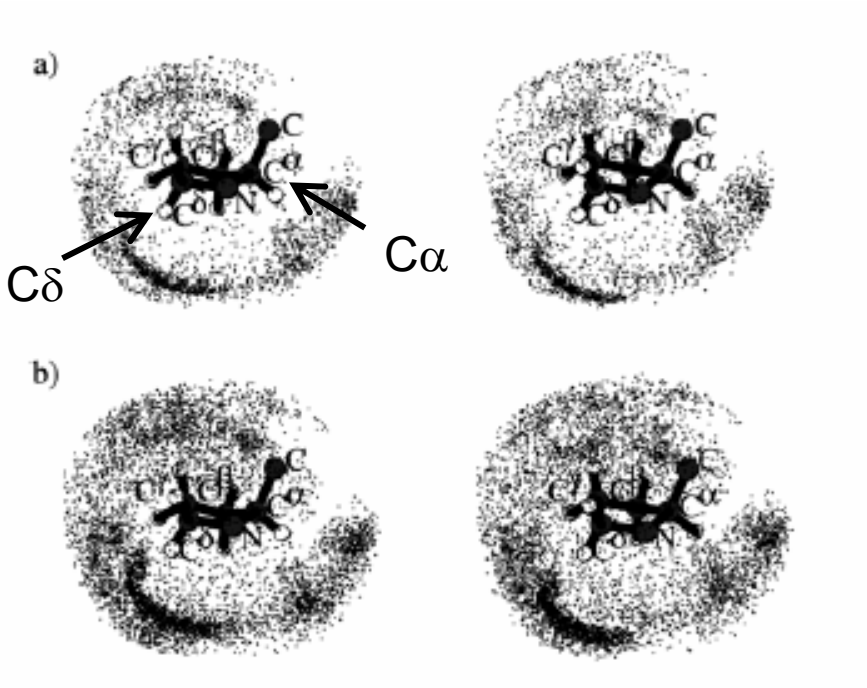

Fig. VII.5. Scatterplots of superimposed positions of oxygen atoms, participating in C–H· · ·O interactions, relative to the pyrrolidine ring, in stereo. The oxygen atoms are represented by dots. The cut-off distance is 3.5 Å in (a) and 4.0 Å in (b) [26]. It can be seen that at 3.5 A ° the points are more clustered, especially around the protons at Cα and Cδ atoms. This suggests that the C–H· · ·O interaction could be stronger and as directional as the conventional hydrogen bonding when the C–H groups at Cα and Cδ, rather than at Cβ and Cγ are involved. This is in conformity with the position of Cα and Cδ atoms being next to the electron-withdrawing ring N atom, whereby the protons at these positions carry more partial positive charge, which brings about a stronger electrostatic interaction for the C–H· · ·O bond. Cδ and Cα are indicated.

VII.7. Analysis of the Role of Prolines in the stability of Bacteriorhodopsin

A comparison of a simulated against experimental thermal denaturation of Bacteriorhodopsin is presented in **Chapter VI.** This method permits us to relate experimental events with predicted changes in the crystal structures. Nevertheless, the simulation does not allow us to change some conditions as pH, which may affect to protonable groups by changing their pK_as. In addition, more variables may be needed to be introduced in the algorithm to make a more reliable approach to what happens in real experiental conditions. For instance, low energy hydrogen bonds (C-H···O) should be taken into account to emphasize the role of Pro in the stability. However, as a preliminar approach to what it happens in a single transition thermal denaturation, the simulation helps

to identify relevant rigid clusters. Implementing the results of FIRST software by experimental thermal denaturation permits to elucidate relevant aspects on the structure of the protein. As shown in **Chapter VI** experimental and simulation data indicate that the stability of the P186A is somewhat decreased, and some conclusions are extracted from the simulation as the fact that the mutation seems to affect the clusters involved in the Retinal Binding to Lys216. This can be deduced a priori by knowing that Pro186 forms part of the Retinal binding Pocket **Chapter I.2**, but confirming it by a simulation encourages us in the use of FIRST for preliminary approaches.

VII.7.References

1. Zhang, Y.N., et al., Effects of mutagenetic substitution of prolines on the rate of deprotonation and reprotonation of the Schiff base during the photocycle of bacteriorhodopsin. Photochem Photobiol, 1993. **57**(6): p. 1027-31.
2. Rothschild, K.J., et al., Vibrational spectroscopy of bacteriorhodopsin mutants: evidence for the interaction of proline-186 with the retinylidene chromophore. Biochemistry, 1990. **29**(25): p. 5954-60.
3. Rothschild, K.J., et al., Conserved amino acids in F-helix of bacteriorhodopsin form part of a retinal binding pocket. FEBS Lett, 1989. **250**(2): p. 448-52.
4. Mogi, T., et al., Structure-function studies on bacteriorhodopsin. VIII. Substitutions of the membrane-embedded prolines 50, 91, and 186: the effects are determined by the substituting amino acids. J Biol Chem, 1989. **264**(24): p. 14192-6.
5. Lu, H., T. Marti, and P.J. Booth, Proline residues in transmembrane alpha helices affect the folding of bacteriorhodopsin. J Mol Biol, 2001. **308**(2): p. 437-46.
6. Lansing, J.C., et al., Solid-state NMR investigation of the buried X-proline peptide bonds of bacteriorhodopsin. Biochemistry, 2003. **42**(12): p. 3586-93.
7. Kira, A., et al., Significance of low-frequency local fluctuation motions in the transmembrane B and C alpha-helices of bacteriorhodopsin, to facilitate efficient proton uptake from the cytoplasmic surface, as revealed by site-directed solid-state (13)C NMR. Eur Biophys J, 2004.
8. Deber, C.M., B.J. Sorrell, and G.Y. Xu, Conformation of proline residues in bacteriorhodopsin. Biochem Biophys Res Commun, 1990. **172**(2): p. 862-9.
9. Yohannan, S., et al., The evolution of transmembrane helix kinks and the structural diversity of G protein-coupled receptors. Proc Natl Acad Sci U S A, 2004. **101**(4): p. 959-63.
10. Faham, S., et al., Side-chain contributions to membrane protein structure and stability. J Mol Biol, 2004. **335**(1): p. 297-305.
11. Ihara, K., et al., Evolution of the archaeal rhodopsins: evolution rate changes by gene duplication and functional differentiation. J Mol Biol, 1999. **285**(1): p. 163-74.
12. Edman, K., et al., Deformation of helix C in the low temperature L-intermediate of bacteriorhodopsin. J Biol Chem, 2004. **279**(3): p. 2147-58.
13. Russell, T.S., et al., Threonine-89 participates in the active site of bacteriorhodopsin: evidence for a role in color regulation and Schiff base proton transfer. Biochemistry, 1997. **36**(24): p. 7490-7.
14. Kandori, H., et al., Tight Asp-85--Thr-89 association during the pump switch of bacteriorhodopsin. Proc Natl Acad Sci U S A, 2001. **98**(4): p. 1571-6.

15. Kandori, H., et al., Structural change of threonine 89 upon photoisomerization in bacteriorhodopsin as revealed by polarized FTIR spectroscopy. Biochemistry, 1999. **38**(30): p. 9676-83.
16. Lanyi, J.K. and B. Schobert, Local-global conformational coupling in a heptahelical membrane protein: transport mechanism from crystal structures of the nine States in the bacteriorhodopsin photocycle. Biochemistry, 2004. **43**(1): p. 3-8.
17. Metzger, T.G., et al., An analysis of the conserved residues between halobacterial retinal proteins and G-protein coupled receptors: implications for GPCR modeling. J Chem Inf Comput Sci, 1996. **36**(4): p. 857-61.
18. Deupi, X., et al., Ser and Thr residues modulate the conformation of pro-kinked transmembrane alpha-helices. Biophys J, 2004. **86**(1 Pt 1): p. 105-15.
19. Bright, J.N. and M.S.P. Sansom, The flexing/twirling helix: Exploring the flexibility about molecular hinges formed by proline and glycine motifs in transmembrane helices. Journal of Physical Chemistry B, 2003. **107**(2): p. 627-636.
20. Luecke, H., et al., Structure of bacteriorhodopsin at 1.55 A resolution. J Mol Biol, 1999. **291**(4): p. 899-911.
21. Subramaniam, S., et al., Protein conformational changes in the bacteriorhodopsin photocycle. J Mol Biol, 1999. **287**(1): p. 145-61.
22. Lanyi, J.K. and B. Schobert, Mechanism of proton transport in bacteriorhodopsin from crystallographic structures of the K, L, M1, M2, and M2' intermediates of the photocycle. J Mol Biol, 2003. **328**(2): p. 439-50.
23. Sansom, M.S. and H. Weinstein, Hinges, swivels and switches: the role of prolines in signalling via transmembrane alpha-helices. Trends Pharmacol Sci, 2000. **21**(11): p. 445-51.
24. Slepkov, E.R., et al., Proline residues in transmembrane segment IV are critical for activity, expression and targeting of the Na+/H+ exchanger isoform 1. Biochem J, 2004. **379**(Pt 1): p. 31-8.
25. Cordes, F.S., J.N. Bright, and M.S. Sansom, Proline-induced distortions of transmembrane helices. J Mol Biol, 2002. **323**(5): p. 951-60.
26. Bhattacharyya, R. and P. Chakrabarti, Stereospecific interactions of proline residues in protein structures and complexes. J Mol Biol, 2003. **331**(4): p. 925-40.
27. Chakrabarti, P. and S. Chakrabarti, C--H.O hydrogen bond involving proline residues in alpha-helices. J Mol Biol, 1998. **284**(4): p. 867-73.
28. Bright, J.N., et al., Conformational dynamics of helix S6 from Shaker potassium channel: simulation studies. Biopolymers, 2002. **64**(6): p. 303-13.

And I won't make the same mistakes
Because I know how much time that wastes
And function is the key
Inside the waiting room

Fugazi.

CHAPTER VIII.

CONCLUSIONS

VIII. CONCLUSIONS

1. Mutants P50A, T90A, T90V, P91A, D115A and P186A of Bacteriorhodopsin have been produced by site directed mutagenesis and expressed in the L33 strain of *Halobacterium salinarum.*

2. An altered behaviour of the retinal is observed when Thr90 is mutated to Ala or Val or Asp115 is mutated to Ala. Thus, Thr90 through its interactions is a relevant residue for placing properly the chromophore. Moreover, the protonation of Asp85 is faster in T90A mutant arguing for an altered environment of the Schiff Base counter-ion.

3. Thr90 is involved through its interactions in the correct helical packing as shown by a decreased thermal stability of all three mutants (T90A, T90V and D115A). Thr90 also contributes to purple membrane para-crystalline arrangement. This indicates that the interactions established by Thr90 favours the packing of the trimers to correctly form the 2D natural crystal.

4. The accessibility to the Schiff Base is increased in T90A. This results in an altered environment for the retinal induced by changes in Helix packing. The interactions performed by Thr90 seem to be indispensable both for Helix packing and retinal placing. The interactions established by Thr90 are important for proton pumping; despite of this residue is not involved directly to this function.

5. Alterations in the photocycle determine that the interactions established by Thr90 are important for the dynamics of the protein. The conformational changes occurring near the retinal all along the photocycle are dependent of the nature of the residue 90 of Bacteriorhodopsin.

6. The altered behaviour in dark-light adaptation of helix-embedded proline mutants argues for an altered environment of the retinal. Shifted maximum of absorbance of P91A and P186A comes from the fact that these residues (91 and 186) are nearer to the chromophore than 50. Moreover, a higher Asp85 accessibility to the proton compared to WT is noticeable in all the mutants, with a higher pKa for P186A followed by P50A and P91A. The counter-ion environment and the Schiff Base are more accessible demonstrating that the structure is somewhat changed.

7. Proton pumping function of the mutants is altered when studied by reconstitution of purple membrane patches into liposomes. The monitoring of pyranine signal also shows a decreased efficiency compared to WT. The dynamics of the protein are somewhat distorted providing a less effective function in the mutants. The less affected is P50A, and P186A and P91A show a similar level of pumping but lower than P50A and WT.

8. In spite of the crystal structures of the mutants P50A, P91A and P186A do not report any structural changes; a dynamic role for Helix-embedded Prolines can be inferred from the experimental results. I.e., The α-helical hydrogen bond established by Ala50 with the backbone of Helix B is not enough to recover the properties of the native protein. The 3_{10} turn in Helix F established by mutant Ala186 is not enough to recover the properties of WT Bacteriorhodopsin.

9. The steric clash induced by Pro in Helices B, C and F is removed by the mutation to Ala. The Cδ-H$\cdots$O interactions performed by Pro50, Pro91 and Pro186 are lost. This provides a strong argument for all the alterations found in the dynamical structure of the mutant proteins. In addition, this points to a dynamic role of these Prolines both in the resting state and during the photocycle of Bacteriorhodopsin.

10. Thr90-Pro91 motif in Helix C of Bacteriorhodopsin plays a vital role in the environment of the main groups involved in proton pumping (Asp85, Asp96, Arg82 and Schiff Base). This is an efficient and dynamic mechanism to drive the function of Bacteriorhodopsin.

11. The conclusions obtained in this work can be extended to other archaeal rhodopsins due to the conservation degree of the residues studied (Thr90, Pro91 and Pro186). The dynamic role of Helix-embedded prolines (Pro50, Pro91 and Pro186) can be also extended to other transmebrane proteins as G-protein coupled receptors, due to its high degree of conservation and by the same dynamical need to perform the proper conformational changes.

12. FIRST algorithm becomes, when summed up with experimental results, a good approach to determine the structural stability of Bacteriorhodopsin. Both experimental and simulation data coincide in a less stable structure for P186A mutant.

13. A general conclusion that can be derived from this work is that crystal structures tend to overlook dynamic fluctuations of the protein.

Index of Figures and Tables

Chapter I

Fig. I.1. *Salt lake inhabited by Halobacterium salinarum with the characteristic purple coloration due to Bacteriorhodopsin.* 6

Fig. I.2. *Basic scheme of light-to-chemical energy transformation carried out by Halobacterium salinarum. PM, which is induced by low oxygen concentration generates an electrochemical gradient of protons when stimulated by light. ATP synthases enter a proton into the cell and release two sodium molecules to the external medium through an antiport mechanism. As a result ATP molecules are produced and used as a source of energy to live until the environmental stress disappears. This is an endurance form of living, in these conditions H. salinarum is not capable of growing.* 7

Fig. I.3. *A. Primary and secondary structure of BR.B. Tertiary structure of BR. It comes from the X-ray diffraction of a crystal (PDB code 1c3w). The N- and C-terminal are not complete because they don't appear in the diffraction pattern due to their high mobility. C. The lattice of a 2D crystal is formed by three molecules of BR forming a trimer, and these trimers are later distributed forming hexamers.* 9

Fig. I.4. *Plot of the Schiff Base between the side-chain Nitrogen of the Lysine 216 and the Carbon of the retinal molecule. The plus sign indicates the protonated state.* 10

Fig. I.5. *Two conformations of retinal are displayed: all-trans and 13-cis retinal.* 11

Fig. I.6*. A. Set of aromatic residues surrounding retinal. Despite not being aromatic, Pro186 is included in this figure due to its proximity to Tyr185. B. Non-aromatic residues enclosing retinal. Thr90 is emphasized, although not considered as a part of the Retinal Binding Pocket, it contacts directly with retinal through steric interactions.* 12

Fig. I.7. *A. The BR photocycle can be defined as a sum of three different processes: Isomerization (I), Proton Transport or Translocation (T) and Switch of accessibilities (S). The first process is the retinal isomerization from all trans to 13-cis, followed by a proton transfer from the Schiff base to the proton acceptor Asp-85. Then, the accessibility of the Schiff base changes from the extracellular to the cytoplasmic side to be reprotonated from the Asp96. After reprotonation of Asp-96 from the cytoplasmic surface (O intermediate), retinal reisomerizes thermally and the accessibility of the Schiff base switches back to extracellular to re-establish the initial state. Chronologically, the photocycle seems to be divided into two halves, the first one with the main processes occurring in the extracellular side, and the second one happening in the cytoplasmic one. B. Intermediates can be identified by its maximum of absorbance (displayed as a sub index in Fig. I.6.A.), indicating an evolution in the absorption spectra shown by a color change of each intermediate.* 15

Fig.I.8. *Plot of an average right-handed α-helix. The general features explained in the text are presented. The amino acid R-group is displayed in green. Oxygen and Nitrogen are represented in red and blue respectively.* 17

Fig. I.9. *Disposition of the residues related to proton pumping in Helix C. Moreover Thr90 and Pro91 are displayed to show the kinking of this helix. These two residues are not directly involved in the translocation of the proton through the BR channel. Retinal is also shown.* 18

Fig. I.10. *Molecular plot of Threonine.* *19*

Fig. I.11. *Molecular plot of Proline.* *20*

Fig I.12. *Diagram of a proline residue in a helix, highlighting how the loss of an i ← (i - 4) H-bond and the distortion (steric clash) induced by the close contact of the Cγ atom of the proline ring at position i with the carbonyl O atom of residue i - 4 leads to a change in direction of the helix axes (broken lines) before and after the proline.* *21*

Fig. I.13. *Helix C of BR kinked at the level of Thr90 and Pro91. Cylinders are overlapped to the helix to show the degree of bending.* *22*

Fig.I.14. *Interactions established by Pro91 in helix C. Distance from Cδ of Pro91 to Leu87 (i-4) is displayed indicating the presence of a hydrogen bond. The bond between Pro91 with Phe88 and/or Trp86 is not easily established (distance between atoms above 3.2 Å). Atomic coordinates from the 1py6 structure of the PDB.* *23*

Fig. I.16. *Comparison of the bacteriorhodopsin sequence to those of 28 archaerhodopsins having a coincidence of at least 25%, as shown by the multiple sequence alignment program MaxHom. Amino acid sequence 1-240 is shown. The side chains with a 100% consensus are indicated in bold. Symbols: o, alcohol; l, aliphatic; a, aromatic; c, charged; h, hydrophobic; -, negative; p, polar; +, positive; s, small; u, tiny; t, turnlike. Residues of interest in this work are yellow marked.* *26*

Fig. I.17. *Overlay of halobacterial retinal and G-protein coupled receptors sequences. An asterisk (*) notes the conserved positions common to both families. A plus sign (+) indicates residues found in BR that align with residues highly conserved among GPCRs. Sequences for the halobacterial retinal proteins were taken from the Swissprot database. Representative GPCR sequences were taken from the EMBL database. BR) bacteriorhodopsin, HR) halorhodopsin, SR) sensory rhodopsin I, Hh) H. Halobium, SG1) Halobacterium sp. strain SG1, Au2) Halobacterium sp. strain Au2.* *27*

Fig.I.18. *Plot of the projected mutants to study the function of Thr90. T90A mutant in comparison to WT (Fig. I.12.) loses all the interactions. Ala90 is not able to interact through hydrogen bonding nor with Asp115 nor with Trp86. The Van der Wals contact is not possible as well. T90V as T90A loses the hydrogen bond with Asp115 and Trp86, nevertheless, the side chain of Valine is supposed to emulate the steric contact with retinal. D115A mutant cannot form hydrogen bond between Thr90 and Asp115. The contact between retinal and Thr90 remains unaltered.* *28*

Fig. I.19. *Comparison of the structures of WT (PDB code 1PY6) versus transmembranal Prolines mutants. Doted yellow lines are plotted just to display distances, not as an evidence of an hydrogen bond. The maximal distance considered for the existence of a hydrogen bond is 3.2Å, although Chakrabarti et al. showed C-H···O bonds of about 3.7 Å . The residues represented correspond to the i-3 and i-4 amino acids before Pro (i). In the case of WT, the distance considered reflects the space between the Cδ of the Pro versus the peptydil Oxygen of the i-3 and the i-4 residue. In the case of the mutant structures, the distance represented is the one between the peptydil Nitrogen of the Ala respect the peptydil Oxygen of the i-3 and the i-4 residue. The PDB code for the mutants P50A, P91A and P186A are 1PXR, 1Q5J and 1Q5I respectively.* *29*

Chapter III

Fig.III.1. *Purple-to-blue transition of dark-adapted T90A. (A) Absorption spectra of T90A in 150 mM KCl at pH 7.2 (——) and 2.0 (---). (B) Absorption spectra of deionised T90A at pH 7.0 (——) and 3.6 (---). (C) Curves 1-6 are the difference spectra (pH_i-$pH_{7.2}$) of T90A in 150 mM KCl, where pH_i values are 7.2, 6.2, 5.0, 4.1, 3.5 and 3.2. (D) Curves 1-6 are the difference spectra (pH_i-$pH_{8.0}$) of deionised T90A, where pH_i values are 7.0, 6.4, 5.9, 5.1, 4.3 and 3.6.* ____ *45*

Table III.1.*Apparent pK_a of Asp85 (the purple-to-blue transition), as obtained from the plot of absorption changes as a function of pH.* ____ *45*

Fig.III.2. *Rate of hydroxylamine reaction with wild type BR (circles) and T90A (triangles) as measured by the absorption change in the visible. The reactions were carried out in dark (filled symbols) or under illumination with light of 300 lux (empty symbols).* ____ *47*

Fig. III.3. *DSC thermograms of wild type and T90A. The membranes were suspended in H_2O at 1.5-2.0 mg/ml, pH 7.0. All curves were corrected with the instrumental and chemical baselines. Scans were taken at 1.5 ºK/min.* ____ *48*

Fig. III.4. *Proton pumping rates of wild type BR (circles) and T90A (triangles) incorporated into liposomes, as a function of time. Data are the mean values from 3 independent samples. The bars represent half of the corresponding standard error. The initial pumping rate of T90A was about 16% of that of wild type, and the photo steady pumping amount, about 20%.* ____ *48*

Chapter IV

Fig. IV.1. *Structure of helices C and D of bacteriorhodopsin. The structure was taken from the PDB entry 1kgb. (A) Locations and orientations of key residues of helices C and D. (B) Detail of the hydrogen bonds formed by the –OH group of Thr90 with Asp115 and with the carbonyl oxygen of Trp86. The steric interaction of the methyl group of Thr90 with the C11-C13 of the retinal is also shown.* ____ *57*

Fig. IV.2. *Light-dark absorption spectra of T90A. Left column: absorption spectra of dark-adapted (dash-dot line) and light-adapted (solid line) membrane suspensions of T90A, at pH 7.0. (A) in water; (B) in 150 mM KCl; (C) in 1 M KCl. Right column: Difference spectra obtained by subtracting light- minus dark-adapted spectra.* ____ *60*

Table IV.1. *Time constants of M rise and decay obtained by fitting the absorption changes at 410 nm from Fig. 3 (1 M KCl, pH 6.5 or 10.0, 293 K) to a biexponential function. In parentheses, the corresponding fraction amplitude. Maximum absorbance values at 150 mM KCl, pH 7.0 are also shown.* ____ *61*

Fig. IV.3. *Kinetics of photocycle intermediates. The traces show the absorption changes corresponding to the M intermediate (410 nm, top), BR depletion and recovery (555 nm for T90A, T90V and D115A; 570 nm for WT, middle) and O intermediate (660 nm, bottom). Column (A), pH 6.5, 1 M KCl, 293 K. Column (B), pH 10.0, 1 M KCl, 293 K. The absorption changes at 410, 660 and 570/555 nm, were normalized to the amplitude of the M intermediate for each pigment at the respective pH.* ____ *63*

Fig. IV.4. *Light-induced pyranine signals. Pyranine absorption changes were measured at 460 nm in suspensions of T90A, T90V, D115A and WT, in 150 mM KCl (pH 7.0) at 293 K. Proton uptake from BR causes an increase of absorbance, while proton release causes a decrease. Protein concentration, 1.5·10^{-5} M.* 64

Fig. IV.5. *FTIR-Difference spectra of T90A. The films were prepared from suspensions in 150 mM KCl at pH 10.0 (A) and pH 7.0 (B). Conditions: (1) dry sample at 277 K; (2) wet sample at 277 K; (3) dry sample at 243 K; (4) wet sample at 243 K. The spectra are scaled so that all of them have the same intensity.* 66

Fig. IV.6. *N-like FTIR difference spectra and carboxylic region of the FTIR deconvoluted spectra of T90A, T90V, D115A and WT. A, comparison of T90A, T90V, D115A and WT FTIR difference spectra under conditions for WT to yield the N intermediate (pH 10.0, wet sample, at 277 K). (1) WT; (2) T90A; (3) T90V; (4) D115A. B, Carboxylic region of the deconvoluted spectra of purple membrane dry films at 293 K obtained from membrane suspensions in 150 mM KCl, pH 7.0. (1) WT; (2) T90A; (3) T90V; D115A. The parameters used for deconvolution are a full bandwidth at half height of 10 cm^{-1} and a narrowing factor k of 2.* 68

Fig. IV.7. *DSC-thermograms of wild type and mutants D115A, T90V and T90A. Purple membrane patches were suspended in H_2O at a concentration of 2.0 mg/ml, pH 7.0. The curves were corrected with the instrumental and chemical baselines. Scans were taken at 1.5 K/min. Scale bar represents an apparent heat capacity of 5.10^{-4} cal/ºC.* 70

Chapter V

Fig. V.1. *Diagram of the helix C. Up, plot of the steric clash induced by Pro91 and Leu87. Proton pumping related groups are displayed. Thr90 and Trp86 hydrogen bond enhances the kink in Helix C. Down, The clash prevents Asp85 and Asp96 from moving further away the Schiff Base (PDB coordinates from 1M0L).* 80

Fig. V.2. *Location of transmembrane prolines in bacteriorhodopsin wild type structure (PDB code 1PY6). The C_δ-H···O hydrogen bonds involving Pro residues are plotted taking into account the relative distances shown in* ***Table V.2***. 82

Table V.1 *Spectral features of bacteriorhodopsin WT and proline mutants.* 85

Fig. V.3. *Hydroxylamine reactions. (A) Rates of Schiff base accessibility to hydroxylamine in the absence of light recorded for WT (●) and mutants P50A (■), P91A (▲) and P186A (★). (B) Rates of Schiff base accessibility performed under illumination for WT (○), P50A (□), P91A (△) and P186A (☆), using a light of 300 lux of luminance.* 86

Table V.2. *Distances in Å between $C_{\delta i}$ of Pro (50, 91 and 186) and the peptidyl O of the i-3, i-4 and i-5 residues of bacteriorhodopsin.* 87

Fig. V.4. *Kinetics of M photointermediate. Changes in absorbance at 410 nm of WT (1), P50A (2), P91A (3) and P186A (4) suspensions in 1M KCl, pH 6.5 at room temperature were averaged to determine the time constants of M rise. τ_{ave} were: WT 60 μs, P50A 45 μs, P91A 7 μs and P186A 35 μs.* 88

Fig. V.5. *Light-induced proton changes as measured with the pH dye pyranine signals. Pyranine absorption changes were measured at 460 nm in suspensions of WT (1), P50A (2), P91A (3) and P186A (4) in 1M KCl (pH 7.2) at 298 K. Proton uptake from BR causes an increase of absorbance, while proton release causes a decrease. Protein concentration, $1.5 \cdot 10^{-5}$ M.* ___ *89*

Fig. V.6. *Light-induced pH changes of BR-incorporated liposomes as a function of time. WT (●), P50A (■), P91A (▲) and P186A (★). Initial pH, 6.5, in KCl 150 mM.* ___ *90*

Table V.3. *Bacteriorhodopsin relative proton pumping activity* ___ *90*

Fig. V.7. A. *Fourier transform infrared difference spectra corresponding to BR-M state. Spectra for WT, P50A, P91A and P186A were collected under M-yielding conditions (dry film, pH 10, 243 K).* ***B.*** *Fourier transform infrared difference spectra corresponding to BR-N state. Spectra for WT, P50A, P91A and P186A were collected under N-yielding conditions (wet film, pH 10, 277 K).* ___ *92*

Chapter VI

Fig. VI.1. (a) *Plot of the ΔAbs at 560nm as a function of temperature for WT Bacteriorhodopsin. The fitting to a sigmoid function is also displayed. The T_m corresponds to the inflexion point of the function.* ***(b)*** *The first derivative of the sigmoid function in (a) is represented. It yields a one peak curve corresponding to the T_m of the reaction.* ___ *108*

Fig. VI.2. (a) *Order parameter of the denaturation simulation of Bacteriorhodopsin. It corresponds to the fraction of the number of atoms participating in the largest cluster (X_c) as a function of the mean coordination number <r>.* ***(b)*** *Composite graph of the negative of the 1st derivative of ΔAbs at 560nm (Y, left) as a function of the temperature (X, bottom) and the 2nd derivative of the number of floppy modes (Y, right) with respect to <r> (X, top). Both the order parameter and the 2nd derivative serves as indicators of the different states occurring during the denaturation of BR. It should be pointed out that no correspondence between the particular values of temperature and <r> is proposed in this plot; it is used solely to suggest that some sort of relationship is likely to exist between both magnitudes when considering the denaturation process of a protein.* ___ *109*

TABLE VI.1. *Identification of the three main states during simulated denaturation. T_m for the experimental transition state.* ___ *110*

Fig. VI.3. *Difference spectra of the UV-Vis thermal denaturation of BR.* ***(a)*** *WT;* ***(b)*** *P50A;* ***(c)*** *P91A;* ***(d)*** *P186A. Gradual heating of PM samples at pH 7.0 was performed.* ___ *111*

Fig. VI.4. *Hydrogen dilution plot for chain A of the crystal structure of WT Bacteriorhodopsin (1py6). From left to right, in the first column the number of hydrogen bonds remaining in the structure is displayed. The Energy of the removed hydrogen bond is in the 2nd column. The 3rd column displays the average number of atom neighbours for the atoms involved in the hydrogen bond. The following item, the dilution plot, is a linear representation of the protein structure, divided in rigid (thick colored) and flexible regions (thin black lines). The two last colums represent the donor (blue) and acceptor (red) of the broken hydrogen bond at each dilution step. Taking into account if the atoms involved are from the main chain (backbone) or from the side chain of the amino acid, a M or a S is respectively written. To easily identify where the residues are located, small red and blue arrows are plotted in the dilution plot.* ___ *112*

Fig. VI.5. (a) *Order parameter (see legend to Fig* ***VI.2.****) of the PDB structures of WT (1py6), P50A (1pxr), P91A (1q5j) and P186A (1q5i).* ***(b)*** *2^{nd} derivative of the floppy modes for the indicated structures. Related to the order parameter by the mean coordination, the values for the main states of the simulation of each structure are represented in Table VI.1.* ***(c)*** *The T_m for the UV-Vis Thermal denaturation are displayed for WT and mutant proteins.* ___ *113*

Fig. VI.6. *Remaining rigid structure in the transition state obtained by simulated denaturation. (1) WT; (2) P50A; (3) P91A; (4) P186A. The thick colored regions correspond to rigid clusters and the thin black lines represent flexible ones. This linear representations are extracted from the respective hydrogen dilution plot (****see Fig. VI.4****)* ___ *115*

Fig. VI.7. *Evolution of the simulated thermal denaturation in the 3D structure. The red thick structures display rigid regions while the grey thin ones represent denatured structures. Retinal is displayed in yellow in the native state, light-yellow in transition state and no represented in denaturation state. This figuration of retinal presence is done to relate the simulation with what happens in UV-Vis experiments. In the case of the denaturated state (not solely on Bacteriorhodopsin structure), it must be emphasized that all the prolines are present. This limitation of the FIRST algorithm comes from the fact that Pro is always considered as rigid. Furthermore, in the case of some Heteroatoms (with no O, N or S atoms) present in the structure (i.e. retinal), the only interactions are the hydrophobic ones, not taking into account low energy hydrogen bonds.* ___ *116*

Chapter VII

Fig. VII.1. *Diagram of Helix C of Bacteriorhodopsin. Disposition of Asp85 and Asp96 respect to the Schiff Base is represented. The steric clash induced between Leu87 and Pro91 is displayed in order to show the division of the helix in two segments (dotted white line). Arrow are quantitative, indicating the degree of bending that the egments may reach by each side. X indicates restriction of movement induced by the steric clash.Atomic coordinates are from 1M0L from the Protein Data Bank (PDB).* ___ *127*

Fig. VII.2. *Distances from the Cδ of Pro91 to the i-5, i-4 and i-3 residues. In this PDB coordinates of the ground state of BR (1M0L), Pro91 is prone to form hydrogen bonds with 3 residues. Taking into account that Pro can perform from none to 2 hydrogen bonds, this yields the chance of 2^N-1 possibilities of hydrogen bonding, where N is the number of residues which are in the immediate environment of Pro (least than 3.7Å).* ___ *128*

Fig. VII.3. *Plot of a simulation for a poly-Alanine helix (A) and for a poly-Alanine helix with one single Pro at the center of the helix (B). The kink angle (bending) vs. the swivel angle is represented. An homogeneous distribution is shown for poly-ala meanwhile for Pro-containing helix, certain angles are restricted. This restriction comes from the steric clash induced by Pro.* ___ *129*

Fig. VII.4.*Proline positions along Transmembrane helices. The frequency of proline residues is shown as a function of normalised proline position (where -1 corresponds to the N terminus and +1 corresponds to the C terminus of a Transmembrane helix, so that 0 is the centre of the helix).* ___ *134*

Fig. VII.5. *Scatterplots of superimposed positions of oxygen atoms, participating in C–H· · ·O interactions, relative to the pyrrolidine ring, in stereo. The oxygen atoms are represented by dots. The cut-off distance is 3.5 Å in (a) and 4.0 Å in (b). It can be seen that at 3.5 A ° the points are more clustered, especially around the protons at Cα and Cδ atoms. This suggests that the C–H· · ·O interaction could be stronger and as directional as the conventional hydrogen bonding when the C–H groups at Cα and Cδ, rather than at Cβ and Cγ are involved. This is in conformity with the position of Cα and Cδ atoms being next to the electron-withdrawing ring N atom, whereby the protons at these positions carry more partial positive charge, which brings about a stronger electrostatic interaction for the C–H· · ·O bond. Cδ and Cα are indicated.* ___ *135*